

**UNIVERSIDADE FEDERAL DE ITAJUBÁ
PROGRAMA DE PÓS-GRADUAÇÃO EM
ENGENHARIA ELÉTRICA**

**Electromagnetic procedures to support main components design of
synchronous machines**

Paulo Victor Viana da Silva

**Itajubá
February 2020**

**UNIVERSIDADE FEDERAL DE ITAJUBÁ
PROGRAMA DE PÓS-GRADUAÇÃO EM
ENGENHARIA ELÉTRICA**

Paulo Victor Viana da Silva

**Electromagnetic procedures to support main components design of
synchronous machines**

**A Dissertation Presented to Federal
University of Itajubá in Fulfillment of
Requirements for the Degree of Master of
Science in Electric Engineering.**

**Concentration Area: Methods for Analyzing,
Planning and Management of Energy
Systems.**

**Supervisor: Edson da Costa Bortoni
Co-Supervisor: J. Johnny Rocha E.**

**Itajubá
February 2020**

DEDICATION

This work is dedicated to my parents, Ledilson and Vanilda, and my sister Victoria, who unconditionally have supported me through this journey.

To Ana Paula, my beloved one, who cheered me up even in the hardest moments.

Finally, I would like to dedicate this dissertation to all my closest friends from R7, Cassino, and COPOVO, who were always there in moments of need, even when I did not know that I needed them.

Thanks for all their support, which without I could not have done this work.

ACKNOWLEDGEMENTS

I want to acknowledge all the support and love I received from my family and friends during my graduation and post-graduation, which was critical to keep me on the right track in both personal and academic matters. I thank especially my parents, who always believed in my success, regardless of how absurd or far away my goals would send me.

I am thankful to my supervisors, Professor Dr. Edson da Costa Bortoni and Dr. Jorge Johnny Rocha Echeverría, that were not only advisors but friends. They were able to learn and teach all the same, always with great enthusiasm about machinery. I thank them for embracing me since the beginning, when I chose to follow an academic path, until this day, with continuous support, patience, faith in our work, and when needed, a friendly scold. In a few words, thank you two for being the guides in a world that I want to wonder more.

I acknowledge all my colleagues and collaborators at Federal University of Itajubá, not only for their support but also for sharing their time for different matters, as for a chat about soccer, a laugh, a coffee. I could find this kind of environment in many places and moments: in my post-graduation classes, in some project groups, and specially in EXCEN (Excellence Center in Energetic Efficiency), where I spent most of my days.

I want to acknowledge the CAPES, CNPq, FAPEMIG, and INERGE for their financial assistance and primarily for continuous support to conduct research.

ABSTRACT

Synchronous generators have proven over the decades to be the feasible solution for three-phase power systems and have consolidated as the vital piece in power plants in which the source of energy is renewable, as hydraulic or wind. Thus, with a constant increase in environmental concerns in current times, it is also expected an increase in synchronous machine usage, along with more research and development. A challenge would be to integrate the traditional consolidated knowledge with modern computational tools. Since when it comes to electrical machines, there is more than one procedure or technique to solve the same question, many combinations of new algorithms and books from a century ago have yet space to be approached. This work proposes and develops a set of tools to allow the analysis of magnetics effects in a salient pole machine with general, accurate, and fast solutions, applying what has been taught for the first “machinerists”, as Tingley and Park, alongside with MATLAB and Finite Element Method. Its objectives are to get Magnetomotive Force and Magnetic Flux Density of a given machine so then, in future work, to calculate the inductance matrix. MMF is calculated through Tingley Box, Winding Matrix, and Fourier Series, allowing the analysis for every single turn. Flux density is calculated through Finite Element Analysis, which allows the calculation of enclosure factors that support the accuracy of the tool by comparing it with manufacturers' benchmarks. In the end, a guide in MATLAB is shown, which aggregates everything exposed with a user-friendly interface.

Index terms – Enclosure Factor, Finite Element Analysis, Magnetic Simulation, Magnetomotive Force, Salient Poles, Synchronous Generators, Winding Distribution.

LIST OF FIGURES

Figure 1.1 - Electricity generation by source, World 1990-2017 Source: [1].....	15
Figure 1.2 - Renewable electricity generation by source (non-combustible), World 1990-2017 Source: [1]	15
Figure 1.3 - Magnetic flux lines and flux density map in Induction Motor. Source: [5]	17
Figure 2.1- Cross section of different types of a SM rotor. Source: [11].....	19
Figure 2.2 - Cross section of a SM stator. Source: [11]	20
Figure 2.3 - Different slots shapes. Source: [12].....	20
Figure 2.4 - Double layer slot in a salient poles SG.....	21
Figure 2.5 – Itaipu’s SG salient poles rotor being installed, 1760 ton and 90 rpm. Source: [14]	22
Figure 2.6 - Lap Winding for AC machine with 2 poles and 24 slots. Source: [15].....	24
Figure 2.7 - Wave Winding in AC machine with 4 poles and 24 slots. Source: [15]	25
Figure 2.8 – Salient poles SG, with a single pair of poles.....	27
Figure 2.9 - Vector diagram in $0dq$ axis.....	28
Figure 2.10 – Phasorial diagram for phase A.	31
Figure 2.11- Phase A Flux linkage.	34
Figure 2.12 - MMF diagrams for phase A.....	34
Figure 2.13 – Angles σ for phases B and C.....	37
Figure 2.14 - Mutual flux linkages diagram for phases A and B.	38
Figure 2.15 – Example of mesh grids, created by FEATool MATLAB. Source: [21]	45
Figure 2.16 - Color flux density plot of an example solution in FEMM website. Source: [23]	46
Figure 2.17 - Boundary Property window.....	47
Figure 2.18 - FEMM Air property.....	48
Figure 3.1- Phasorial rosettes for different examples.....	51
Figure 3.2 - Winding scheme corresponding to Rosette 3.1a.....	52
Figure 3.3 - Winding scheme corresponding to Rosette 3.1b.	52
Figure 3.4 - Winding scheme corresponding to Rosette 3.1c.....	52
Figure 3.5 - Winding Matrix corresponding to Figure 3.1a ($y = 5$).	53
Figure 3.6 - Winding Matrix corresponding to Figure 3.1b ($y = 3$).	53
Figure 3.7 - Winding Matrix corresponding to Figure 3.1c ($y = 3$).	53
Figure 3.8 - Winding Matrix for each phase.	53

Figure 3.9- MMF of a single turn. Source: [28]	55
Figure 3.10 - 24 slots, 2 pair of poles, phase A MMF for a constant current.....	55
Figure 3.11 - 75 slots, 10 pair of poles, phase A MMF for a constant current.....	56
Figure 3.12 - 72 slots, 10 pair of poles, phase A MMF for a constant current.....	56
Figure 3.13 - 24 slots, 2 pair of poles, resulting MMF at $t = 0$	57
Figure 3.14 - 75 slots, 10 pair of poles, resulting MMF at $t = 0$	57
Figure 3.15 - 72 slots, 10 pair of poles, resulting MMF at $t = 0$	58
Figure 3.16 - 24 slots, 2 pair of poles, resulting MMF and fundamental at $t = 0$	58
Figure 3.17 - 75 slots, 10 pair of poles, resulting MMF and fundamental at $t = 0$	59
Figure 3.18 - 72 slots, 10 pair of poles, resulting MMF and fundamental at $t = 0$	59
Figure 3.19 – Illustrations of three pole shoes types addressed in this work, depicting where the arcs are located.	60
Figure 3.20 - One arc pole shoe dimensions parameters.	61
Figure 3.21 - Two arcs pole shoe dimensions parameters.....	62
Figure 3.22 - Three arcs pole shoe dimensions parameters.....	63
Figure 3.23 - Three arcs pole shoe example in FEMM.....	65
Figure 3.24 - Boundaries properties for pole shoe simulation.	66
Figure 3.25 – Magnetic flux lines and color density plot.....	67
Figure 3.26 - Magnetic flux density plot over air-gap line.....	67
Figure 3.27 - Magnetic Flux Density with some extracted parameters.....	68
Figure 3.28 - Axial dimensions around air-gap.....	70
Figure 3.29 - A SM axial extremity in FEMM.....	71
Figure 3.30 - A SM axial extremity in FEMM (Detail).	72
Figure 3.31 - Boundaries properties for pole end simulation.....	73
Figure 3.32 - Magnetic flux lines and color density plot.	73
Figure 3.33 - Magnetic flux lines and color density plot (Detail).	74
Figure 3.34 - Magnetic flux density over region of interest.....	74
Figure 3.35 - Simulated geometry and normalized magnetic flux density plot.	75
Figure 4.1 - Phasorial rosette and winding scheme for SG1.	77
Figure 4.2 - Stator data for SG1.	78
Figure 4.3 - Winding Matrix for SG1.....	78
Figure 4.4 - Resulting MMF for SG1.....	79
Figure 4.5 - Pole Shoe for SG1.	79
Figure 4.6 - Pole Shoe Magnetic Analysis for SG1.	80

Figure 4.7 - Benchmark pole field curve for SG1.	80
Figure 4.8 - Effective Magnetic Length analysis for SG1.....	81
Figure 4.9 - Benchmark airgap field in axial direction for SG1.....	81
Figure 4.10 - Stator with poles for SG1.	82
Figure 4.11 - Phasorial rosette and winding scheme for SG2.	82
Figure 4.12 - Stator data for SG2	83
Figure 4.13 - Winding Matrix for SG2.....	83
Figure 4.14 - Resulting MMF for SG2.	84
Figure 4.15 - Pole Shoe for SG2.	84
Figure 4.16 - Pole Shoe Magnetic Analysis for SG2.	85
Figure 4.17 - Benchmark pole field curve for SG2.	85
Figure 4.18 - Effective Magnetic Length analysis for SG2.....	86
Figure 4.19 - Benchmark airgap field in axial direction for SG2.....	86
Figure 4.20 - Stator with poles for SG2.	87
Figure 4.21 - Pole Shoe for SG3.	87
Figure 4.22 - Pole Shoe Magnetic Analysis for SG3.	88
Figure 4.23 - Benchmark pole field curve for SG3.	88
Figure 4.24 - Stator with poles for SG3	89

LIST OF TABLES

Table 4.1 - SGs parameters for validation.....	76
Table 4.2 - Pole enclosure results compared to benchmark	89
Table 4.3 - Axial enclosure results compared to benchmark.	90

LIST OF ACRONYMS

AC	Alternating Current
DC	Direct Current
EMF	Electromotive Force
FEA	Finite Element Analysis
FEM	Finite Element Method
MMF	Magnetomotive Force
MSE	Minimum Square Error
PDE	Partial Differential Equation
PM	Permanent Magnet
PMSG	Permanent Magnet Constant-speed-synchronous Generator
SG	Constant-speed-synchronous Generator
SM	Constant-speed-synchronous Machine

LIST OF SYMBOLS

n	Rotor speed, in rpm
f	Frequency
p	Number of pairs of poles
q	Slots per pole per phase ratio
N_s	Number of stator slots
m	Number of phases
a	Integer part when is written as a fractional mixed numeral
b	Reduced numerator in slots pole ratio (without integer part)
c	Reduced denominator in slots pole ratio, reduced number of poles
d	Reduced numerator in slots pole ratio, reduced number of slots
v	Voltage
λ	Flux linkage
S	Start of coil
E	End of coil
L	Winding inductance
r	Winding resistance
i	Current
θ	Angle between direct axis and reference (“A” axis)
ω	Rotor speed, in rad/s
X_a	Subscript a, quantity referent to phase “A”
X_b	Subscript b, quantity referent to phase “B”
X_c	Subscript c, quantity referent to phase “C”
X_o	Subscript o, quantity referent to zero sequence
X_d	Subscript d, quantity referent to direct axis
X_q	Subscript q, quantity referent to quadrature axis
X_F	Subscript F, quantity referent to field winding
X_D	Subscript D, quantity referent to direct axis damper winding
X_Q	Subscript Q, quantity referent to quadrature axis damper winding
K	Proportionality constant
t	Time
I_P	Peak current

\mathbb{P}	Modified Park Transform operator
\bar{E}	Electromotive Force phasor
\bar{V}	Voltage phasor
δ	Synchronous torque angle
\bar{Z}	Impedance phasor
φ	Magnetic flux
X_0	Subscript 0, quantity referent to initial value
X_R	Subscript R, quantity referent to rated value
P	Active power
\mathcal{F}	MagnetoMotive Force
N	Number of turns in a coil
\mathcal{P}	Specific Permeance
\wp	Permeance of a material
A	Area
Y	Admittance
X_l	Subscript l, quantity referent to sparse
X_m	Subscript m, quantity referent to mutual
X_s	Subscript m, quantity referent to self
σ	Phase angle
Δ	Auxiliary angle
U_3	3x3 Identity Matrix
X_{AA}	Subscript AA, quantity referent to armature-armature
X_{AR}, X_{RA}	Subscripts AR and RA, quantity referent to armature-rotor
X_{RR}	Subscript RR, quantity referent to rotor-rotor
A_m	Magnetic vector potential
μ_0	Permeability of free space
μ_r	Relative permeability
D_p	Number of slots in one virtual machine
C_p	Number of pair of poles in one virtual machine
N_{vm}	Number of virtual machines
τ_f	MMF fundamental period
τ_p	Pole pitch
R_δ	Air-gap average radius

y	Coil pitch
γ	Slot shift, in radians
s	Slot width
h_b	Pole core height
ω_b	Pole core width
ω_1	Pole shoe minor width
ω_2	Pole shoe greater width
h_1	Pole shoe height
δ_0	Minimum air-gap
R_e	Pole shoe corner radius
R_1	Pole shoe greater radius
R_2	Pole shoe second radius
ωR_1	Shoe width with greater radius
W_{ld}	Stator extremity “ladder” width
H_{ld}	Stator extremity “ladder” height
l_s	Stator axial length
l_{PS}	Pole Shoe axial length
l_{PC}	Pole Core axial length
H_{damp}	Damper ring slot height
l_{damp}	Damper ring slot length
H_1	Difference height between Pole core and end
H_2	Pole extremity heel height
α	Pole extremity ramp angle
l_1	Damper ring slot ramp length
l_2	Pole extremity minor length
l_3	Pole extremity greater length
α_e	Pole axial enclosure factor
l	Length of interest

SUMMARY

DEDICATION	2
ACKNOWLEDGEMENTS	3
ABSTRACT	4
LIST OF FIGURES.....	5
LIST OF TABLES.....	8
LIST OF ACRONYMS	9
LIST OF SYMBOLS	10
SUMMARY	13
1. INTRODUCTION	15
1.1. Dissertation Outline	17
1.2. Objectives	18
2. LITERATURE REVIEW	19
2.1. Synchronous Machines	19
2.1.1. SMs Windings	23
2.1.2. SM Mathematical Modeling and Park Transformation.....	26
2.1.3. Magnetic Circuits Preamble	32
2.1.4. Flux Linkage Equations.....	33
2.2. Finite Element Method	45
2.2.1. Software - Finite Element Method Magnetics.....	46
3. METHODOLOGY	49
3.1. TINGLEY BOX AND WINDING MATRIX	49
3.1.1. Building an induced voltage phasorial rosette (slot star)	50
3.1.2. Obtaining a regular three-phase winding scheme.....	51
3.1.3. Obtaining the Winding Matrix	52
3.2. MAGNETOMOTIVE FORCE	54
3.2.1. MMF – Single Turn.....	54
3.2.2. MMF – Resultant and Fundamental Waveforms	55
3.3. POLE SHOE ENCLOSURE FACTOR.....	60

	14
3.3.1. Pole shoe Geometry	60
3.3.1.1. One arc pole shoe	61
3.3.1.2. Two arcs pole shoe	62
3.3.1.3. Three arcs pole shoe	63
3.3.2. Finite element Simulation.....	65
3.4. EFFECTIVE PACKAGE MAGNETIC LENGTH	69
4. INTERACTION WITH MATLAB AND APPLICATIONS.....	76
4.1. Results for SG1	77
4.2. Results for SG2.....	82
4.3. Results for SG3	87
4.4. Results.....	89
4.4.1. Pole enclosure factor	89
4.4.2. Axial enclosure factor.....	90
5. CONCLUSIONS.....	91
6. FUTURE WORKS	92
7. BIBLIOGRAPHY.....	93
ANNEX A.....	96

1. INTRODUCTION

Currently, scarcity of resources along with environmental and social conditions brings a global concern on energy supplies; those are some of the factors that make renewable generation experience a constant expansion, as seen in Figure 1.1 and Figure 1.2 [1]. There is a total hydropower generation capacity of 1.267 GW installed around the globe, and pumped storage capacity of 153 GW [2], which suggests it as a reasonable choice among renewable sources for large-scale production. Developing technologies and tools that allow better utilization of these resources help to maintain this growth, bringing investment and opportunities altogether.

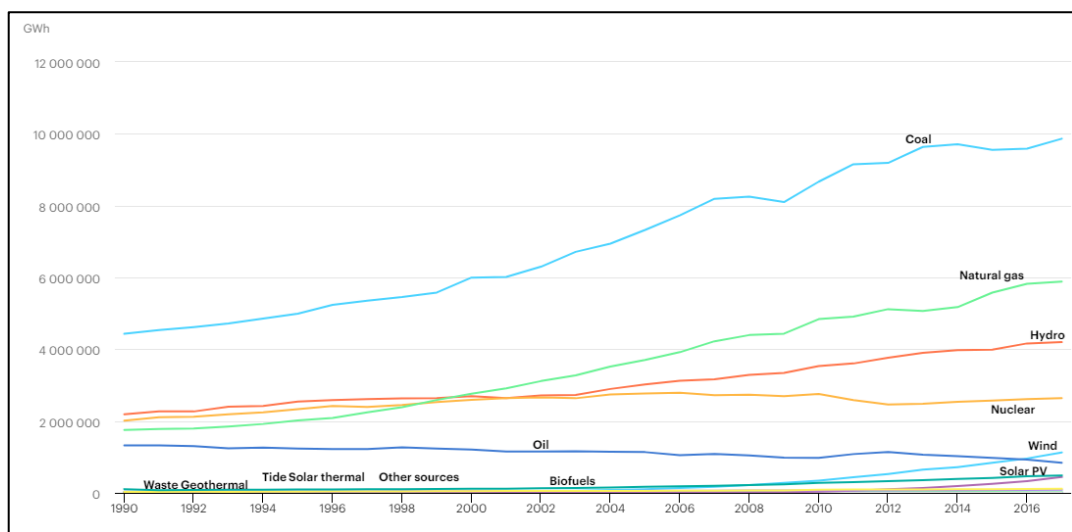


Figure 1.1 - Electricity generation by source, World 1990-2017

Source: [1]

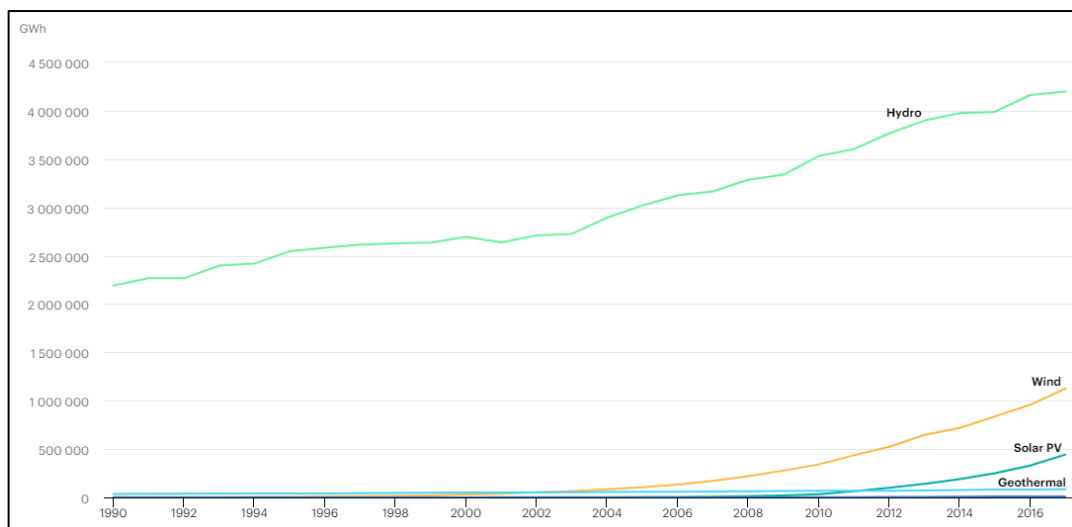


Figure 1.2 - Renewable electricity generation by source (non-combustible), World 1990-2017

Source: [1]

Improvements in electrical power generation as a centennial technology requires to target more than in the system physically, as much has been done in a macro scenario. Hence, unless another big breakthrough of physics or materials towards energy is made, changes tend to come from studying effects and behaviors that govern these systems. Studies can indicate generation's vulnerabilities as well as points where improvements are more significant, and they are also essential to help to validate theories and simulating different scenarios, which is often impractical.

This dissertation focus is in Synchronous Machines, a type of energy converter commonly adopted in hydro-generation and as a load for many applications, due to their advantageous characteristics such as:

- Controllable power factor, by changing its excitation;
- High efficiency, usually over 90%;
- Wider air-gap lengths grant mechanical stability.

As the use of mathematical modeling for the representation of actual phenomena, simulations are used in various fields as natural sciences, social sciences, and, of course, engineering. They enable studying different effects of what it is modeled, predicting, and, sometimes, controlling its behaviors. Such a powerful tool finds limitations in how complex a model can become, and the resources needed to solve it. Numerous models exist for synchronous generators, many coming from Park's two reaction theory [3], and all use inputs from reality or acceptable presumptions of it.

Modeling has constantly been evolving due to better analytical solutions and computation progress, in both hardware (better processors, memory, refrigeration techniques) and software (finite element methods, artificial intelligence, parallel processing).

Finite element analysis (FEA) is suitable for handling magnetic problems, such as energy converters. Both motors and generators have been studied using this technique ([4], [5], [6], and [7]). FEA is mentioned in most recent books about SM, with chapters dedicated to it [8]. An example of an FEA output is seen in Figure 1.3.

For this work, it is used MATLAB and FEMM (Finite Element Method Magnetics), which is a suite of programs for solving low-frequency electromagnetic problems on two-dimensional planar and axisymmetric domains.

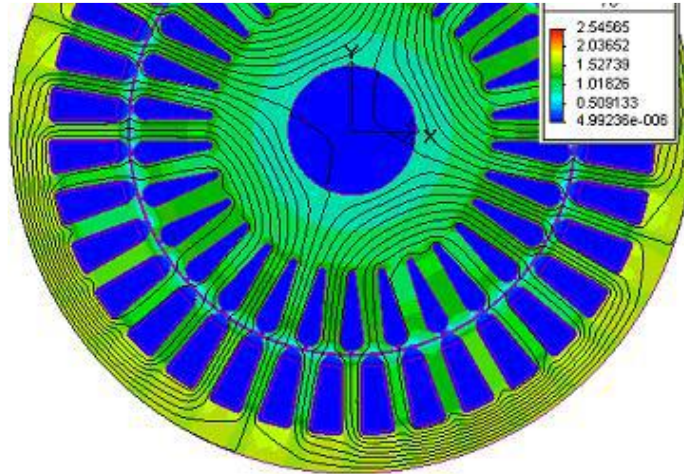


Figure 1.3 - Magnetic flux lines and flux density map in Induction Motor.

Source: [5]

1.1. Dissertation Outline

This dissertation is composed of 5 chapters. In this chapter, a brief introduction is presented about the present scenario in energy sources and the importance of SGs and studies on them.

The second chapter is a literature review, synthesizing SMs and FEM, and their elements that matter most for this work.

The third chapter goes through this work methodology, separated into four sections, one for each tool:

- Tingley Box and Winding Matrix, which is this work first objective, to set winding in a standard fashion and getting the Winding Matrix as a result.
- Magnetomotive Force, which clarifies how MMF is obtained for any SG condition, from any given Winding Matrix.
- Pole Shoe Enclosure Factor, which describes pole shoe geometry to thereby, used as FEM input, obtain their magnetic simulation overview and enclosure factor.
- Effective Core Magnetic Length, goes through axial enclosure factor, getting the actual core length for magnetic calculations.

The fourth chapter shows the Interaction with MATLAB and some Applications, with results from an interface that integrates all magnetic study done.

The fifth chapter concludes this dissertation, analyzing its results and the usability of the created interface.

The sixth and last chapter points to some future opportunities left open with this work, along with some improvements.

1.2. Objectives

To provide a complete and more reliable set of tools for analyzing main components in a usual SM design. Grouping traditional procedures and Finite Element Analysis that enable validation of essential aspects, as MMF and flux density waveforms as well as pole and axial enclosure factors, based only in some machine dimensions and rated data. All together in a user-friendly interface using MATLAB and FEMM.

2. LITERATURE REVIEW

With the intention of achieving tools development, some definitions need to be stated, both for Synchronous Machines and Finite Element Analysis. This chapter presents some key elements that one can understand and repeat the results.

2.1. Synchronous Machines

A SG, mostly, is constituted of elements that make use of Faraday's principle, which foresee that the interaction of a magnetic field with an electric circuit creates an EMF, effect known as electromagnetic induction [9]. Therefore, one element is responsible for producing the magnetic field and another composed by a set of armature coils in which voltage is induced, uniquely when there is relative motion between these elements. This induced current, flowing through armature windings, also produces a magnetic field, which is opposite to the one that caused it. This phenomenon is called armature reaction, and it is based on Park's theory [3].

The rotor is the moving part of a machine. In a SM rotor, an exciting magnetic field is produced by a set of coils on the rotor periphery, known as field winding [9]. There are two types of poles: salient (salient pole rotor) and non-salient (cylindrical, solid or round rotor), a cross-section of both types can be seen respectively in Figures 2.1a and 2.1b. There are some rotors with no windings on them, as for PMSG (excitation field is generated by PM) and reluctance machines (torque is created through magnetic reluctance [10]).

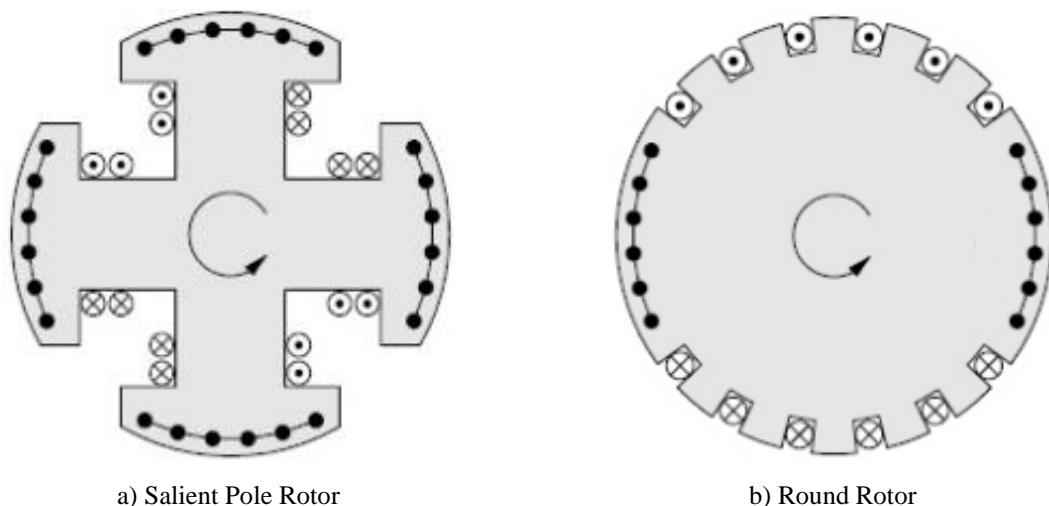


Figure 2.1- Cross-section of different types of a SM rotor.

Source: [11]

The second and stationary element, the stator (or armature), supports and provides a magnetic flux path for the armature windings [9]. For a vast majority of cases, SGs generate three-phase

power. Thus there are three sets of armature coils distributed in intervals of 120° (electrical degrees), so that is the difference between voltages phases. More about the disposition of armature windings and the difference between electrical and mechanical degrees are discussed further. A general stator cross-section can be seen in Figure 2.2.

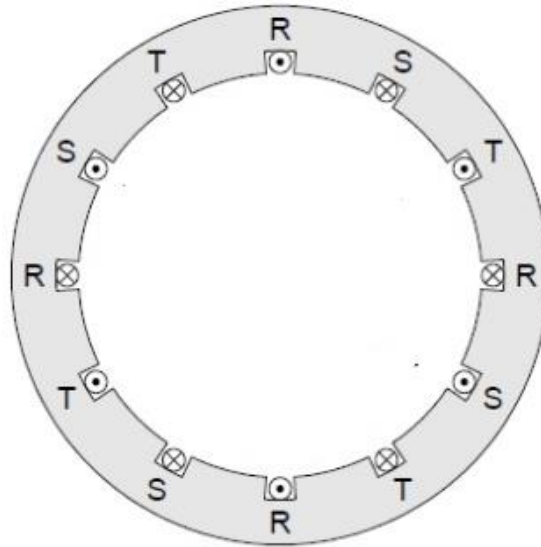


Figure 2.2 - Cross-section of a SM stator.

Source: [11]

Stator slots can be built as a) open, b) semi-open, c) and d) semi-closed, e) closed, as can be seen in Figure 2.3. Open and semi-open are usually rectangular, while semi-closed and closed ones can present rectangular or trapezoidal shapes with round angles [12].

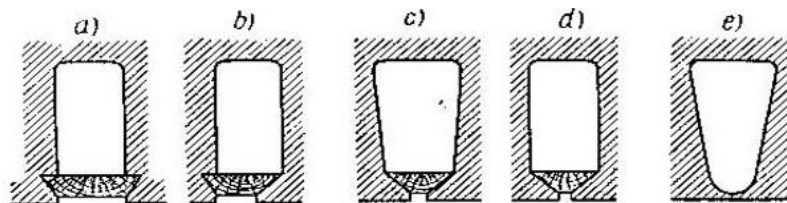


Figure 2.3 - Different slots shapes.

Source: [12]

A slot shape depends mainly on the winding and how it is insulated, which in turn depends on the machine power. Closed slots are for specific purposes; semi-closed are applied in low voltage and low and medium power machines; semi-open slots are applied in low voltage and medium power machines; and open slots are applied in all high voltage machines and low voltage with medium or high-power machines [9].

Armature slots are built as single- or double-layer slots. Single-layer is more common in smaller machines, with a number of windings as half of the number of slots (to each winding occupies

two slots). For this configuration, it is preferable the use of semi-closed or closed slots. The double-layer reduces costs, allowing the number of windings to be equal to the number of slots, granting a uniform shape for the coils. Figure 2.4 shows a merely illustrative machine design with double layer slots.

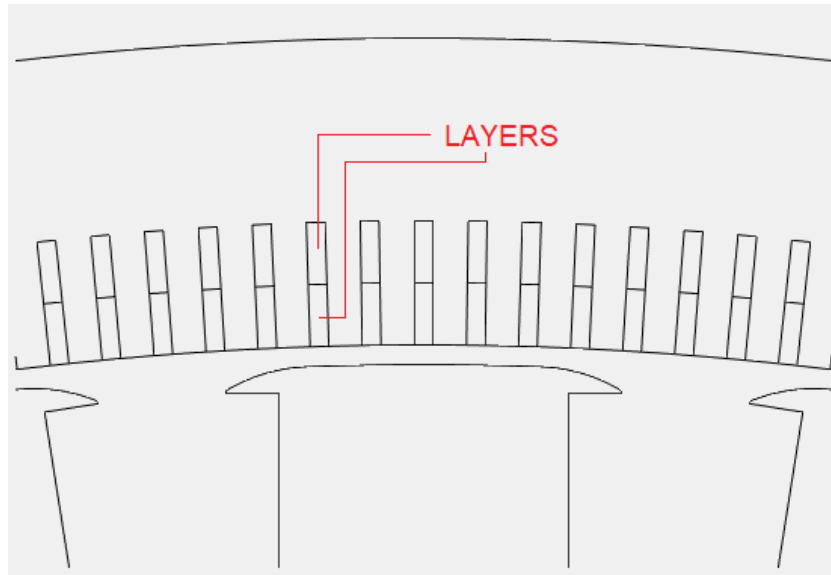


Figure 2.4 - Double-layer slot in a salient poles SG.

One of the most significant SM features is the relationship between frequency, speed, and the number of pairs of poles, expressed in Equation 2.1. SM rotor, due to field excitation (or PM, depending on the machine), follows the magnetic field produced by the armature, rotating at the same speed [13]. This behavior is reciprocal to a machine working as a generator or a motor.

$$n = \frac{60 \times f}{p} \quad (2.1)$$

Salient poles SGs may present from a single pair of poles as in small machines to dozens of pairs of poles as in vertical generators (Figure 2.5), depending on the practice demand. As seen in Equation 2.1, a more significant number of poles means lower rotor speeds for a given frequency, setting it as a preferential generator to use in hydroelectric power plants, where turbines speeds are lower than 200 rpm.



Figure 2.5 –SG salient poles rotor being installed in Itaipu, 1760 ton, and 90 rpm.

Source: [14]

Although more elements of a machine are applicable for magnetic studies, this work focuses on armature windings and salient rotor design, which are vital information to calculate Magnetomotive Force and Magnetic Flux Density in air-gap. For this reason, more of these subjects are addressed in further chapters.

2.1.1. SMs Windings

Three-phase windings require special attention in their construction because generated voltage wave shape depends directly on it. In [12] there is specific care at explaining the most common winding scenarios, whereas, for this work, only double layers windings are addressed. There is an essential link among the number of slots (N_s), number of phases (m) and number of pair of poles (p) that dictates how to organize windings, and q is commonly used to express this relation.

$$q = \frac{N_s}{m \times 2p} \quad (2.2)$$

Reducing q to minimum factors:

$$q = a \frac{b}{c} = \frac{d}{c} \quad (2.3)$$

Some ponderations can be done concerning Equation 2.3 factors, which are:

- Integral q ($c = 1$)

An integral q is where first harmonic in pole fields coincide with armature reaction first harmonic (MMF). Different phases start in an interval of $2q$ (120°).

- Fractional q ($c > 1$)

This case creates as good as a waveform than an integer q , and with fewer slots.

A fractional q also gives more options of placements; in a further chapter, a procedure known as Tingley Box is presented, which standardizes this work choice of placement.

a) Lap Winding

Lap winding applies the same coil pitch for all coils, starting at a top layer, passing through a bottom layer, and then coming back, forming then, q groups of phases. These groups are connected and form the machine terminals.

Figure 2.6 shows an example of lap winding in AC machines.

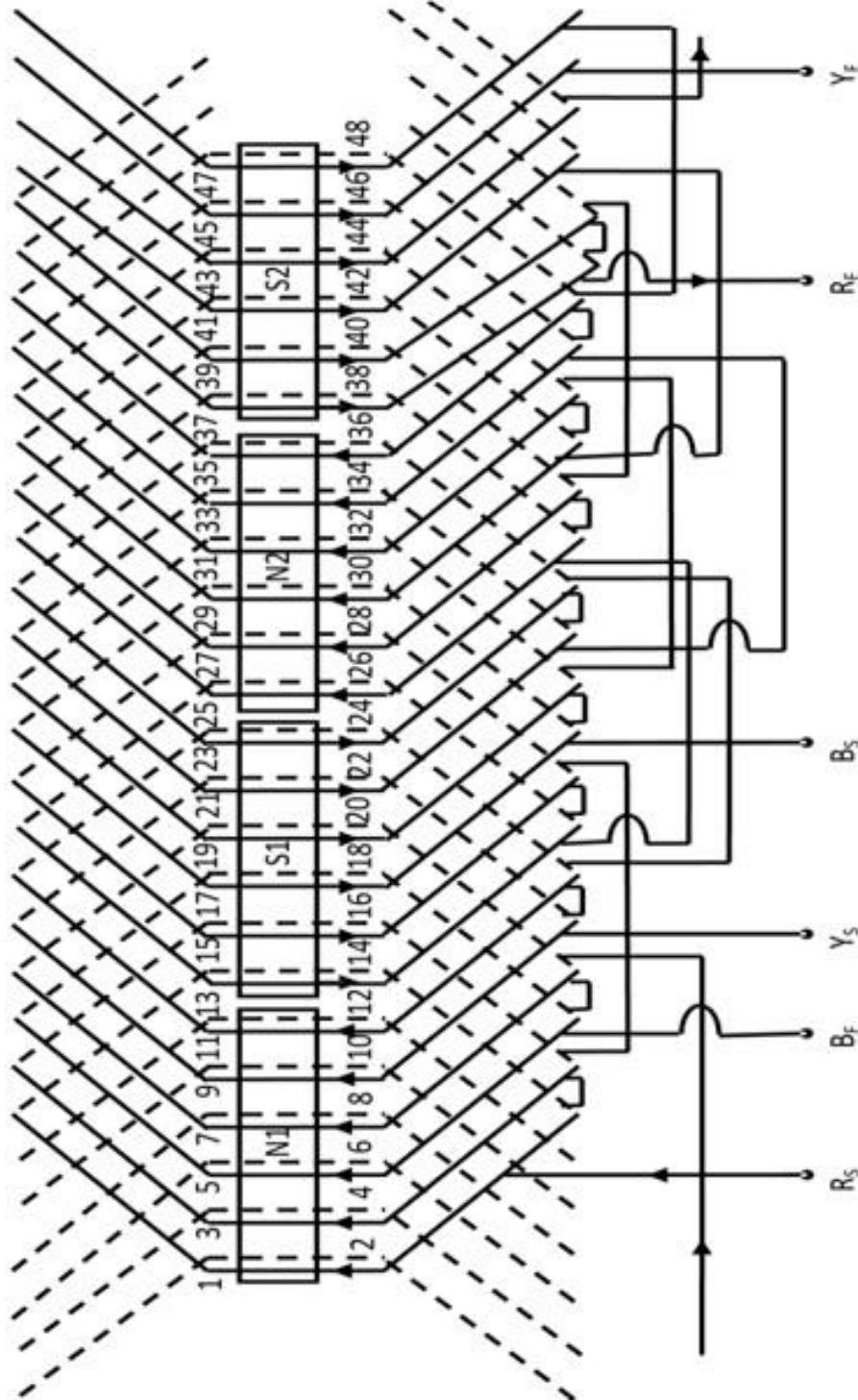


Figure 2.6 - Lap Winding for AC machine with 2 poles and 24 slots.

Source: [15]

b) Wave Winding

Wave winding presents no deviation in the magnetic field, which happens when windings from different phases share the same slot. One continuous coil goes from a slot to another spaced by one coil pitch, in a corrugated way. This coil composes a phase, and its terminals are then the machine terminals for that phase.

Figure 2.7 shows an example of wave winding in AC machines.

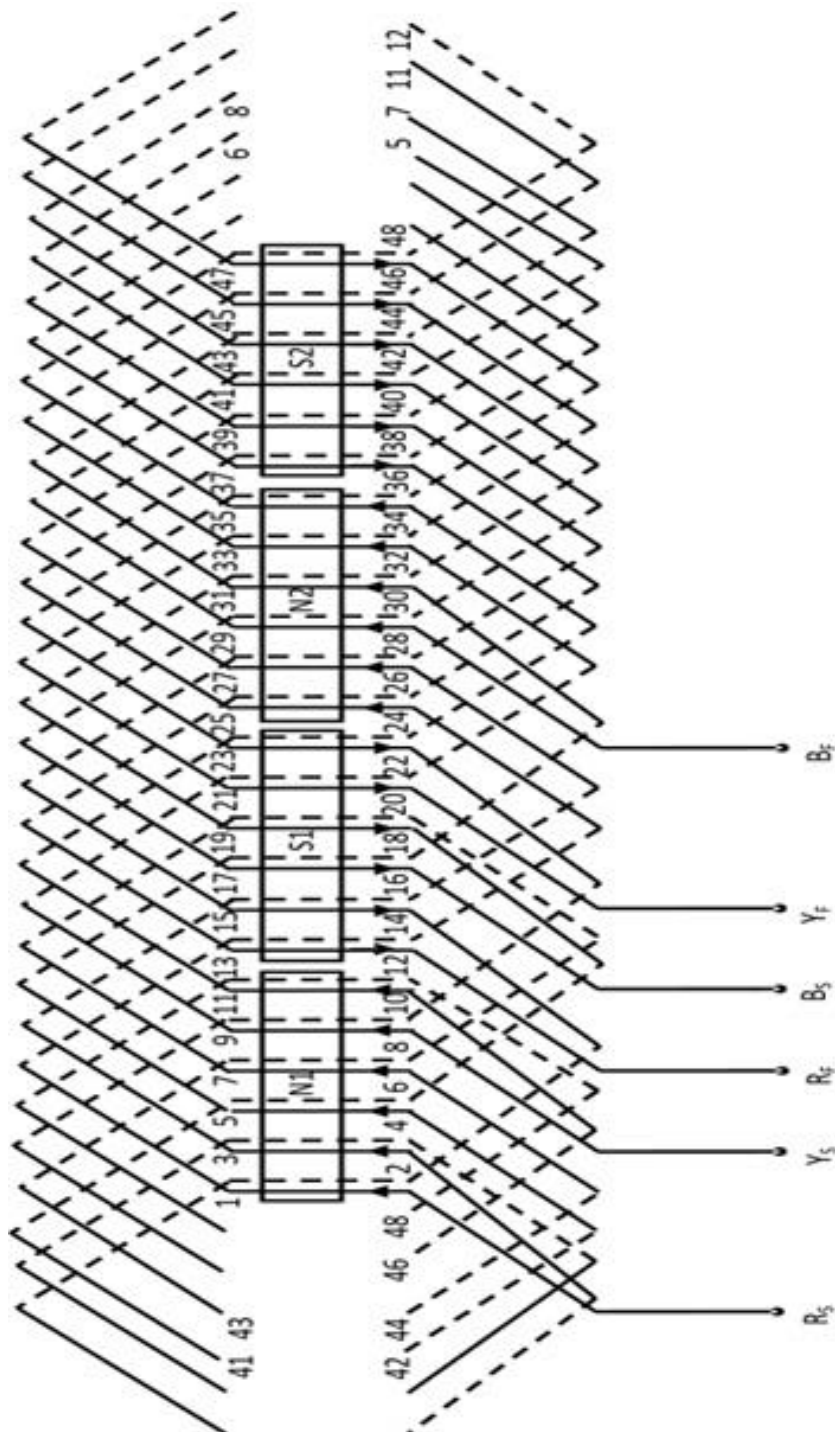


Figure 2.7 - Wave Winding in AC machine with 4 poles and 24 slots.

Source: [15]

2.1.2. SM Mathematical Modeling and Park Transformation

In this subchapter, it is shown how SM models can be deduced from elements previously exposed in this work. Park Transformation [3], which allows one to calculate machine quantities in a more comfortable and natural universe, changes an ordinary abc axis to one moving alongside the rotor, called $0dq$. The following demonstration makes explicit why describing accurately magnetic quantities is fundamental for modeling.

Firstly, it is considered a machine with 03 coils in its stator, 01 field winding, and 02 damper windings. Terminal voltages can be calculated using Equation 2.4. For magnetically coupled circuits, it is needed to consider voltage drops in windings (the first element in the equation) and reactions due to flux linkages (second element in the equation). The sums are to consider all drops (resistances) and flux linkages.

$$v = \pm \sum (r \times i) \pm \sum \frac{d\lambda}{dt} \quad (2.4)$$

- v - Terminal voltage
- r - Winding resistance
- i - Current flowing in the winding
- λ - Total flux linkage

Where:

$$\lambda = L \times i \quad (2.5)$$

- L - Winding inductance

Figure 2.8 shows a generator with one pair of poles, rotating at speed ω . Stator windings a , b and c are out of phase by 120° . S represents where a coil starts, and E where it ends. Subscripts are used as follows:

- a Phase A
- b Phase B
- c Phase C
- o Zero sequence
- d Direct axis
- q Quadrature axis

- F Field winding
 D Direct axis damper winding
 Q Quadrature axis damper winding

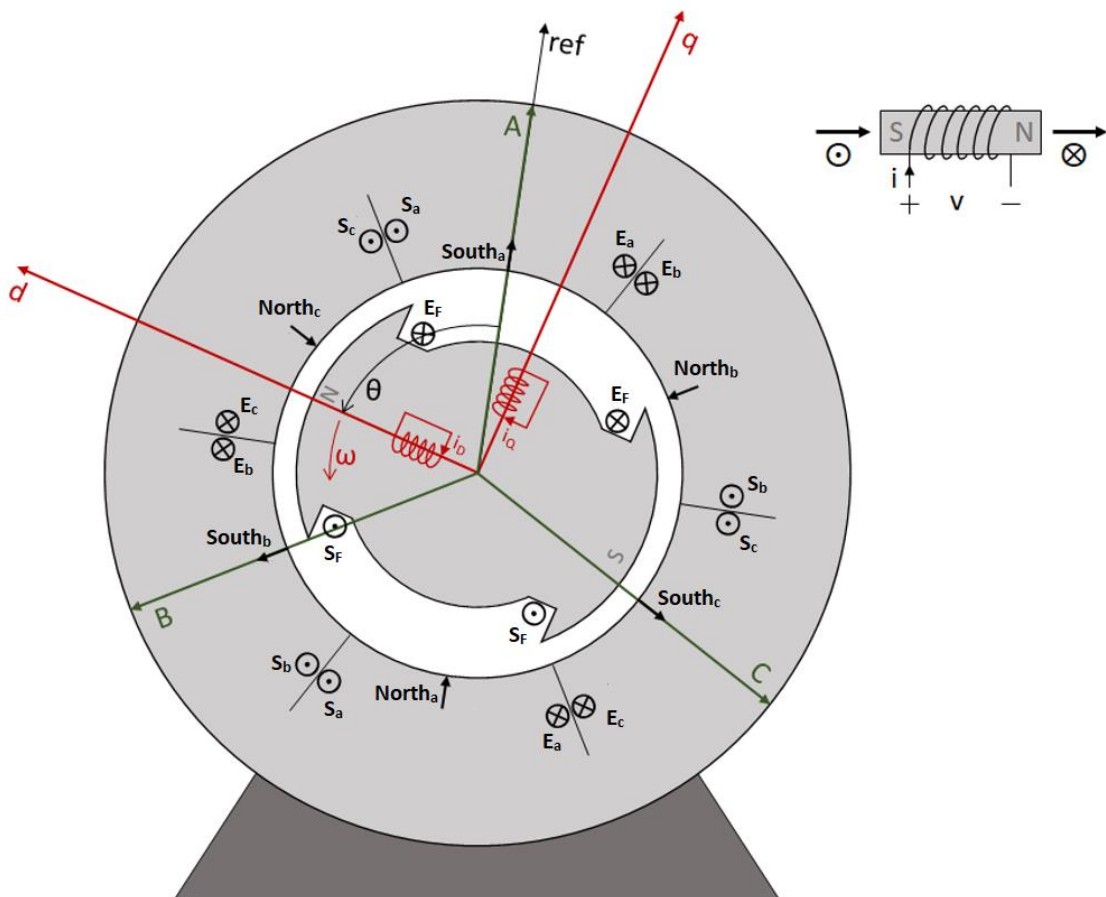


Figure 2.8 – Salient poles SG, with a single pair of poles.

There are some considerations to be pointed out before further analysis:

- d axis is placed in minimum air-gap reluctance direction, and q axis is 90° lagged, electrically;
- The rotor rotation direction is counterclockwise;
- The distance between adjacent poles is 180° (electrical degrees), where for a p number of pair of poles:

$$p \times (\text{mechanical degrees}) = \text{electrical degrees} \quad (2.6)$$

- Magnetic flux flows from south to north (inside the core);
- “A” axis is taken as reference for any angular displacement;

Thus, defining two fictitious currents, i_d and i_q , as follows:

$$\begin{cases} i_d \propto (\Sigma \text{ of } d \text{ axis currents}) \\ i_q \propto (\Sigma \text{ of } q \text{ axis currents}) \end{cases} \quad (2.9)$$

$$\begin{cases} i_d \triangleq K \left[i_a \cos \theta + i_b \cos \left(\theta - \frac{2\pi}{3} \right) + i_c \cos \left(\theta + \frac{2\pi}{3} \right) \right] \\ i_q \triangleq K \left[i_a \sin \theta + i_b \sin \left(\theta - \frac{2\pi}{3} \right) + i_c \sin \left(\theta + \frac{2\pi}{3} \right) \right] \end{cases} \quad (2.10)$$

The value of K that is used here comes from an improvement introduced by Leweis in [17]. There is defined K to obtain a transformation invariant in power. More can be read in Lewis work, here it is just defined:

$$K \triangleq \sqrt{\frac{2}{3}} \quad (2.11)$$

To handle Equation 2.10 in matrix notation, a new variable must be created. So, the third reference quantity is stationary proportional to the zero-sequence current:

$$i_o \triangleq \frac{1}{\sqrt{3}}(i_a + i_b + i_c) \quad (2.12)$$

In equilibrium conditions $i_a + i_b + i_c = 0$, and considering a peak current value of I_p :

$$\begin{cases} i_a = I_p \sin(\omega t) \\ i_b = I_p \sin \left(\omega t - \frac{2\pi}{3} \right) \\ i_c = I_p \sin \left(\omega t + \frac{2\pi}{3} \right) \end{cases} \quad (2.13)$$

Then, there is the following set of equations:

$$\begin{cases} i_o = \frac{1}{\sqrt{3}}(i_a + i_b + i_c) = \sqrt{\frac{2}{3}}\left(\frac{1}{\sqrt{2}}i_a + \frac{1}{\sqrt{2}}i_b + \frac{1}{\sqrt{2}}i_c\right) \\ i_d = \sqrt{\frac{2}{3}}\left[i_a \cos \theta + i_b \cos\left(\theta - \frac{2\pi}{3}\right) + i_c \cos\left(\theta + \frac{2\pi}{3}\right)\right] \\ i_q = \sqrt{\frac{2}{3}}\left[i_a \sin \theta + i_b \sin\left(\theta - \frac{2\pi}{3}\right) + i_c \sin\left(\theta + \frac{2\pi}{3}\right)\right] \end{cases} \quad (2.14)$$

In matrix form:

$$\begin{bmatrix} i_o \\ i_d \\ i_q \end{bmatrix} = \sqrt{\frac{2}{3}} \begin{bmatrix} \frac{1}{\sqrt{2}} & \frac{1}{\sqrt{2}} & \frac{1}{\sqrt{2}} \\ \cos \theta & \cos\left(\theta - \frac{2\pi}{3}\right) & \cos\left(\theta + \frac{2\pi}{3}\right) \\ \sin \theta & \sin\left(\theta - \frac{2\pi}{3}\right) & \sin\left(\theta + \frac{2\pi}{3}\right) \end{bmatrix} \begin{bmatrix} i_a \\ i_b \\ i_c \end{bmatrix} \quad (2.15)$$

A simplified notation of Equation 2.15 is defined:

$$I_{odq} \triangleq \mathbb{P}I_{abc} \quad (2.16)$$

\mathbb{P} is the modified Park Transformation operator, so:

$$\mathbb{P} \triangleq \sqrt{\frac{2}{3}} \begin{bmatrix} \frac{1}{\sqrt{2}} & \frac{1}{\sqrt{2}} & \frac{1}{\sqrt{2}} \\ \cos \theta & \cos\left(\theta - \frac{2\pi}{3}\right) & \cos\left(\theta + \frac{2\pi}{3}\right) \\ \sin \theta & \sin\left(\theta - \frac{2\pi}{3}\right) & \sin\left(\theta + \frac{2\pi}{3}\right) \end{bmatrix} \quad (2.17)$$

Similar equations can be written for voltages and fluxes:

$$V_{odq} = \mathbb{P}V_{abc} \quad (2.18)$$

$$\lambda_{odq} = \mathbb{P}\lambda_{abc} \quad (2.19)$$

Using the inverse of \mathbb{P} :

$$I_{abc} = \mathbb{P}^{-1}I_{odq} \quad (2.20)$$

It can be shown that the inverse matrix of Equation 2.17 is as follows: [18]

$$\mathbb{P}^{-1} = \sqrt{\frac{2}{3}} \begin{bmatrix} \frac{1}{\sqrt{2}} & \cos \theta & \sin \theta \\ \frac{1}{\sqrt{2}} & \cos\left(\theta - \frac{2\pi}{3}\right) & \sin\left(\theta - \frac{2\pi}{3}\right) \\ \frac{1}{\sqrt{2}} & \cos\left(\theta + \frac{2\pi}{3}\right) & \sin\left(\theta + \frac{2\pi}{3}\right) \end{bmatrix} \quad (2.21)$$

It can be noticed that $\mathbb{P}^T = \mathbb{P}^{-1}$, which makes \mathbb{P} orthogonal and invariant with power. And so, the following equation is valid:

$$\begin{aligned} P &= v_a i_a + v_b i_b + v_c i_c = [v_a \quad v_b \quad v_c] \begin{bmatrix} i_a \\ i_b \\ i_c \end{bmatrix} = V_{abc}^T \times I_{abc} \\ P &= V_{abc}^T \times I_{abc} = (\mathbb{P}^{-1} V_{odq})^T \times (\mathbb{P}^{-1} I_{odq}) \\ P &= V_{odq}^T (\mathbb{P}^{-1})^T \mathbb{P}^{-1} I_{odq} = V_{odq}^T \mathbb{P} \mathbb{P}^{-1} I_{odq} \\ P &= V_{odq}^T \times I_{odq} = [v_o \quad v_d \quad v_q] \begin{bmatrix} i_o \\ i_d \\ i_q \end{bmatrix} = v_o i_o + v_d i_d + v_q i_q \end{aligned} \quad (2.22)$$

Equation 2.22 makes explicit that Park Transformation only changes the reference of variables, without changing anything physically, creating fictional variables in axes d and q that turns solving synchronous machines problems more natural.

In order to proceed with the demonstration, an explanation about the angle θ is presented, where it is considered a machine with EMF \bar{E} has a terminal voltage \bar{V} lagged δ electrical degrees by the impedance \bar{Z} . The EMF is induced by the magnetic flux φ_F , being perpendicular to each other. Figure 2.10 illustrates this example for phase A.

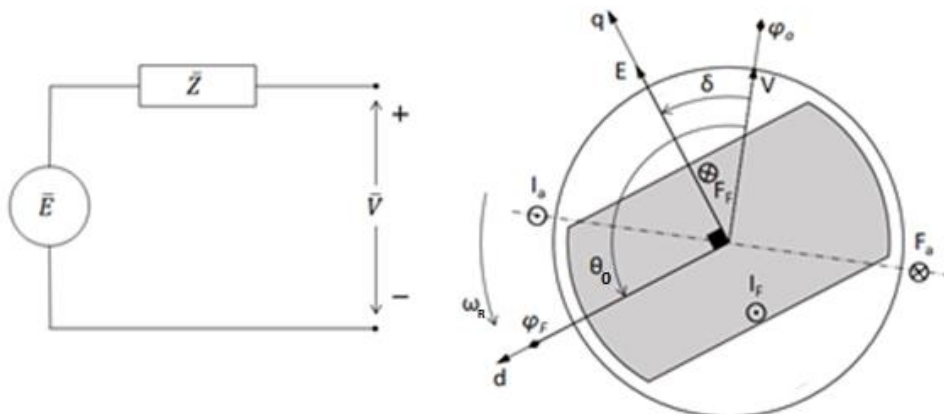


Figure 2.10 – Phasorial diagram for phase A.

If at instant $t = 0$ phasor \bar{V} is over the phase A-axis (reference), then the q axis is δ far from it and the d axis is $\theta_0 = \delta + \pi/2$.

For an instant $t > 0$, the rotational axis moved $\omega_R t$. And d axis is displaced with angle θ :

$$\theta = \theta_0 + \omega_R t = \omega_R t + \delta + \frac{\pi}{2} \quad (2.23)$$

2.1.3. Magnetic Circuits Preamble

Before advancing, a short preamble about electromagnetics with the equations needed to get to the inductances matrices.

Defining MMF as \mathcal{F} , N number of turns, i current flowing on each turn, μ_0 permeability of free space, A the area and l the length covered by magnetic flux, and \wp the permeance:

$$\mathcal{F} = N \times i \quad (2.24)$$

And:
$$\lambda = N \times \varphi \quad (2.25)$$

$$\text{Specific permeance} = \mathcal{P} = \frac{\varphi}{\mathcal{F}} \quad (2.26)$$

$$\text{Magnetic flux} = \varphi = \mathcal{F} \mu_0 \frac{A}{l} = \mathcal{F} \mu_0 \wp \quad (2.27)$$

$$\text{Magnetic induction} = B = \mu_0 \frac{\mathcal{F}}{l} = \mu_0 \frac{\wp}{A} \mathcal{F} = \mathcal{P} \mathcal{F} \quad (2.28)$$

$$\text{Inductance} = L = \frac{N\phi}{i} = N^2 \mu_0 \frac{A}{l} = N^2 \mu_0 \wp \quad (2.29)$$

From Equation 2.27 one can get to $\varphi = \mathcal{P} \mathcal{F}$, something analogous to $i = Yv$ in electric circuits, concluding that:

$$\boxed{\lambda = N \mathcal{P} \mathcal{F}} \quad (2.30)$$

2.1.4. Flux Linkage Equations

Figures 2.8 and 2.9 depict 6 coils mutually coupled, each one starting from S and ending in E . Those coils are from three phases $S_a - E_a$, $S_b - E_b$ and $S_c - E_c$; Coil from field winding $S_F - E_F$; and two coils from damper windings $S_D - E_D$ and $S_Q - E_Q$.

Adopting a matrix form to the flux linkage equations:

$$\begin{bmatrix} \lambda_a \\ \lambda_b \\ \lambda_c \\ - \\ \lambda_F \\ \lambda_D \\ \lambda_Q \end{bmatrix} = \begin{bmatrix} L_{aa} & L_{ab} & L_{ac} & | & L_{aF} & L_{aD} & L_{aQ} \\ L_{ba} & L_{bb} & L_{bc} & | & L_{bF} & L_{bD} & L_{bQ} \\ L_{ca} & L_{cb} & L_{cc} & | & L_{cF} & L_{cD} & L_{cQ} \\ - & - & - & \div & - & - & - \\ L_{Fa} & L_{Fb} & L_{Fc} & | & L_{FF} & L_{FD} & L_{FQ} \\ L_{Da} & L_{Db} & L_{Dc} & | & L_{DF} & L_{DD} & L_{DQ} \\ L_{Qa} & L_{Qb} & L_{Qc} & | & L_{QF} & L_{QD} & L_{QQ} \end{bmatrix} \begin{bmatrix} i_a \\ i_b \\ i_c \\ - \\ i_F \\ i_D \\ i_Q \end{bmatrix} \Rightarrow [\lambda] = [L][i] \quad (2.31)$$

Where:

$$L_{jk} = \begin{cases} \text{if } j = k \Rightarrow \text{self inductance} \\ \text{if } j \neq k \Rightarrow \text{mutual inductance} \end{cases}$$

And:

$$L_{jk} = L_{kj} \text{ in every case}$$

The matrix in Equation 2.31 is divided in four parts, upper left destined to stator fluxes and bottom right to rotor fluxes.

Next, inductances are calculated as a function of rotor position θ , and the following subscripts are used:

l	Leakage
m	Mutual
s	Self

a) Stator self-inductances

Figures 2.11 and 2.12 show two SM diagrams, respectively, with flux linkage and MMF, corresponding to phase A.

However:

$$\begin{cases} \mathcal{F}_{da} = \mathcal{F}_a \cos \theta = N_a i_a \cos \theta \\ \mathcal{F}_{qa} = \mathcal{F}_a \sin \theta = N_a i_a \sin \theta \end{cases} \quad (2.35)$$

$$\begin{cases} \lambda_{da} = N_a \mathcal{P}_d \mathcal{F}_{da} \\ \lambda_{qa} = N_a \mathcal{P}_q \mathcal{F}_{qa} \end{cases} \quad (2.36)$$

$$\begin{cases} \lambda_{da} = N_a \mathcal{P}_d (N_a i_a \cos \theta) = N_a^2 i_a \mathcal{P}_d \cos \theta \\ \lambda_{qa} = N_a \mathcal{P}_q (N_a i_a \sin \theta) = N_a^2 i_a \mathcal{P}_q \sin \theta \end{cases} \quad (2.37)$$

Equation 2.37 in Equation 2.34:

$$\lambda_m = (N_a^2 i_a \mathcal{P}_d \cos \theta) \cos \theta + (N_a^2 i_a \mathcal{P}_q \sin \theta) \sin \theta$$

$$\lambda_m = N_a^2 i_a (\mathcal{P}_d \cos^2 \theta + \mathcal{P}_q \sin^2 \theta) \quad (2.38)$$

Using the following identities:

$$\begin{cases} \cos^2 \theta = \frac{1}{2} + \frac{1}{2} \cos(2\theta) \\ \sin^2 \theta = \frac{1}{2} - \frac{1}{2} \cos(2\theta) \end{cases}$$

It comes:

$$\lambda_m = N_a^2 i_a \left[\frac{\mathcal{P}_d}{2} + \frac{\mathcal{P}_d}{2} \cos(2\theta) + \frac{\mathcal{P}_q}{2} - \frac{\mathcal{P}_q}{2} \cos(2\theta) \right]$$

$$\boxed{\lambda_m = N_a^2 i_a \left[\left(\frac{\mathcal{P}_d + \mathcal{P}_q}{2} \right) + \left(\frac{\mathcal{P}_d - \mathcal{P}_q}{2} \right) \cos(2\theta) \right]} \quad (2.39)$$

Analyzing Equation 2.33:

$$\lambda_l = N_a \mathcal{P}_l \mathcal{F}_a = N_a \mathcal{P}_l (N_a i_a)$$

$$\boxed{\lambda_l = N_a^2 i_a \mathcal{P}_l} \quad (2.40)$$

Equations 2.39 and 2.40 in Equation 2.32:

$$\lambda_a = N_a^2 i_a \mathcal{P}_l + N_a^2 i_a \left[\left(\frac{\mathcal{P}_d + \mathcal{P}_q}{2} \right) + \left(\frac{\mathcal{P}_d - \mathcal{P}_q}{2} \right) \cos(2\theta) \right] \quad (2.41)$$

And:

$$L_a = N_a^2 \mathcal{P}_a$$

$$\lambda_a = L_a i_a$$

$$L_a = \frac{\lambda_a}{i_a}$$

From Equation 2.41:

$$\lambda_a = \underbrace{N_a^2 \mathcal{P}_l}_{L_l} i_a + \underbrace{N_a^2 \left(\frac{\mathcal{P}_d + \mathcal{P}_q}{2} \right)}_{L_1} i_a + \underbrace{N_a^2 \left(\frac{\mathcal{P}_d - \mathcal{P}_q}{2} \right)}_{L_2} i_a \cos(2\theta) \quad (2.42)$$

Then, it is defined:

$$\begin{cases} L_l \triangleq N_a^2 \mathcal{P}_l \\ L_1 \triangleq N_a^2 \left(\frac{\mathcal{P}_d + \mathcal{P}_q}{2} \right) \\ L_2 \triangleq N_a^2 \left(\frac{\mathcal{P}_d - \mathcal{P}_q}{2} \right) \end{cases} \quad (2.43)$$

Equation 2.43 in 2.42:

$$\lambda_a = L_a i_a = L_l i_a + L_1 i_a + L_2 i_a \cos(2\theta) \quad (2.44)$$

$$L_a = L_{aa} = L_l + L_1 + L_2 \cos(2\theta)$$

$$L_s \triangleq L_l + L_1$$

$$L_m \triangleq L_2$$

L_s and L_m are constants and $L_s > L_m$, finally:

$$\boxed{L_{aa} = L_s + L_m \cos(2\theta)} \quad (2.45)$$

Similarly, the deduction can be done for both L_{bb} and L_{cc} , changing the angle σ for each phase correspondence, as can be seen in Figure 2.13.

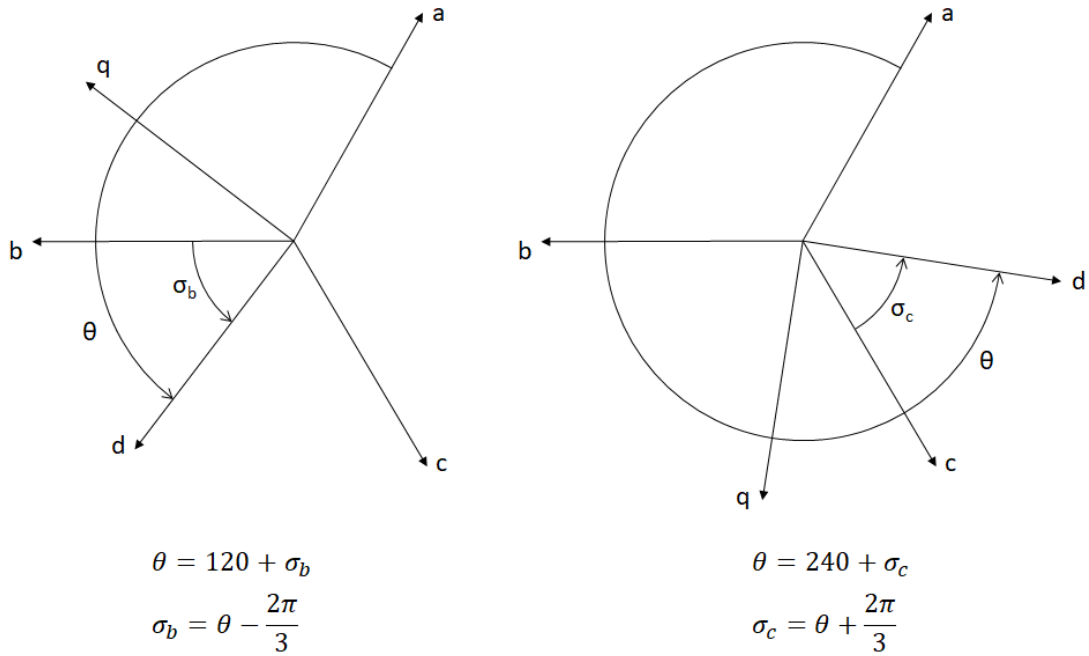


Figure 2.13 – Angles σ for phases B and C.

Lastly, the stator inductances are:

$$\begin{cases} L_{aa} = L_s + L_m \cos(2\theta) \\ L_{bb} = L_s + L_m \cos\left[2\left(\theta - \frac{2\pi}{3}\right)\right] [H] \\ L_{cc} = L_s + L_m \cos\left[2\left(\theta + \frac{2\pi}{3}\right)\right] \end{cases} \quad (2.46)$$

As can be seen in Figure 2.14, mutual flux is decomposed in λ_{da} and λ_{qa} , which are project on b axis, and then calculated how much flux from phase A is concatenated on B.

$$\lambda_{ab} = \vec{u} - \vec{v} \quad (2.49)$$

$$\vec{u} = \lambda_{da} \cos\left(\frac{2\pi}{3} - \theta\right)$$

$$\vec{u} = \lambda_{da} \cos\left(\theta - \frac{2\pi}{3}\right) \quad (2.50)$$

$$\vec{v} = \lambda_{qa} \cos\left(\theta - \frac{\pi}{6}\right) = -\lambda_{qa} \sin\left(\theta - \frac{\pi}{6} - \frac{\pi}{2}\right)$$

$$\vec{v} = -\lambda_{qa} \sin\left(\theta - \frac{2\pi}{3}\right) \quad (2.51)$$

Equations 2.50 and 2.51 in Equation 2.49:

$$\lambda_{ab} = \lambda_{da} \cos\left(\theta - \frac{2\pi}{3}\right) + \lambda_{qa} \sin\left(\theta - \frac{2\pi}{3}\right) \quad (2.52)$$

And Equation 2.37 in Equation 2.34:

$$\lambda_{ab} = (N_a^2 i_a \mathcal{P}_d \cos \theta) \cos\left(\theta - \frac{2\pi}{3}\right) + (N_a^2 i_a \mathcal{P}_q \sin \theta) \sin\left(\theta - \frac{2\pi}{3}\right) \quad (2.53)$$

Using the following identities:

$$\begin{cases} \cos \theta \cos\left(\theta \pm \frac{2\pi}{3}\right) = -\frac{1}{4} - \frac{1}{4} \cos(2\theta) \mp \frac{\sqrt{3}}{4} \sin(2\theta) \\ \sin \theta \sin\left(\theta \pm \frac{2\pi}{3}\right) = -\frac{1}{4} + \frac{1}{4} \cos(2\theta) \pm \frac{\sqrt{3}}{4} \sin(2\theta) \end{cases}$$

$$\lambda_{ab} = N_a^2 i_a \left[-\frac{\mathcal{P}_d}{4} - \frac{\mathcal{P}_d}{4} \cos(2\theta) + \frac{\sqrt{3}}{4} \mathcal{P}_d \sin(2\theta) - \frac{\mathcal{P}_q}{4} + \frac{\mathcal{P}_q}{4} \cos(2\theta) - \frac{\sqrt{3}}{4} \mathcal{P}_q \sin(2\theta) \right]$$

$$\lambda_{ab} = N_a^2 i_a \left[-\left(\frac{\mathcal{P}_d + \mathcal{P}_q}{4}\right) - \left(\frac{\mathcal{P}_d - \mathcal{P}_q}{4}\right) \cos(2\theta) + \frac{\sqrt{3}}{4} (\mathcal{P}_d - \mathcal{P}_q) \sin(2\theta) \right]$$

$$\lambda_{ab} = N_a^2 i_a \left\{ -\left(\frac{\mathcal{P}_d + \mathcal{P}_q}{4}\right) + (\mathcal{P}_d - \mathcal{P}_q) \left[-\frac{1}{4} \cos(2\theta) + \frac{\sqrt{3}}{4} \sin(2\theta) \right] \right\}$$

Also:

$$\cos\left(2\theta \pm \frac{2\pi}{3}\right) = -\frac{1}{2} \cos(2\theta) \mp \frac{\sqrt{3}}{2} \sin(2\theta)$$

$$\lambda_{ab} = N_a^2 i_a \left[-\left(\frac{\mathcal{P}_d + \mathcal{P}_q}{4}\right) + \left(\frac{\mathcal{P}_d - \mathcal{P}_q}{2}\right) \cos\left(2\theta - \frac{2\pi}{3}\right) \right]$$

$$\lambda_{ab} = L_{ab} i_a = -\underbrace{N_a^2 \left(\frac{\mathcal{P}_d + \mathcal{P}_q}{4}\right)}_{L_s} i_a + \underbrace{N_a^2 \left(\frac{\mathcal{P}_d - \mathcal{P}_q}{2}\right)}_{L_m} i_a \cos\left[2\left(\theta - \frac{\pi}{3}\right)\right] \quad (2.54)$$

And from Equation 2.43:

$$\begin{cases} \frac{L_1}{2} = N_a^2 \left(\frac{\mathcal{P}_d + \mathcal{P}_q}{4}\right) \\ L_2 = L_m = N_a^2 \left(\frac{\mathcal{P}_d - \mathcal{P}_q}{2}\right) \end{cases}$$

It is defined:

$$M_s \triangleq \frac{L_1}{2}$$

Again, M_s and L_m are constants and $|M_s| > L_m$, and finally:

$$\boxed{L_{ab} = L_{ba} = -M_s + L_m \cos\left[2\left(\theta - \frac{\pi}{3}\right)\right]} \quad (2.55)$$

For phases B and C, and A and C:

$$\begin{cases} L_{bc} = L_{cb} = -M_s + L_m \cos \left[2 \left(\sigma_b - \frac{\pi}{3} \right) \right] \\ L_{ca} = L_{ac} = -M_s + L_m \cos \left[2 \left(\sigma_c - \frac{\pi}{3} \right) \right] \end{cases}$$

And yet:

$$\begin{cases} L_{bc} = L_{cb} = -M_s + L_m \cos[2(\theta - \pi)] \\ L_{ca} = L_{ac} = -M_s + L_m \cos \left[2 \left(\theta + \frac{\pi}{3} \right) \right] \end{cases}$$

$$\begin{cases} L_{ab} = L_{ba} = -M_s + L_m \cos \left[2 \left(\theta - \frac{\pi}{3} \right) \right] \\ L_{bc} = L_{cb} = -M_s + L_m \cos(2\theta) \\ L_{ca} = L_{ac} = -M_s + L_m \cos \left[2 \left(\theta + \frac{\pi}{3} \right) \right] \end{cases} \quad (2.56)$$

$$\begin{cases} L_m \cos(2\theta + 2\pi) = L_m \cos(2\theta) = -L_m \cos(2\theta - \pi) \\ L_m \cos \left(2\theta - \frac{2\pi}{3} \right) = -L_m \cos \left(2\theta - \frac{2\pi}{3} + \pi \right) = -L_m \cos \left(2\theta + \frac{\pi}{3} \right) \\ L_m \cos \left(2\theta + \frac{2\pi}{3} \right) = -L_m \cos \left(2\theta + \frac{2\pi}{3} + \pi \right) = -L_m \cos \left(2\theta + \frac{5\pi}{3} \right) \end{cases}$$

And finally:

$$\begin{cases} L_{ab} = L_{ba} = -M_s - L_m \cos \left[2 \left(\theta + \frac{\pi}{6} \right) \right] \\ L_{bc} = L_{cb} = -M_s - L_m \cos \left[2 \left(\theta - \frac{3\pi}{6} \right) \right] \\ L_{ca} = L_{ac} = -M_s - L_m \cos \left[2 \left(\theta + \frac{5\pi}{6} \right) \right] \end{cases} \quad [H] \quad (2.57)$$

c) Rotor self-inductances

Neglecting saturation and slots effects, self-inductances in the rotor are constants, and using subscript notations:

$$\begin{cases} L_{FF} = L_F \\ L_{DD} = L_D [H] \\ L_{QQ} = L_Q \end{cases} \quad (2.58)$$

d) Rotor mutual inductances

Mutual inductance between field and direct axis damper winding is constant, and there are no mutual inductances among direct and quadrature axes, due to the fact of being 90° apart, so:

$$\begin{cases} L_{FD} = L_{DF} = M_R \\ L_{FQ} = L_{QF} = 0 \\ L_{DQ} = L_{QD} = 0 \end{cases} [H] \quad (2.59)$$

e) Mutual inductances between stator and rotor

They can be expressed directly by inspecting Figures 2.8 and 2.9.

$$\begin{cases} L_{aF} = L_{Fa} = M_F \cos \theta \\ L_{bF} = L_{Fb} = M_F \cos \left(\theta - \frac{2\pi}{3} \right) [H] \\ L_{cF} = L_{Fc} = M_F \cos \left(\theta + \frac{2\pi}{3} \right) \end{cases} \quad (2.60)$$

And M_F is the mutual-inductance maximum value between field winding and a phase winding.

Similarly, M_D for direct axis damper winding and M_Q for quadrature axis damper winding.

$$\begin{cases} L_{aD} = L_{Da} = M_D \cos \theta \\ L_{bD} = L_{Db} = M_D \cos \left(\theta - \frac{2\pi}{3} \right) [H] \\ L_{cD} = L_{Dc} = M_D \cos \left(\theta + \frac{2\pi}{3} \right) \end{cases} \quad (2.61)$$

$$\begin{cases} L_{aQ} = L_{Qa} = M_Q \sin \theta \\ L_{bQ} = L_{Qb} = M_Q \sin \left(\theta - \frac{2\pi}{3} \right) [H] \\ L_{cQ} = L_{Qc} = M_Q \sin \left(\theta + \frac{2\pi}{3} \right) \end{cases} \quad (2.62)$$

f) Inductances Transformation

At once, that all admittance matrix (Equation 2.31) terms are known, the next step is relating all terms to a fixed rotor reference. Using Park Transformation simplifies Equation 2.31.

Still, from Equations 2.4 and 2.5:

$$\dot{\lambda} = L\dot{i} + \dot{L}i \quad (2.63)$$

Treating λ as a vector:

$$[\lambda_{abc}] = [L][i_{abc}] \quad (2.64)$$

Applying Park Transformation:

$$\begin{cases} \lambda_{odq} = \mathbb{P}\lambda_{abc} \Rightarrow \lambda_{abc} = \mathbb{P}^{-1}\lambda_{odq} \\ i_{odq} = \mathbb{P}i_{abc} \Rightarrow i_{abc} = \mathbb{P}^{-1}i_{odq} \end{cases} \quad (2.65)$$

$$\mathbb{P}^{-1}\lambda_{odq} = L\mathbb{P}^{-1}i_{odq}$$

Pre-multiplying both sides by \mathbb{P} :

$$\mathbb{P}\mathbb{P}^{-1}\lambda_{odq} = \mathbb{P}L\mathbb{P}^{-1}i_{odq}$$

$$\begin{cases} \lambda_{odq} = \mathbb{P}L\mathbb{P}^{-1}i_{odq} \\ \mathbb{P}\lambda_{abc} = \mathbb{P}L\mathbb{P}^{-1}\mathbb{P}i_{abc} \end{cases} \quad (2.66)$$

Writing Equation 2.66 in a more general fashion:

$$\begin{bmatrix} \mathbb{P} & 0 \\ 0 & U_3 \end{bmatrix} \begin{bmatrix} \lambda_{abc} \\ \lambda_{FDQ} \end{bmatrix} = \begin{bmatrix} \mathbb{P} & 0 \\ 0 & U_3 \end{bmatrix} \begin{bmatrix} L_{SS} & L_{SR} \\ L_{RS} & L_{RR} \end{bmatrix} \begin{bmatrix} \mathbb{P}^{-1} & 0 \\ 0 & U_3 \end{bmatrix} \begin{bmatrix} \mathbb{P} & 0 \\ 0 & U_3 \end{bmatrix} \begin{bmatrix} i_{abc} \\ i_{FDQ} \end{bmatrix} \quad (2.67)$$

Another way to reach Equation 2.67 is by pre-multiplying Equation 2.31 by $\begin{bmatrix} \mathbb{P} & 0 \\ 0 & U_3 \end{bmatrix}$, Annex

A presents this demonstration.

Equation 2.67 results in the following matrix:

$$\begin{bmatrix} \lambda_o \\ \lambda_d \\ \lambda_q \\ \lambda_F \\ \lambda_D \\ \lambda_Q \end{bmatrix} = \begin{bmatrix} L_o & 0 & 0 & | & 0 & 0 & 0 \\ 0 & L_d & 0 & | & KM_F & KM_D & 0 \\ 0 & 0 & L_q & | & 0 & 0 & KM_Q \\ \hline 0 & KM_F & 0 & | & L_F & M_R & 0 \\ 0 & KM_D & 0 & | & M_R & L_D & 0 \\ 0 & 0 & KM_Q & | & 0 & 0 & L_Q \end{bmatrix} \begin{bmatrix} i_a \\ i_b \\ i_c \\ i_F \\ i_D \\ i_Q \end{bmatrix} \quad (2.68)$$

And the following constants are defined:

$$\begin{cases} L_d \triangleq L_s + M_s + \frac{3}{2}L_m [H] \\ L_q \triangleq L_s + M_s - \frac{3}{2}L_m [H] \\ L_o \triangleq L_s - 2M_s [H] \\ K = \sqrt{3/2} \end{cases} \quad (2.69)$$

A great advantage brought by Park is to use constant values of inductances in calculations since the axes now “move” alongside the rotor.

This transformation, with Lewis modifications, presents invariance in power and results in a symmetric matrix.

In order to use any of these equations to represent a real machine, the magnetic inputs must be reliable, and for so, in this work, it is used Finite Element Analysis to get to some of these parameters. The next chapter goes through FEM and how it is applied in this work.

2.2. Finite Element Method

On previous chapters were presented elements from SM and how to model it mathematically. To obtain a representative model, all parameters that matter must be reliable. Therefore, to obtain some of these parameters, this work makes use of the Finite Element Method (FEM).

The FEM is one of the most widely applied methods in engineering for solving problems in structural analysis, fluid flow, heat transfer, electrostatic, magnetism, and others. It is complicated to give one person the title of FEM inventor. Although some authors like in [19] and [20] have been the pioneers employing similar methods. To discretize a problem in a mesh, i.e., transforming a difficult, maybe unsolvable, domain into lesser difficult elements, as seen in Figure 2.15.

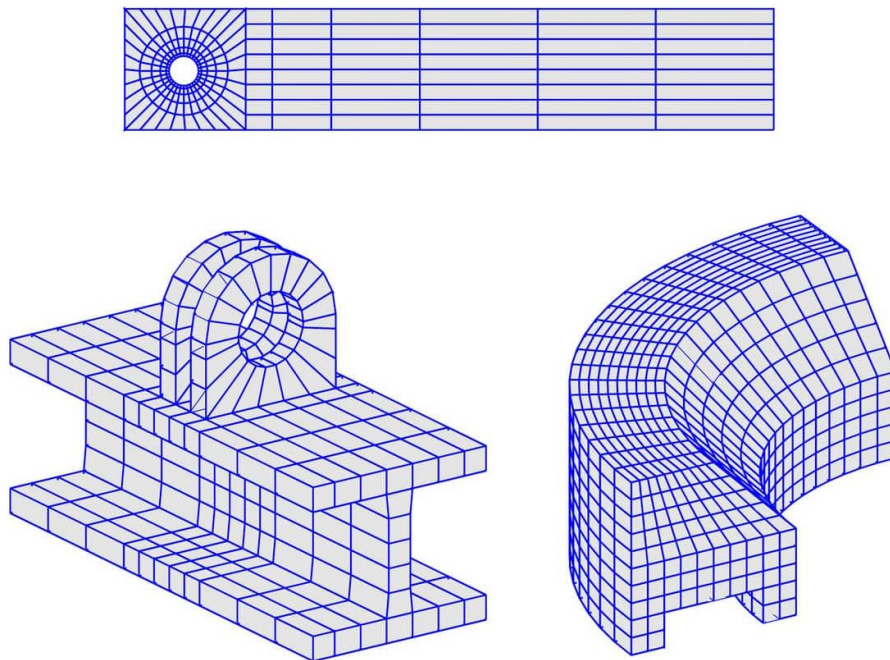


Figure 2.15 – Example of mesh grids, created by FEATool MATLAB.

Source: [21]

Some of FEM features elects it as an appropriate tool to solve magnetic problems [22]. As for this work, the problem is to basically solve Maxwell's equations in complex shapes as salient poles, which FEM solves by "breaking" it in sub-shapes where solving differential equations are simpler.

This work uses a freeware software, FEMM, that simulates a magnetic problem and generates illustrative representations of flux lines and flux densities, as in Figure 2.16.

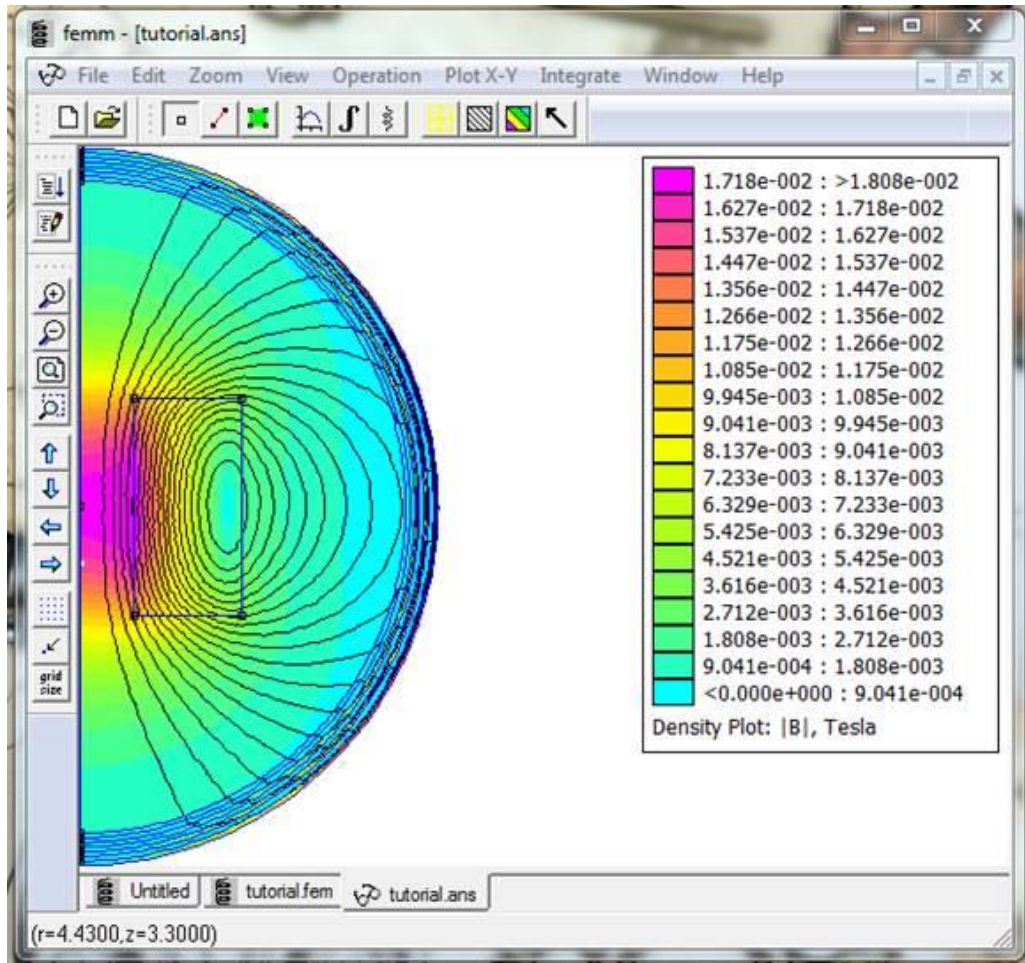


Figure 2.16 - Color flux density plot of an example solution in FEMM website.

Source: [23]

2.2.1. Software - Finite Element Method Magnetics

FEMM is a suite of programs for solving low-frequency electromagnetic problems on two-dimensional planar and axisymmetric domains. The program currently addresses linear/nonlinear magnetostatic problems, linear/nonlinear time harmonic magnetic problems, linear electrostatic problems, and steady-state heat flow problems [23].

For poles shoes and axial extremities, the targets for this dissertation simulations, planar modeling is enough (due to rotor symmetries). It is necessary to define properties in the air-gap and some boundaries, depending on the shape studied. The outputs of interest are magnetic flux densities on air-gap line.

For magnetic problems to properties are the most important: boundaries and materials. Screens to set both are shown, respectively, in Figures 2.17 and 2.18.

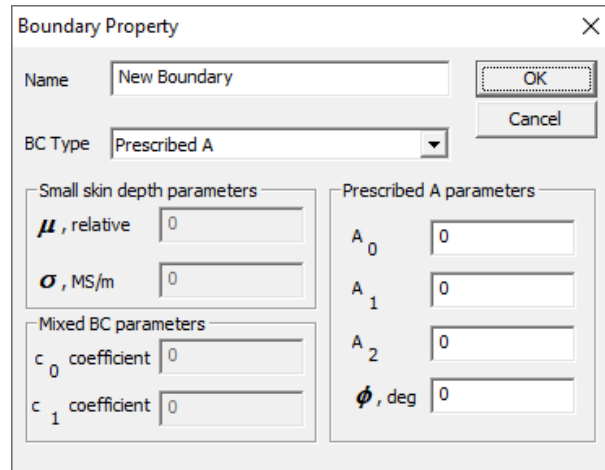


Figure 2.17 - Boundary Property window.

What FEM does in boundary regions, in magnetic problems, is to solve the following equations for the magnetic vector potential when set, respectively, as “Prescribed A” and “Mixed”:

$$\nabla^2 A = 0 \quad (2.67)$$

$$\frac{1}{\mu_0 \mu_r} \frac{\partial A}{\partial n} + c_0 A + c_1 = 0 \quad (2.68)$$

An approach using only air-gap boundaries is much more straightforward than a complete 2D analysis. However, this choice makes it impossible to model any winding, making necessary the normalization of results.

In order to generate a magnetic field, three boundary properties are set:

- $A = 0$ (Dirichlet) For rotor core outer perimeter
- $A = 1$ (Dirichlet) On air-gap
- $\frac{\partial A}{\partial n} = 0$ (Neumann) On iron parts, and over the quadrature imaginary-line (forcing magnetic flux to be perpendicular)

In Figure 2.17, Dirichlet is set by choosing BC type as “Prescribed A” and A_0 as 0 or to 1.

Neumann is set by choosing BC type as “Mixed,” and c_0 and c_1 coefficients as 0.

This work represents only boundaries of metallic parts, then the only material left to be set is air, which is done by using a pre-set “Air” property from FEMM library, as can be seen in Figure 2.18.

The image shows a 'Block Property' dialog box with the following fields and sections:

- Name:** Air
- B-H Curve:** Linear B-H Relationship
- Linear Material Properties:**
 - Relative μ_x : 1
 - Relative μ_y : 1
 - ϕ_{hx} , deg: 0
 - ϕ_{hy} , deg: 0
- Nonlinear Material Properties:**
 - Edit B-H Curve (button)
 - ϕ_{hmax} , deg: 0
- Coercivity:** H_c , A/m: 0
- Electrical Conductivity:** σ , MS/m: 0
- Source Current Density:** J , MA/m²: 0
- Special Attributes: Lamination & Wire Type:**
 - Not laminated or stranded (dropdown)
 - Lam thickness, mm: 0
 - Lam fill factor: 1
 - Number of strands: 0
 - Strand dia, mm: 0
- Buttons:** OK, Cancel

Figure 2.18 - FEMM Air property.

In this work, FEA is used together with MATLAB with commands available in FEMM 4.2 that possibilities its integration with octave.

Finally, the next chapter presents the assimilation of SM theory and procedures and FEM to achieve this work goal, which is to obtain essential magnetic parameters from SM design and rated data.

3. METHODOLOGY

In this chapter, it is presented the four tools that are the fruit of this work. They use the theory exposed so far in this dissertation, together with methods that are described in each tool respective chapter. The four tools are Winding Matrix using Tingley Box, MMF calculation for any given Winding Matrix, Pole shoe magnetic simulation, and Effective magnetic length (package).

In this work, the tools are focused on output parameters that serve as magnetic inputs (listed in section 2.1.2) to get the reactance matrix for any given synchronous machine.

3.1. TINGLEY BOX AND WINDING MATRIX

The first tool is aimed to sort windings in slots using a standard and traditional step by step procedure, Tingley Box.

Tingley's work [24] discusses the distribution of windings for three and two-phase machines, elaborating a procedure not found in no other reference. Tingley's proposal is simple but useful. It is a step-by-step process to set windings in a standard pattern, building a diagram called "Least-Common-Multiple-Diagram," applying which has been used by many authors in a more illustrative method, using tables. Currently, there is a reasonable number of works exploiting techniques to distribute fractional q slots, as [25], [26] and [27], the choice for Tingley Box is due to its simplicity and tradition.

Firstly, some concepts must be redeemed from previous chapters.

Let it be, from Equation 2.2:

$$Q_p = 2mq = \frac{N_s}{p} = \frac{D_p}{C_p} \quad (3.1)$$

Then C_p pair of poles contains in D_p slots. These variables allow to define the number of virtual machines:

$$N_{vm} = \frac{N_s}{D_p} = \frac{p}{C_p} \quad (3.2)$$

MMFs first harmonic stays over D_p slots and covers C_p pairs of poles, repeating it N_{vm} times.

And defining an MMF fundamental period τ_f (equivalent to two-pole pitches τ_p) for a referential air-gap average radius R_δ .

$$\tau_f = 2\tau_p = 2 \frac{2\pi R_\delta}{2p} = \frac{2\pi R_\delta}{p} \quad (3.3)$$

With these concepts, it is possible to get to a SM Winding Matrix following procedures described hereafter.

3.1.1. Building an induced voltage phasorial rosette (slot star)

As introduced in [12], a slot star can be drawn by following these steps:

- Working with Equations 3.1 and 3.2 as a function of chosen p and N_s ;
- Draw two concentric circles;
- If C_p is odd, divide the circles into 6 sections;
- If C_p is even, divide the circles into 3 sections;
- Identify each section following the desired phase sequence:

Positive sequence	$A - C$	$B - A$	$C - B$
Negative sequence	$A - B$	$C - A$	$B - C$
- Divide the inner circle in D_p equal parts;
- Each radius represents a coil voltage induced phasor associated with the slot in question. The center of the circle corresponds to potential zero; the outer vertex of the radius represents the high-potential side;
- The maximum negative or positive potential condition is defined by the phase identification being positive or negative, depending on the sector occupied;
- Enumerate the zero-angle radius (right-hand horizontal radius) as corresponding to slot 1, count C_p times, then slot 2, and so on following a spiral sequence to enumerate all radiuses;
- The radiuses contained within each segment belong to the phasors of the corresponding phase. So, choose 3 colors, one for each phase, and identify the phasors corresponding to each phase;
- The identified sequence of phasors will correspond to the winding unit required to describe one virtual machine;

- If the denominator C_p is an even number, then this unit corresponds to a winding group able to be connected in series and/or parallel circuits;
- If the denominator C_p is odd, then the file sequence with D_p elements that describe one virtual machine may be split into 2 winding-groups. Both subgroups have the same amplitude but with opposite phase angles. After caring upon the phasor directions, there is the possibility to double the parallel circuits when needed. Or just, each winding-subgroup may be arranged in series and/or parallel circuits.

Examples are illustrated in Figure 3.1.

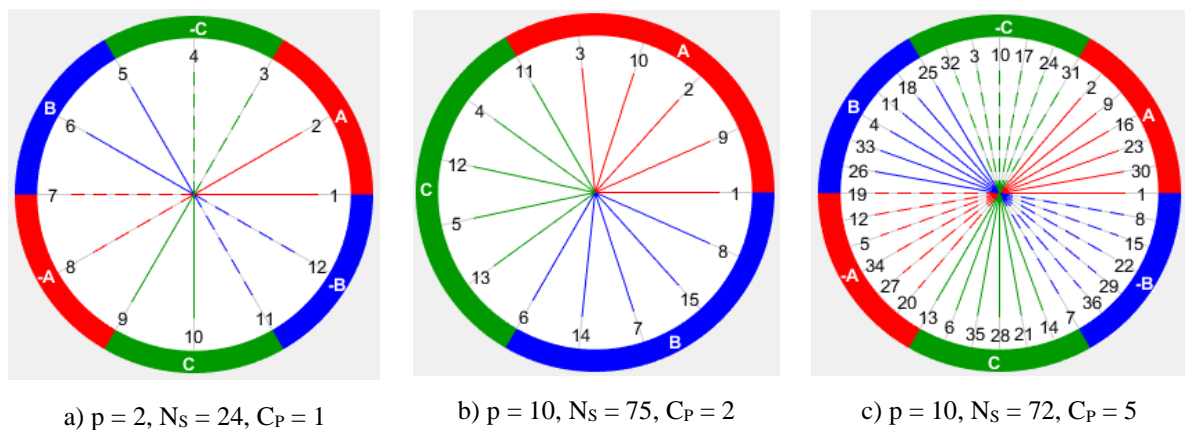


Figure 3.1- Phasorial rosettes for different examples.

3.1.2. Obtaining a regular three-phase winding scheme

Applying a slot star in a “graph paper” can be obtained by following these steps:

- Enumerate D_p columns;
- If C_p is even, divide the columns into 3 vertical sections and identify the phase-sequence (A B C) or (A C B);
- If C_p is odd, divide de columns into 6 vertical sections and determine the phase sequence (A -C B -A C -B) or (A -B C -A B -C);
- Begin the slots occupation, starting in 1, count until C_p and mark 2, count until C_p and mark 3, so on until getting to D_p ;
- This operation occupies C_p rows;
- Relate each phase number in the bottom row and Sort them.

These sets represent each phase winding scheme. For example, schemes in Figures 3.2 to 3.4 correspond to rosettes in Figure 3.1.

A		-C		B		-A		C		-B	
1	2	3	4	5	6	7	8	9	10	11	12
1	2	3	4	5	6	7	8	9	10	11	12
1	2	3	4	5	6	7	8	9	10	11	12

Figure 3.2 - Winding scheme corresponding to Rosette 3.1a.

A					C					B				
1	2	3	4	5	6	7	8	9	10	11	12	13	14	15
1		2		3		4		5		6		7		8
	9		10		11		12		13		14		15	
1	9	2	10	3	11	4	12	5	13	6	14	7	15	8

Figure 3.3 - Winding scheme corresponding to Rosette 3.1b.

A						-C						B						-A						C						-B					
1	2	3	4	5	6	7	8	9	10	11	12	13	14	15	16	17	18	19	20	21	22	23	24	25	26	27	28	29	30	31	32	33	34	35	36
1				2					3					4					5					6					7					8	
			9					10						11					12					13					14					15	
			16					17						18					19					20					21					22	
			23					24						25					26					27					28					29	
			30					31						32					33					34					35					36	
1	30	23	16	9	2	31	24	17	10	3	32	25	18	11	4	33	26	19	12	5	34	27	20	13	6	35	28	21	14	7	36	29	22	15	8

Figure 3.4 - Winding scheme corresponding to Rosette 3.1c.

3.1.3. Obtaining the Winding Matrix

Dealing with windings in the form of a matrix brings a great advantage when applying it to calculate the MMF using Fourier Series. The next procedure explicit how to get from a winding scheme to the winding matrix.

- Sort phases letters in each slot;
- Define a coil pitch y (number of slots between two legs of a coil).

Equation 3.4 presents a value that mitigates 5th harmonic and its multiples;

$$y \triangleq \text{round} \left(\frac{5 N_s}{6 2p} \right) \quad (3.4)$$

- Take a winding scheme and insert a row below it with the same number of slots (representing the slot second layer);

- Repeat the scheme in this new row, shifting it to the right by y slots.

The two resultant rows, with slots as columns, constitute the **Winding Matrix**. Figures 3.5 to 3.7 show Winding Matrix corresponding to rosettes in Figure 3.1.

1	2	3	4	5	6	7	8	9	10	11	12
a	a	-c	-c	b	b	-a	-a	c	c	-b	-b
a	-c	-c	b	b	-a	-a	c	c	-b	-b	a

Figure 3.5 - Winding Matrix corresponding to Figure 3.1a ($y = 5$).

1	2	3	4	5	6	7	8	9	10	11	12	13	14	15
a	a	a	-c	-c	b	b	b	-a	-a	c	c	c	-b	-b
-c	b	b	-a	-a	-a	c	c	-b	-b	-b	a	a	-c	-c

Figure 3.6 - Winding Matrix corresponding to Figure 3.1b ($y = 3$).

1	2	3	4	5	6	7	8	9	10	11	12	13	14	15	16	17	18	19	20	21	22	23	24	25	26	27	28	29	30	31	32	33	34	35	36
a	a	-c	b	-a	c	-b	-b	a	-c	b	-a	c	c	-b	a	-c	b	-a	-a	c	-b	a	-c	b	b	-a	c	-b	a	-c	-c	b	-a	c	-b
a	-c	b	-a	-a	c	-b	a	-c	b	b	-a	c	-b	a	-c	-c	b	-a	c	-b	a	a	-c	b	-a	c	-b	-b	a	-c	b	-a	c	c	-b

Figure 3.7 - Winding Matrix corresponding to Figure 3.1c ($y = 3$).

With the Winding Matrix in hand, it is possible to check the number of windings for each phase. For example, in Figure 3.5, one can separate the matrix in three, taking only slots that contain that phase and adding layers with the same phase, making the three matrices in Figure 3.8.

1	2	6	7	8	12
2	1	-1	-2	-1	1

A

4	5	6	10	11	12
1	2	1	-1	-2	-1

B

2	3	4	8	9	10
-1	-2	-1	1	2	1

C

Figure 3.8 - Winding Matrix for each phase.

These Winding Matrices are required to the next chapter, which plots Magnetomotive Force using them as input.

3.2. MAGNETOMOTIVE FORCE

The second tool uses the Winding Matrix, which is resulted from Tingley Box, to plot the Magnetomotive force in the air-gap of any machine.

Also known as Ohm's law for magnetic circuits, the relationship cited in Equation 2.27, sets MMF as a force analogous to the voltage, in electrics. It is a quantity that forces magnetic flux through a mean and a product of magnetic flux passage.

This work calculates the MMF caused by armature reacting to the excitation field. Which makes current flow through armature winding that, considering its number of turns, respects Equation 2.25.

There is a singularity in a SM case that, besides the current varying with time and space, the number of turns varies with space (along the stator perimeter). For this matter, Fourier series are used, so it is easier to manipulate each spatial point, summing or subtracting effects of each wire in a slot. For that, a method to calculate the MMF of a single turn is exposed.

3.2.1. MMF – Single Turn

[28] depicts a method to calculate MMF for a single wire and further, in the same work, for a turn as sum of two wires with opposite direction currents. Making use of Fourier series for MMF calculation, endorsed with FEM simulations.

Equation 3.5 reveals the MMF for a winding with N turns (considering phase shifting of γ radians for a correct slot placement) [25]. Figure 3.9 illustrates three MMF waveforms of a single turn ($N = 1$): "Proposed" represents an ideal square waveform; "Analytical" represents the use of the Fourier Series, and "FEM" is a plot obtained by simulation using FEM.

$$\mathcal{F}(x) = 2Ni \sum_k b_k \sin\left(k \frac{\pi}{\tau_f} \gamma\right) \cos\left(2k \frac{\pi}{\tau_f} x - k \frac{\pi}{\tau_f} \gamma\right) \quad (3.5)$$

With

$$b_k = \left(\frac{\tau_f}{k\pi}\right)^2 \frac{2}{s(\tau_f - s)} \sin\left(k \frac{\pi}{\tau_f} s\right) \quad (3.6)$$

Considering τ_f defined in Equation 3.3 and s the slot width.

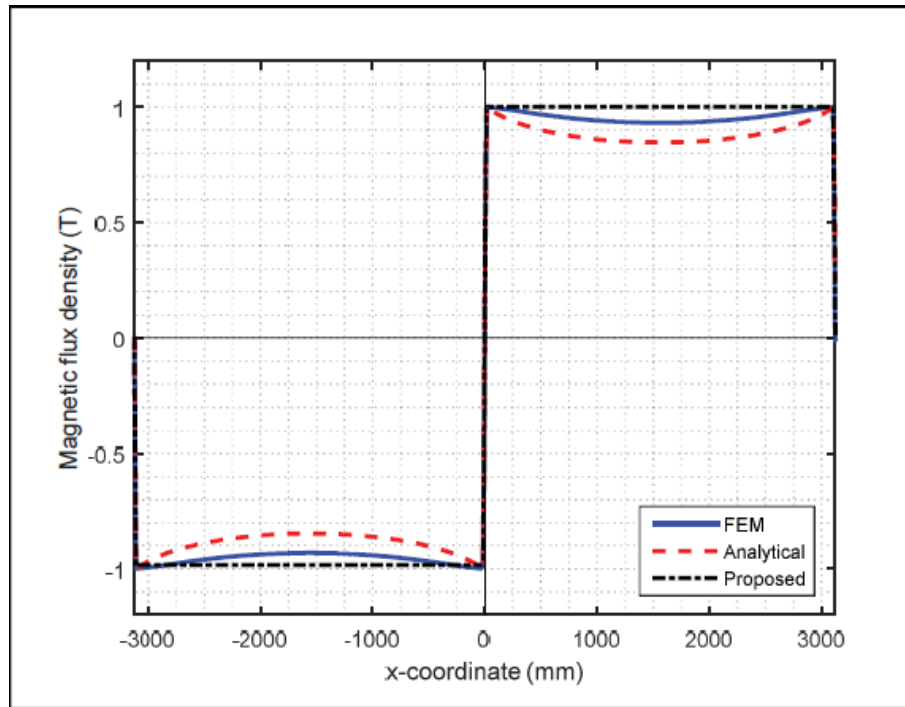


Figure 3.9- MMF of a single turn.

Source: [28]

3.2.2. MMF – Resultant and Fundamental Waveforms

A resultant MMF, i.e., considering all windings and slots, is obtained by using Equation 3.5 and considering the Winding Matrix in the place of N and a pulsating current in the place of i . In a first approach, the current is kept as a variable, and MMF for each phase is calculated using Equation 3.5 and phases Winding Matrix (Figure 3.8). Waveforms for phase A are presented in Figures 3.10 to 3.12, respectively, for examples in Figures 3.1a, 3.1b, and 3.1c. The dashed line marks the end of a virtual machine, from where the waveform repeats itself, marking the ending of a MMF period.

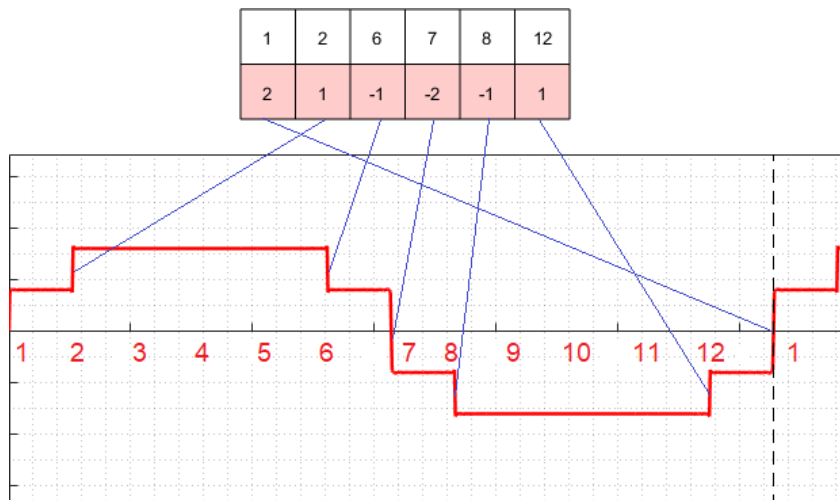


Figure 3.10 - 24 slots, 2 pair of poles, phase A MMF for a constant current.

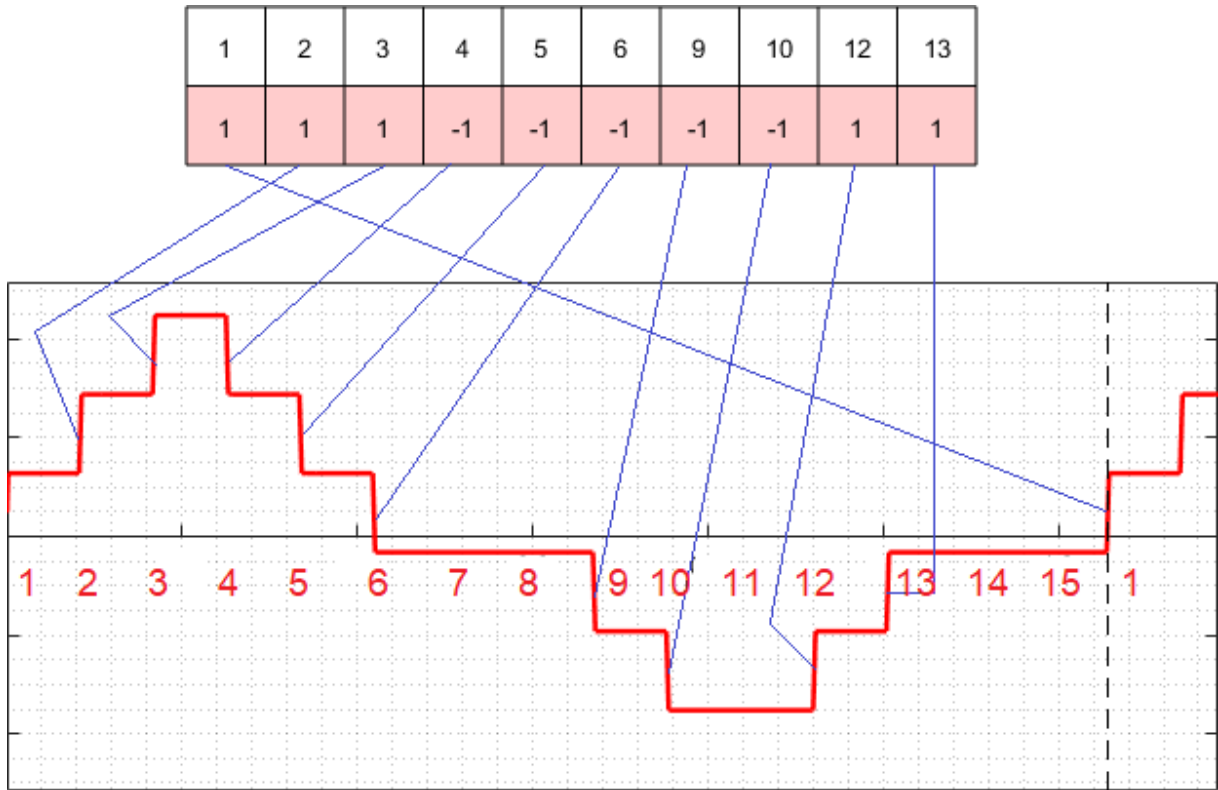


Figure 3.11 - 75 slots, 10 pair of poles, phase A MMF for a constant current.

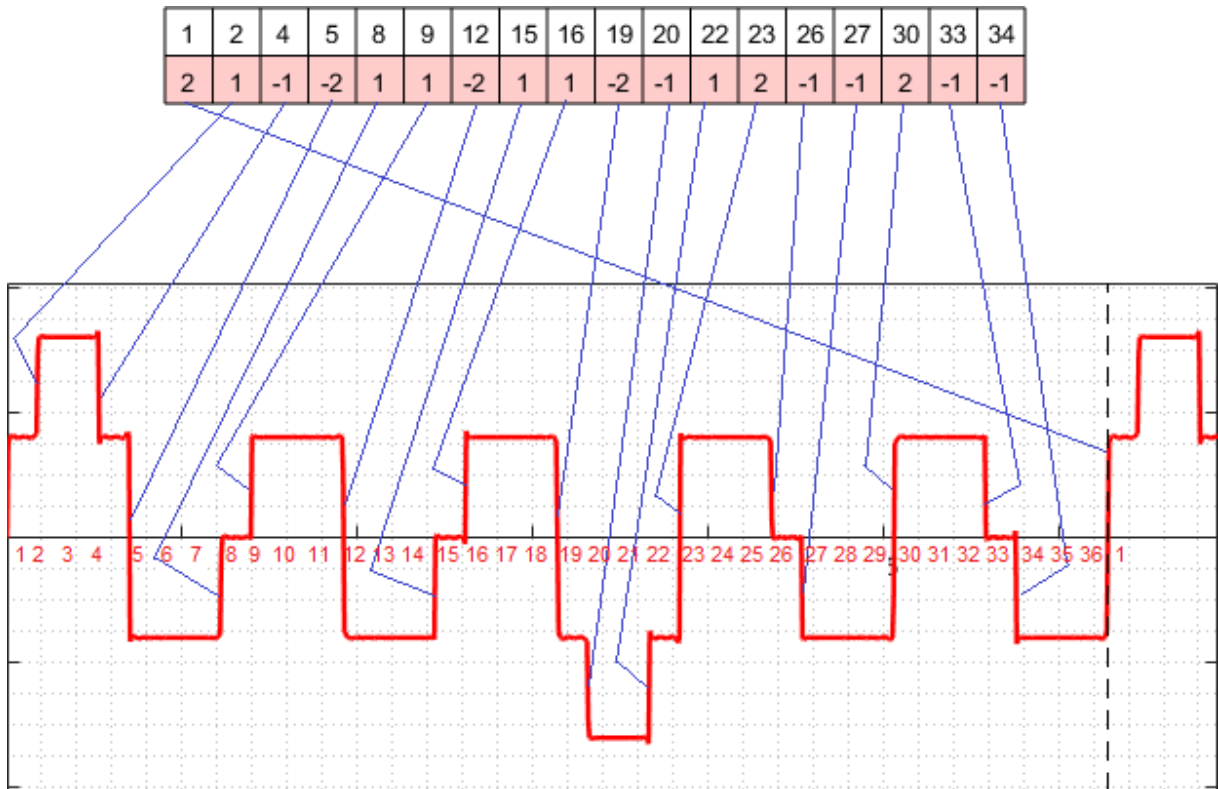


Figure 3.12 - 72 slots, 10 pairs of poles, phase A MMF for a constant current.

Considering the current as a pulsating wave in Equation 3.5 and summing the MMFs from the three phases results in waveforms in Figures 3.13 to 3.15, that are presented at instant $t = 0$ (red line – phase A; blue line – phase B; green line – phase C; and black line – resultant).

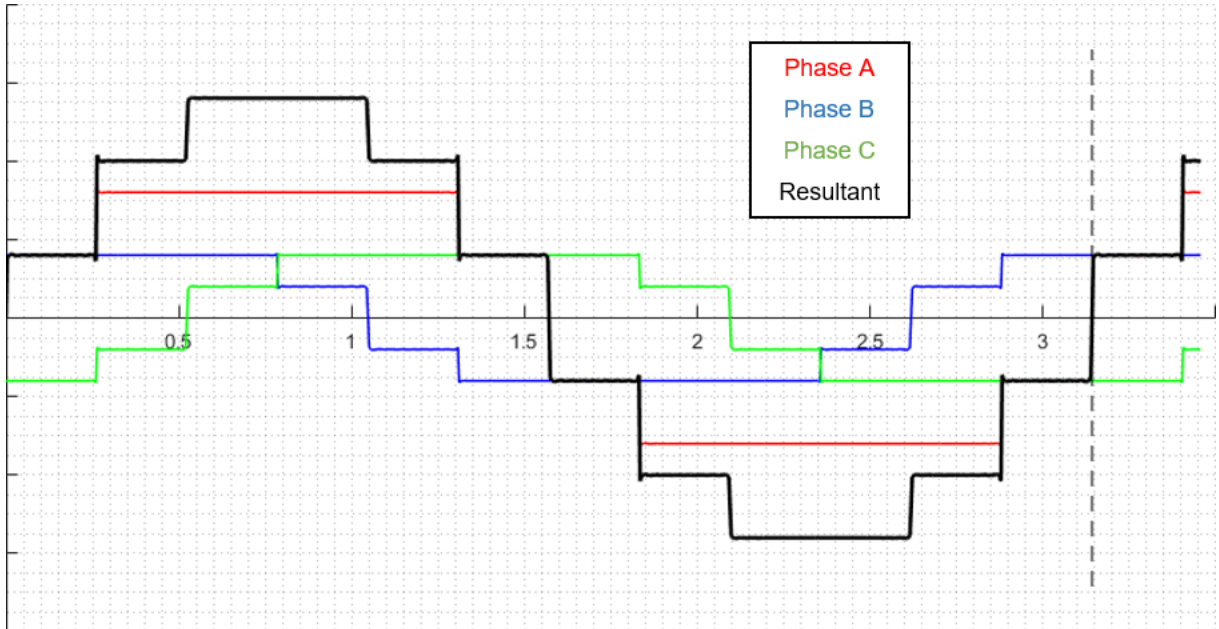


Figure 3.13 - 24 slots, 2 pairs of poles, resulting MMF at $t = 0$.

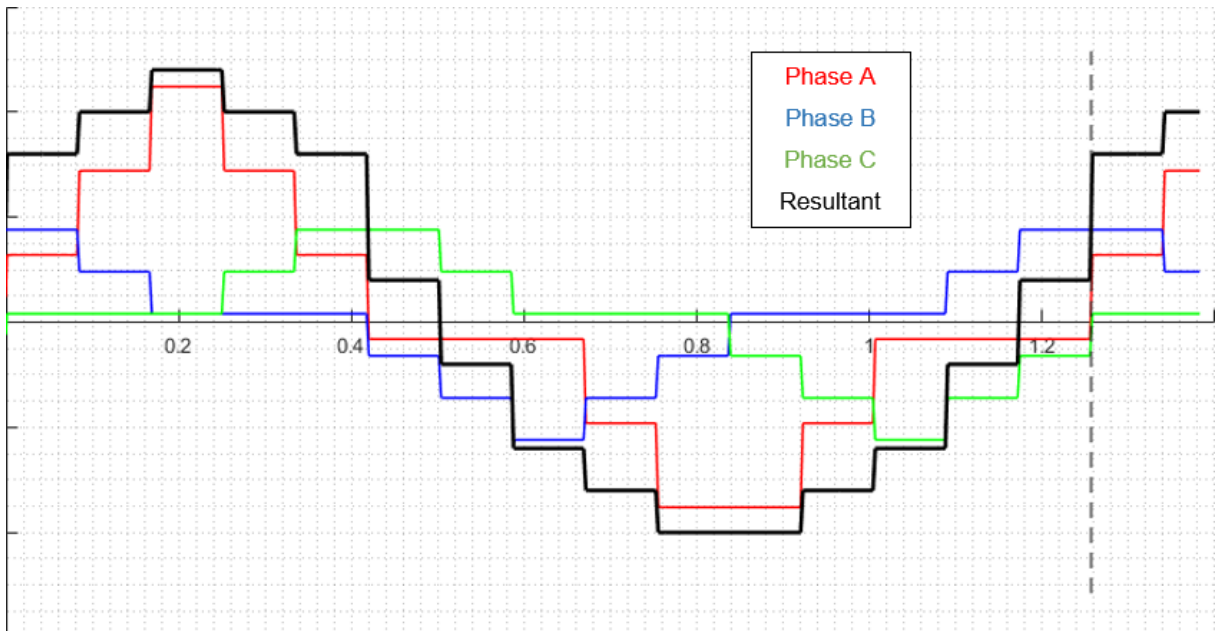


Figure 3.14 - 75 slots, 10 pairs of poles, resulting MMF at $t = 0$.

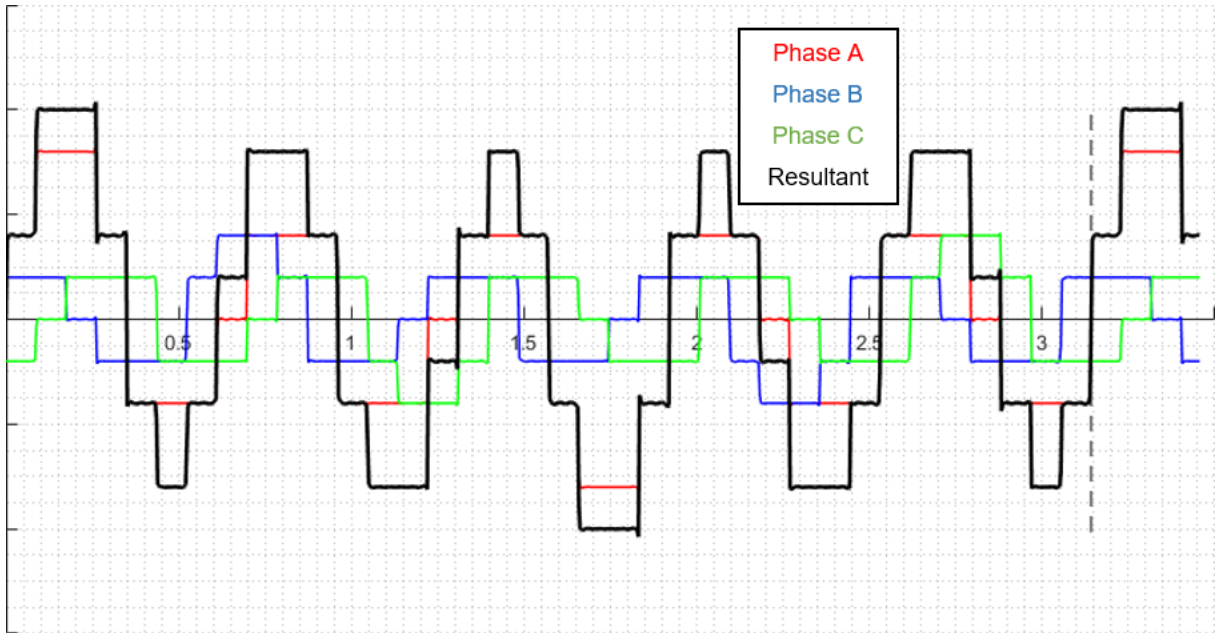


Figure 3.15 - 72 slots, 10 pairs of poles, resulting MMF at $t = 0$.

When introducing time, the current wave pulsates, and the sum of three pulsating waves delayed 120° produces a traveling wave, the resultant MMF for the SG.

What remains is to calculate the fundamental wave from the resultant MMF. From this fundamental, it is obtained the MMF magnitude. Figures 3.16 to 3.18 present resultant MMFs along with their fundamentals.

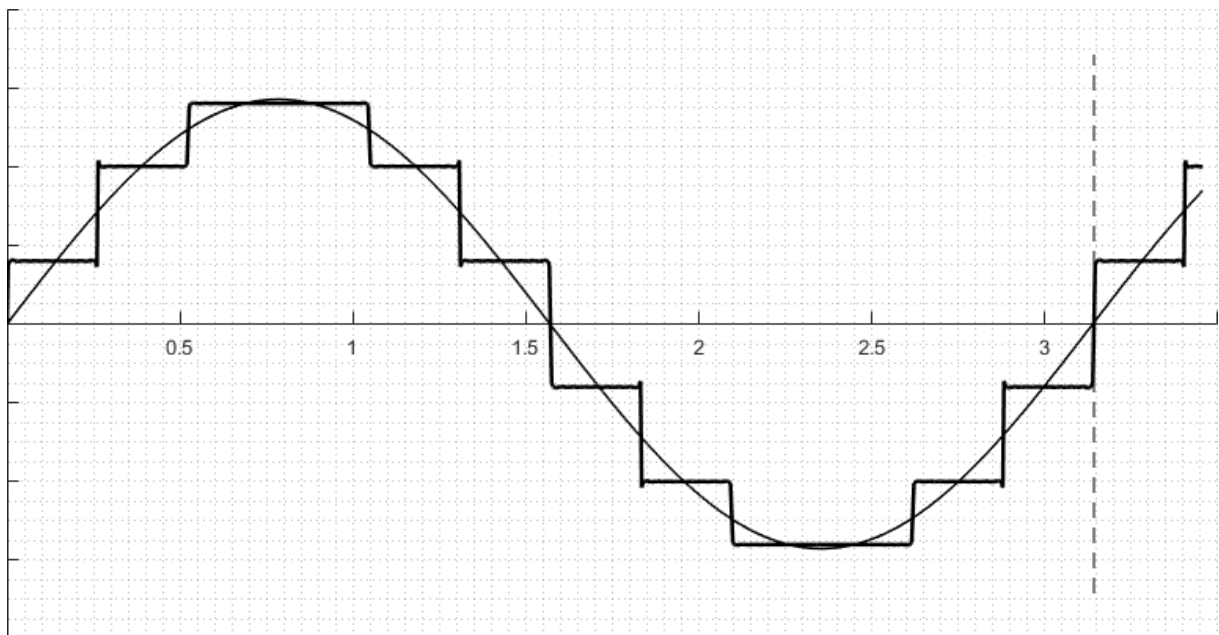


Figure 3.16 - 24 slots, 2 pairs of poles, resultant MMF and fundamental at $t = 0$.

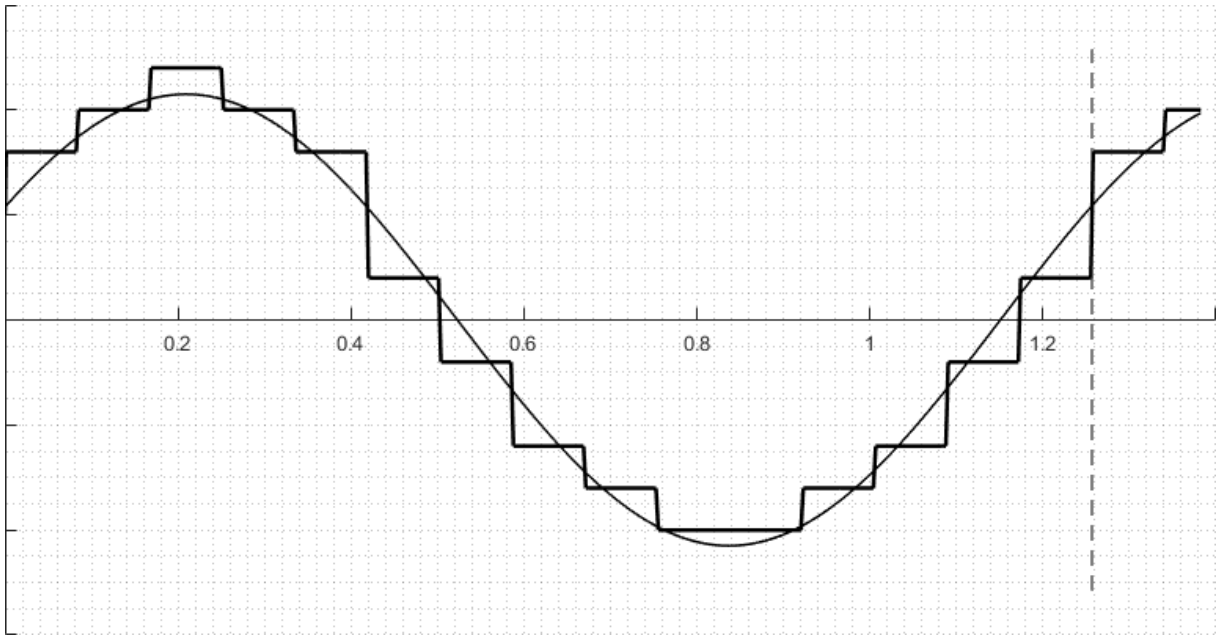


Figure 3.17 - 75 slots, 10 pairs of poles, resultant MMF and fundamental at $t = 0$.

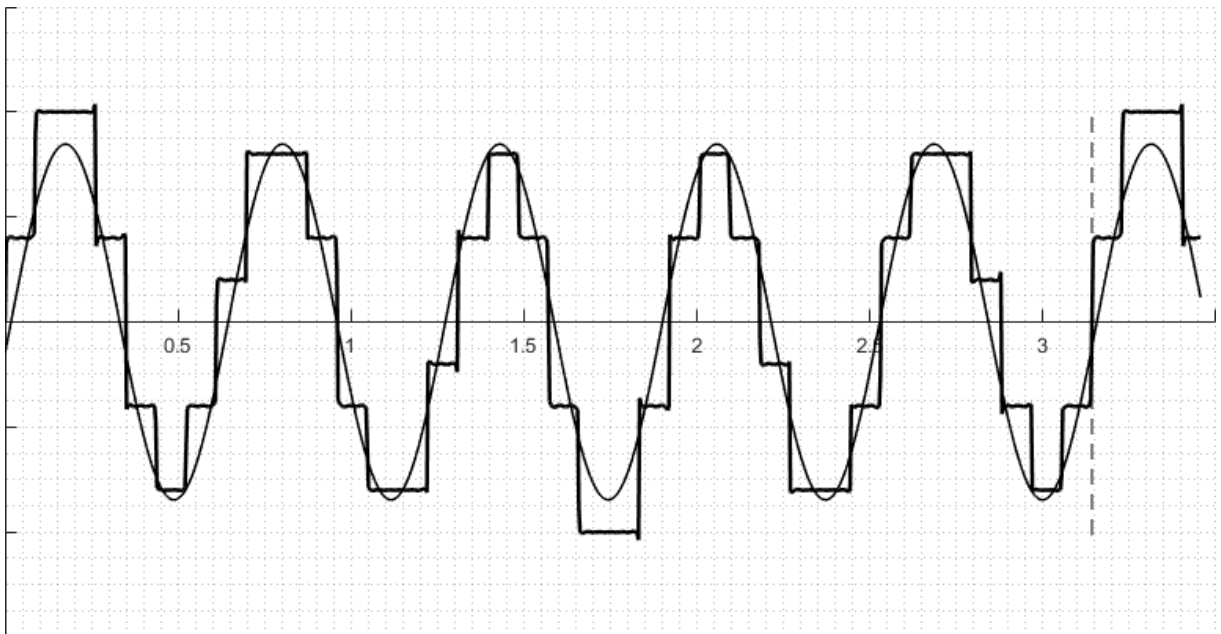


Figure 3.18 - 72 slots, 10 pairs of poles, resultant MMF, and fundamental at $t = 0$.

3.3. POLE SHOE ENCLOSURE FACTOR

The third tool does deal with windings as the two before, but another essential parameter that feeds the reactances calculations, the pole shoe magnetic enclosure factor [29]. This factor is used to correctly represent the magnetic area that goes in the equation presented in section 2.1.3 and varies depending on the pole shoe shape. For that matter, this tool simulates the pole shoe. Simulating salient poles in FEM includes, basically, two actions: defining its geometry in FEMM and its properties.

Drawing a geometry using only FEMM is a laborious task, then a MATLAB interface was made to create a geometry and to export it to FEMM so that it can be simulated. In this interface, it is possible to draw three types of pole shoes, illustrated in Figure 3.19:

- One arc pole shoe;
- Two arcs pole shoe;
- Three arcs pole shoe;

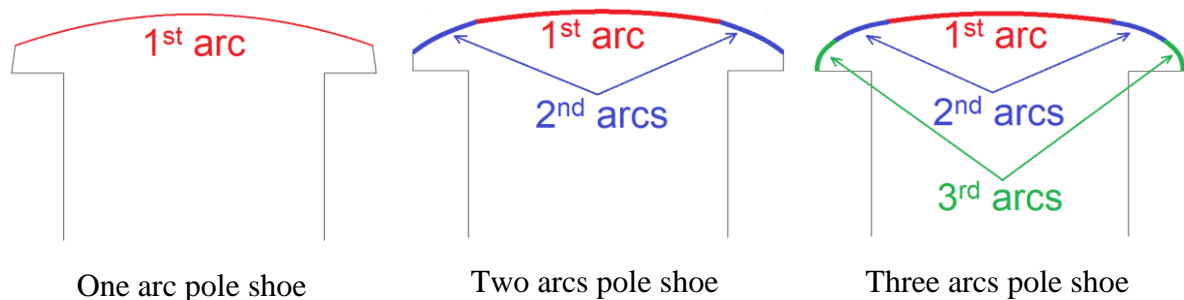


Figure 3.19 – Illustrations of three types of pole-shoe addressed in this work, depicting where the arcs are located.

3.3.1. Pole shoe Geometry

Not all pole parameters need to be inputted, because some are obtainable with others in hand. This section presents input cases used in this work, and the calculations used to obtain the remaining parameters.

Some parameters are common to any type of pole shoe (among those types addressed by this work), which are pole base height and width, respectively h_b and ω_b .

Other parameters are presented next, for each type.

3.3.1.1. One arc pole shoe

General pole-shape with dimension parameters is shown in Figure 3.20.

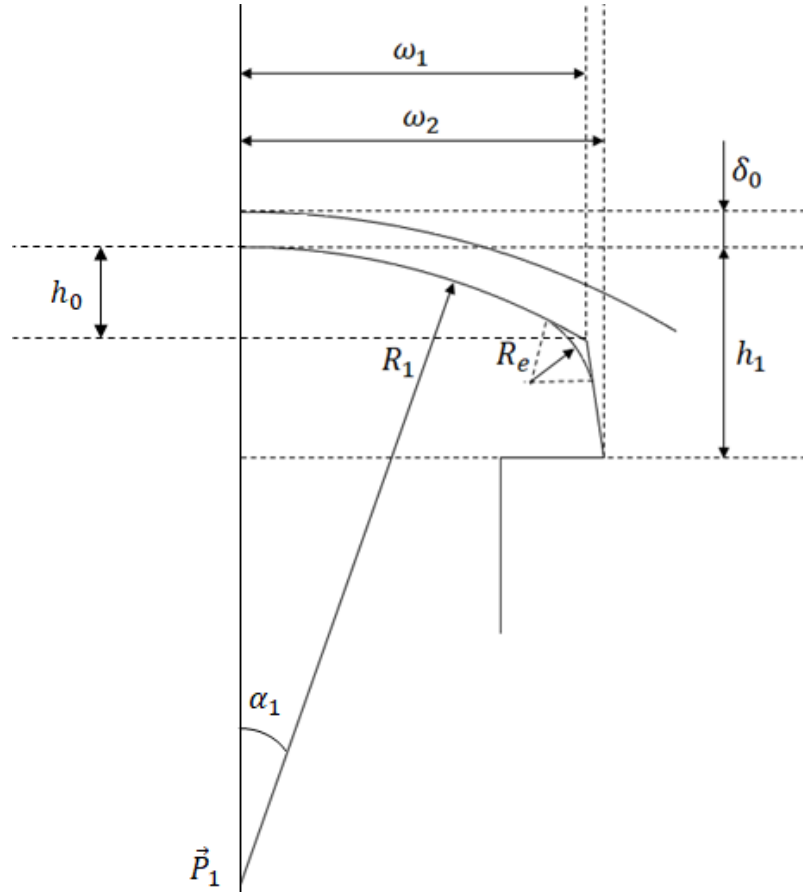


Figure 3.20 - One arc pole shoe dimensional parameters.

- **Input Parameters:**

$$\delta_0 - h_1 - \omega_1 - \omega_2 - R_e - R_1 - h_b - \omega_b$$

- **Calculated Parameters:**

$$\alpha_1 = \arcsin \frac{\omega_1/2}{R_1} \quad (3.7)$$

$$h_0 = R_1 \cos(1 - \cos \alpha_1) \quad (3.8)$$

$$P_1 = \frac{D_i}{2} - \delta_0 - R_1 \quad (3.9)$$

3.3.1.2. Two arcs pole shoe

General pole-shape with dimension parameters is shown in Figure 3.21.

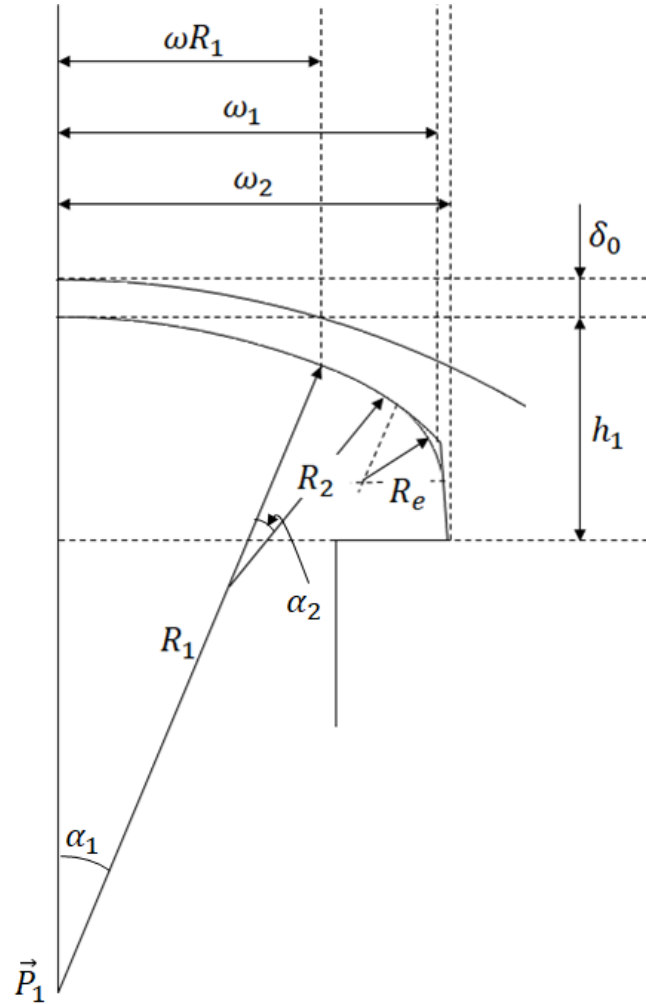


Figure 3.21 - Two arcs pole shoe dimensions parameters.

- **Input Parameters:**

$$\delta_0 - h_1 - \omega_1 - \omega_2 - R_e - R_1 - \omega R_1 - R_2 - h_b - \omega_b$$

- **Calculated Parameters:**

$$\alpha_1 = \arcsin \frac{\omega_1/2}{R_1} \quad (3.10)$$

$$\alpha_2 = \arcsin \frac{\omega_1/2 - (R_1 - R_2) \sin \alpha_1}{R_2} - \alpha_1 \quad (3.11)$$

3.3.1.3. Three arcs pole shoe

General pole-shape with dimension parameters is shown in Figure 3.22.

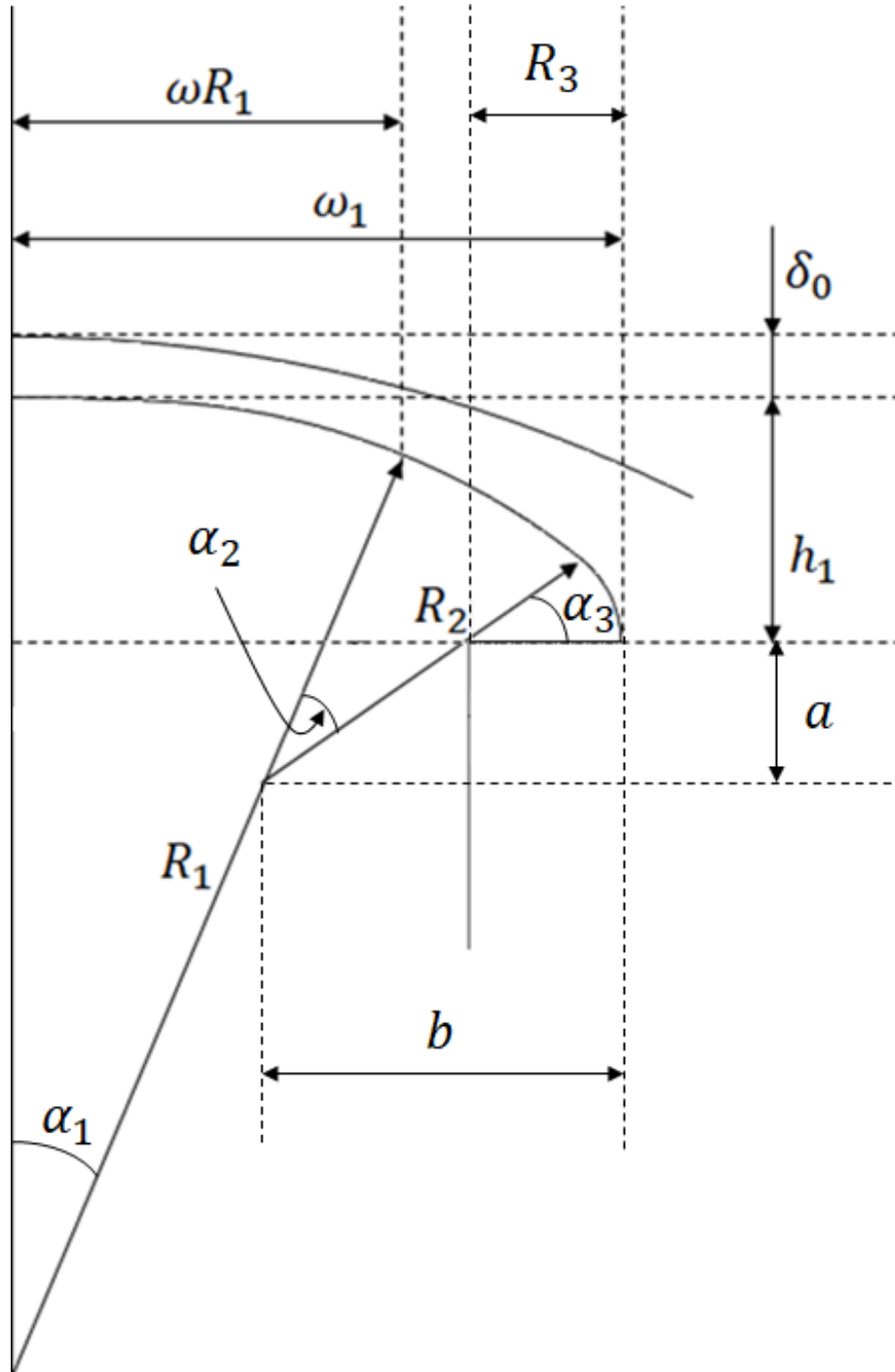


Figure 3.22 - Three arcs pole shoe dimensions parameters.

- **Input Parameters:**

$$\delta_0 - h_1 - \omega_1 - R_1 - \omega R_1 - R_2 - h_b - \omega_b$$

- **Calculated Parameters:**

$$\alpha_1 = \arcsin \frac{\omega R_1 / 2}{R_1} \quad (3.12)$$

$$a = \frac{D_i}{2} - (R_1 - R_2) \cos \alpha_1 - \delta_0 - h_1 \quad (3.13)$$

$$b = \frac{\omega_1}{2} - (R_1 - R_2) \sin \alpha_1 \quad (3.14)$$

$$\frac{R_2 - b}{a} \cos(\alpha_1 - \alpha_2) + \sin(\alpha_1 + \alpha_2) = 1 \quad (3.15)$$

Solving Equation 3.15 for α_2 results in the remaining parameters:

$$R_3 = R_2 - \frac{a}{\cos(\alpha_1 + \alpha_2)} \quad (3.16)$$

$$\alpha_3 = \frac{\pi}{2} - \alpha_1 - \alpha_2 \quad (3.17)$$

3.3.2. Finite element Simulation

With geometry parameters defined and inputted, MATLAB draws and exports to FEMM the pole shoe shape along with appropriate boundaries. An example is shown in Figure 3.23, where not only the pole is drawn, but also the stator inner perimeter, rotor-rim outer perimeter, and symmetry imaginary lines over air-gap (direct and quadrature axes).

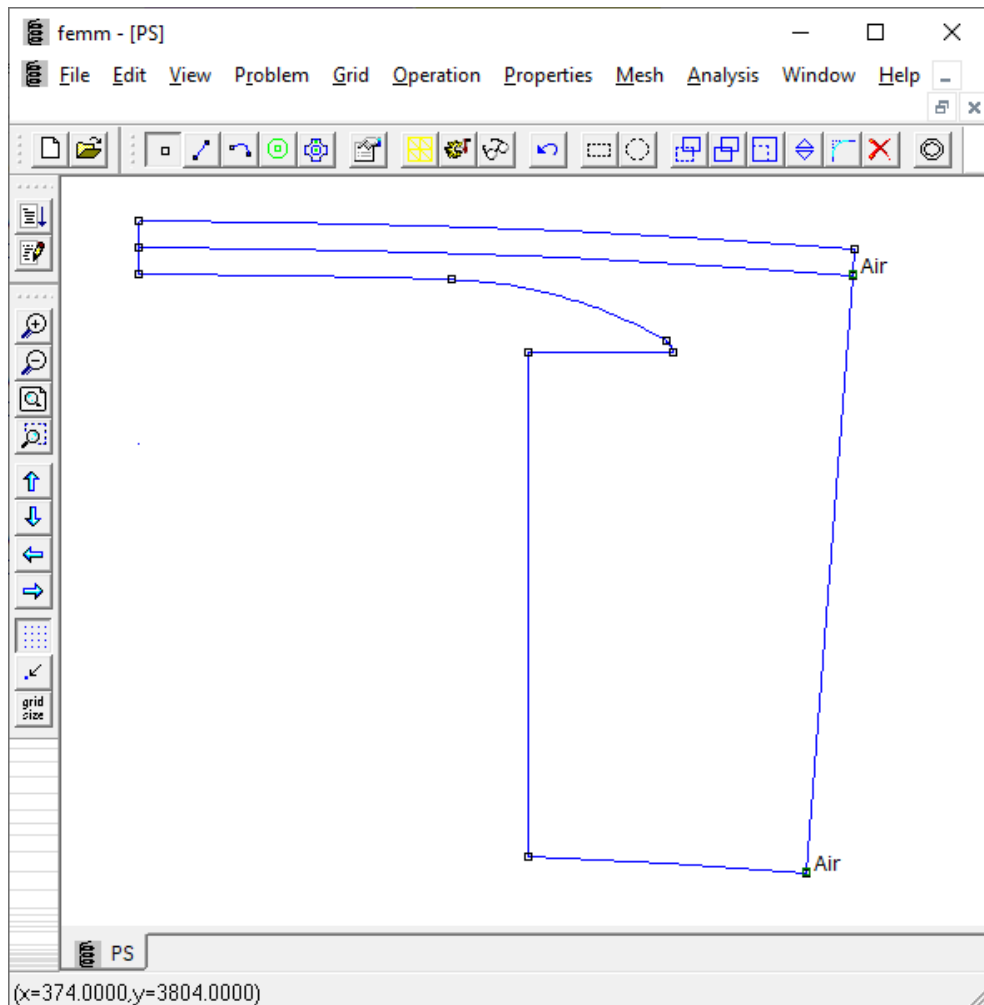


Figure 3.23 - Three arcs pole example in FEMM.

It can be seen that another arc is drawn, concentric to stator inner diameter that passes through the air-gap average “point.” That is due to the FEMM requirement to have a previously defined line (or arc) drawn over which graphics can be plotted. This arc is precisely the region of interest for magnetics studies in this work, where MMF was calculated and, in this section, where magnetic flux densities are plotted.

Materials properties are set for the only two areas inside the boundaries, which are air-gap areas, and as can be seen in Figure 3.23 they are set as “Air.” For the boundaries, correct properties are shown in Figure 3.24.

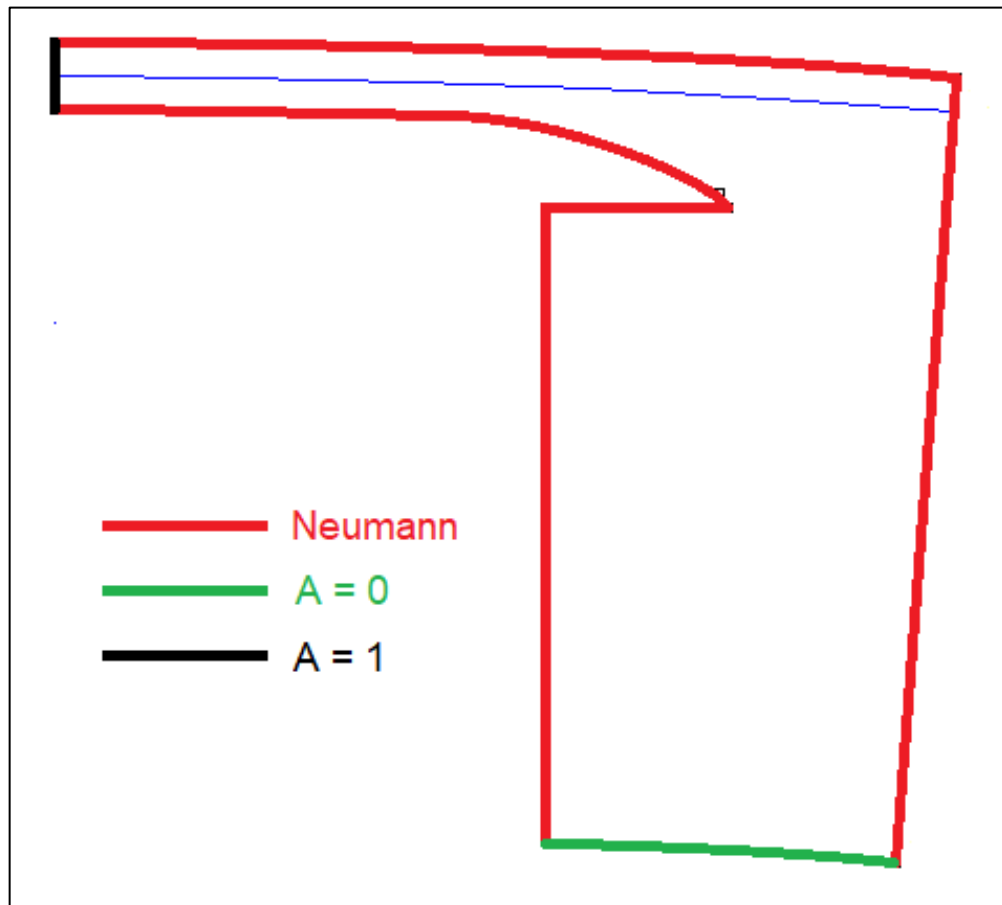


Figure 3.24 - Boundaries properties for pole shoe simulation.

With boundaries and material appropriately set, a simulation can be done. It is interesting to see the example of the magnetic flux lines plot (Figure 3.25) and magnetic flux density over the air-gap arc (Figure 3.26).

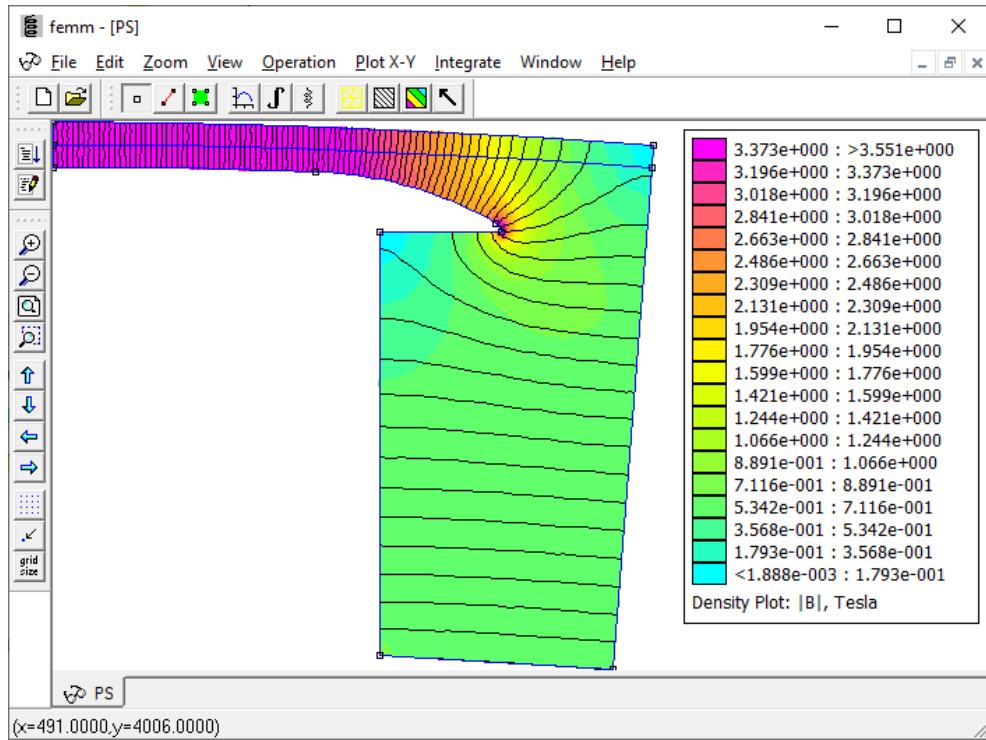


Figure 3.25 – Magnetic flux lines and color density plot.

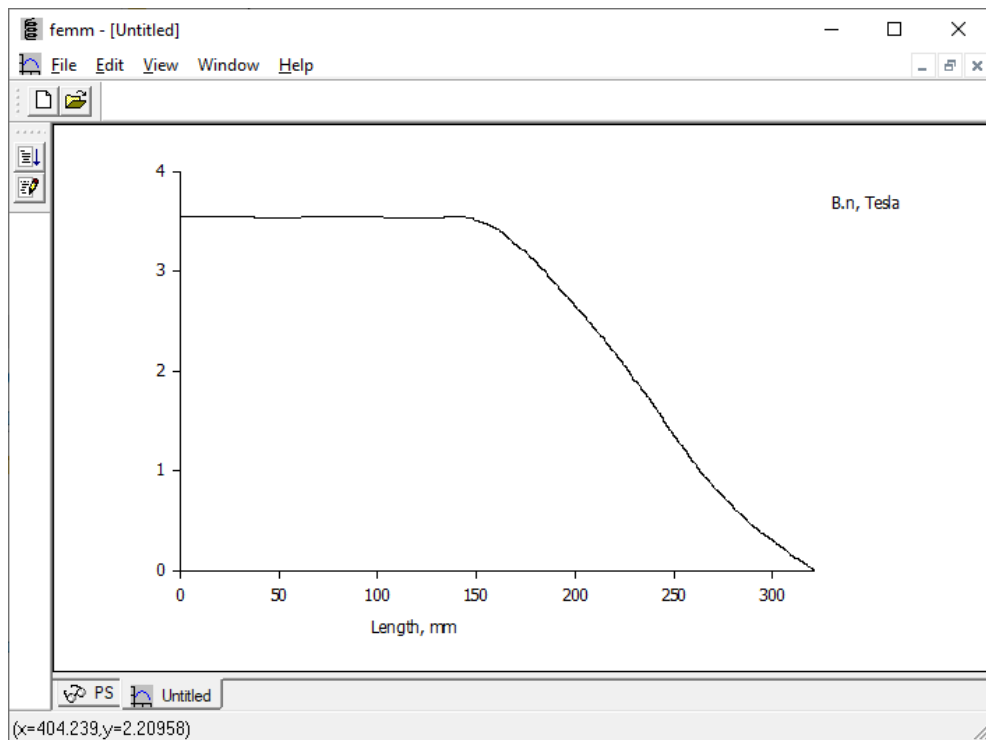


Figure 3.26 - Magnetic flux density plot over the air-gap line.

Data shown in Figure 3.26 is then imported to MATLAB, normalized, and first harmonic and mean value extracted (Figure 3.27). The normalization is done to neglect the saturation effect, as the simulation regards effects from pole shoe shape only. An important parameter is obtained from this tool since this mean value corresponds to the pole enclosure factor [29].

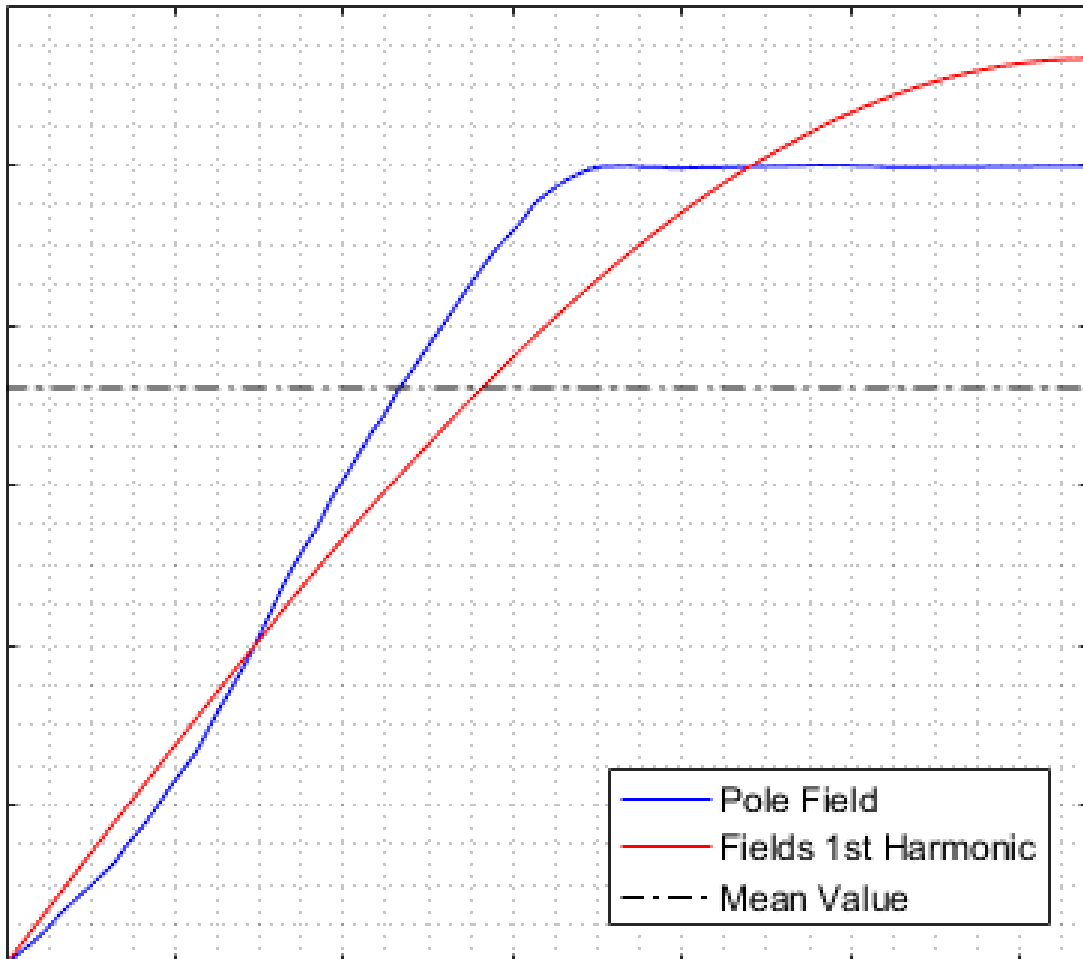


Figure 3.27 - Magnetic Flux Density with some extracted parameters.

3.4. EFFECTIVE PACKAGE MAGNETIC LENGTH

The fourth and last tool calculates the effective package length, which, like the third tool, simulates actual shape to get density flux curves. The Effective Magnetic Length is something to be regarded when calculating magnetic flux in air-gap, because not all flux lines cross the air-gap following a minimum path (straight line). They are sparse in extremities due to leakage flux. Then, for an accurate portrayal of air-gap quantities, simulation is required to compensate for this difference, representing the pole-end actual geometry (damper slots ring and pole end) correctly.

A core axial enclosure factor can be defined as the ratio between the flux density in a length that covers from the stator center to this critical region (pole extremity*) and that density without the critical region. Given a normalized density plot $B(z)$, where z stand for axial length, a pole axial enclosure factor α_e :

$$\alpha_e = \frac{1}{l_s/2} \int_{l-l_s/2}^{l_s} B(z) dz \quad (3.18)$$

* For a stator with length l_s , the reference line l that defines the critical region is chosen by taking some considerations further ahead.

To correctly represent pole and stator extremities, the geometry in Figure 3.28 is applied.

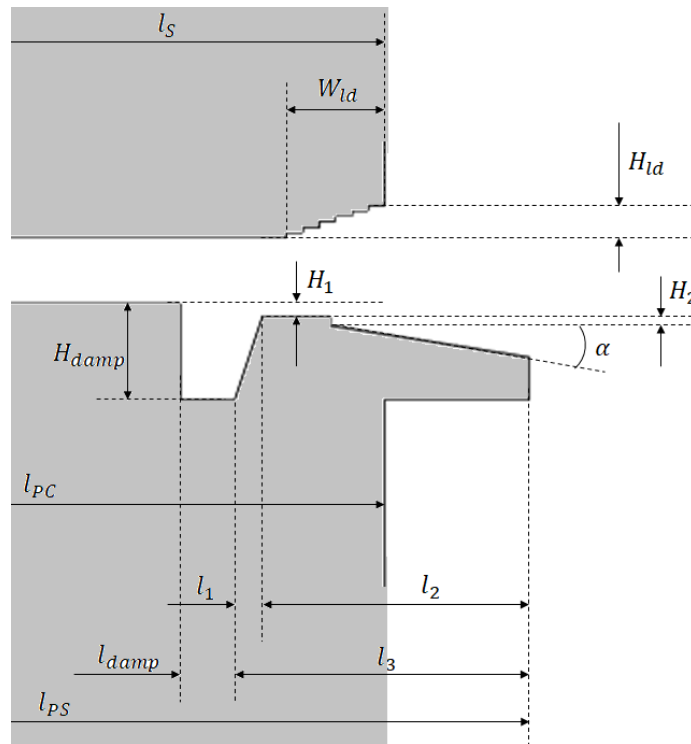


Figure 3.28 - Axial dimensions around air-gap.

Some considerations are made before simulating it:

- It is considered actual stator axial height and pole axial height;
- Length of interest (plotting region):
 - From **4 minimum air-gaps** of distance before the damping winding slot ($l_{damp} - 4\delta_0$);
 - To **half minimum air-gap** beyond stator axial length ($l_s + \delta_0/2$);
 - $l = [l_{damp} - 4\delta_0, l_s + \delta_0/2]^*$

These values were obtained after some simulations, where it was observed that results did not change significantly after increasing this interest region.

- Instead of using open boundaries, it is defined as a squared region of air, with dimensions that do not affect the leakage significantly.

In Figure 3.29 it is shown the geometry in FEMM, zoomed-in Figure 3.30. The geometry is defined by inputting parameters shown in Figure 3.28.

*Figure 3.30 depicts the region of interest with dimensions

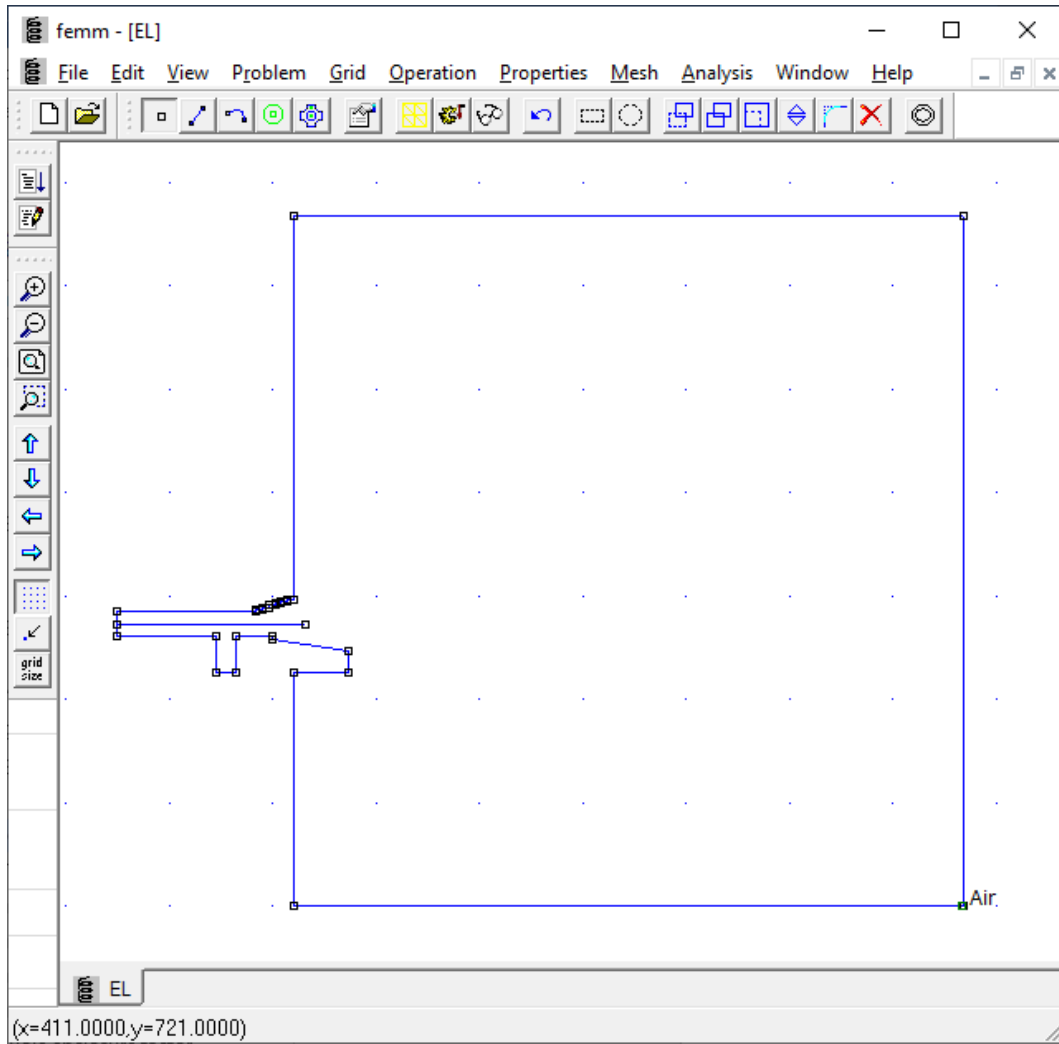


Figure 3.29 - A SM axial extremity in FEMM.

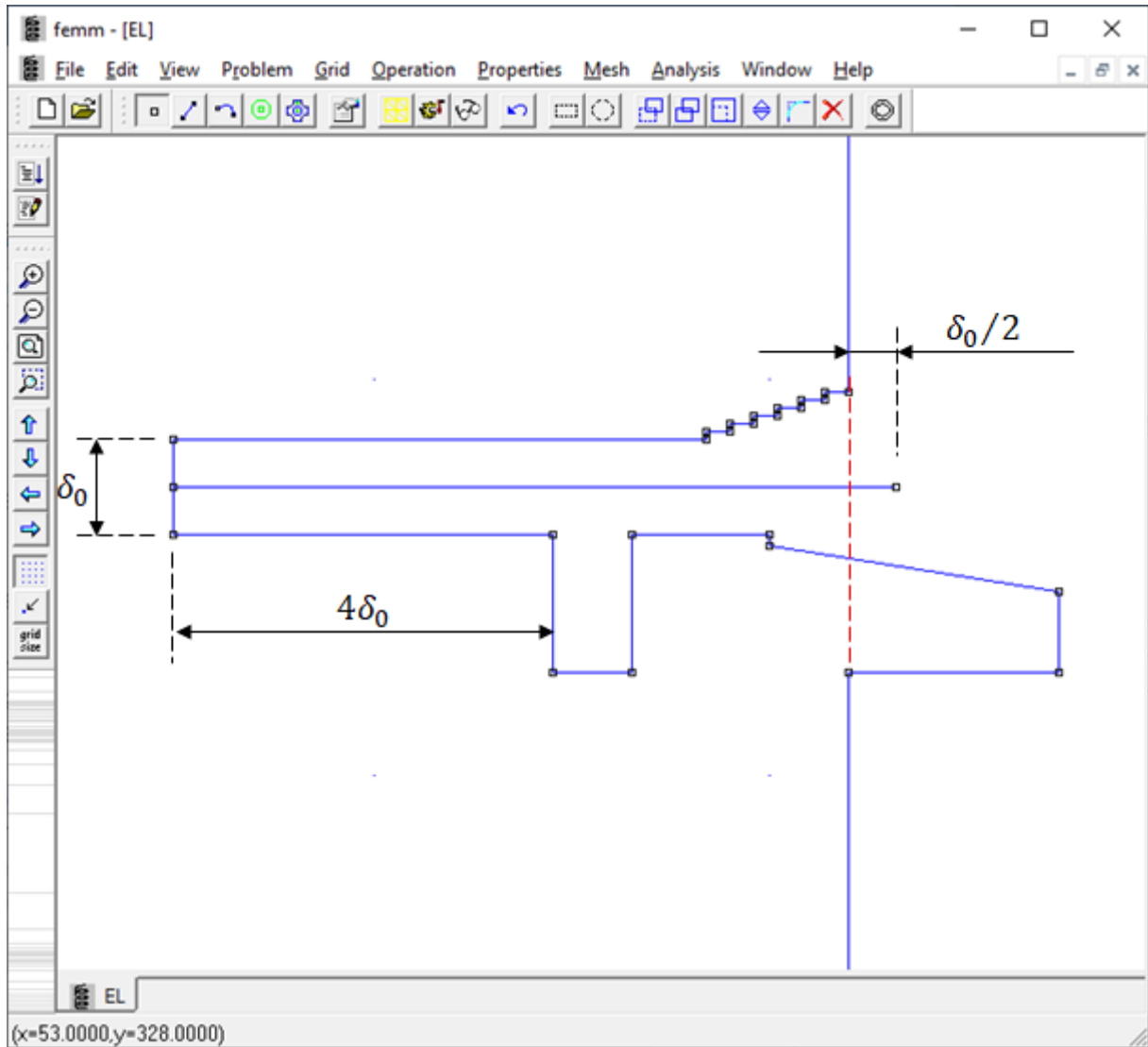


Figure 3.30 - A SM axial extremity in FEMM (Detail).

With boundaries set as in Figure 3.31.

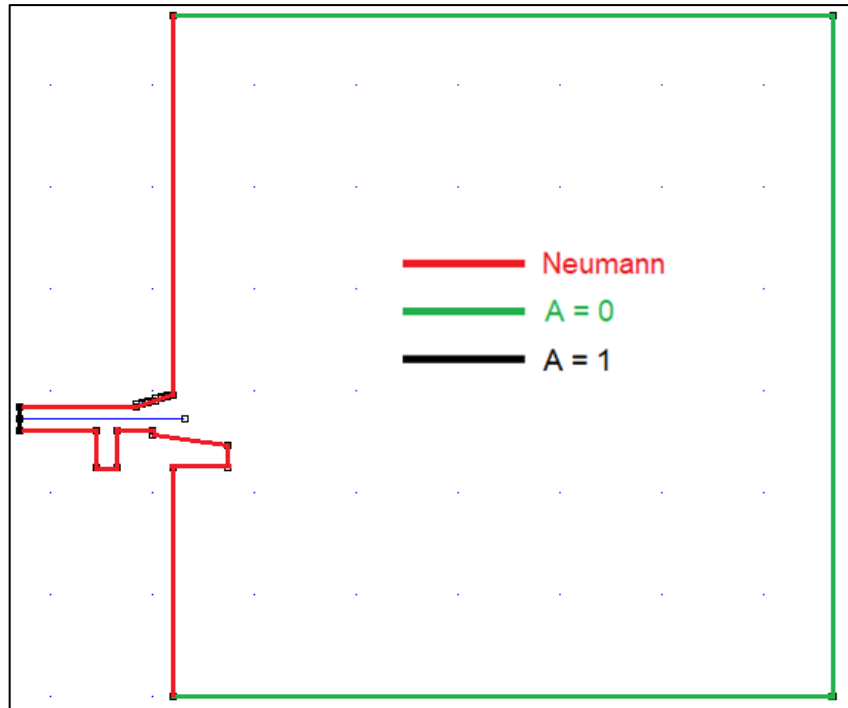


Figure 3.31 - Boundaries properties for pole end simulation

Figures 3.32 to 3.34 show simulation results:

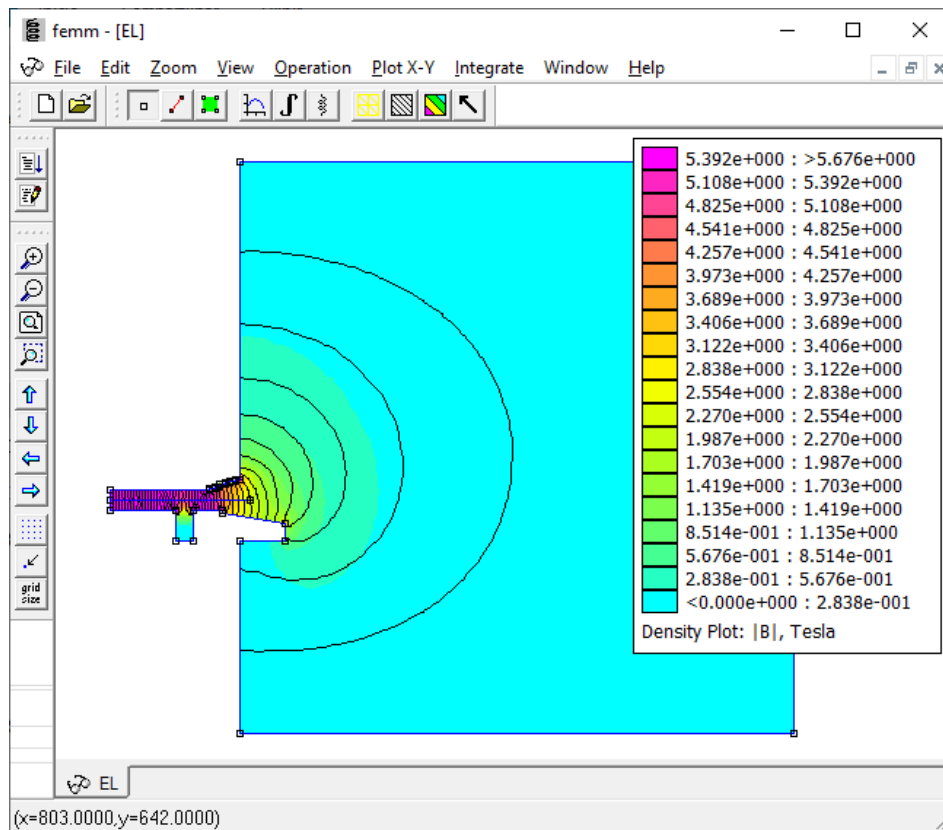


Figure 3.32 - Magnetic flux lines and color density plot.

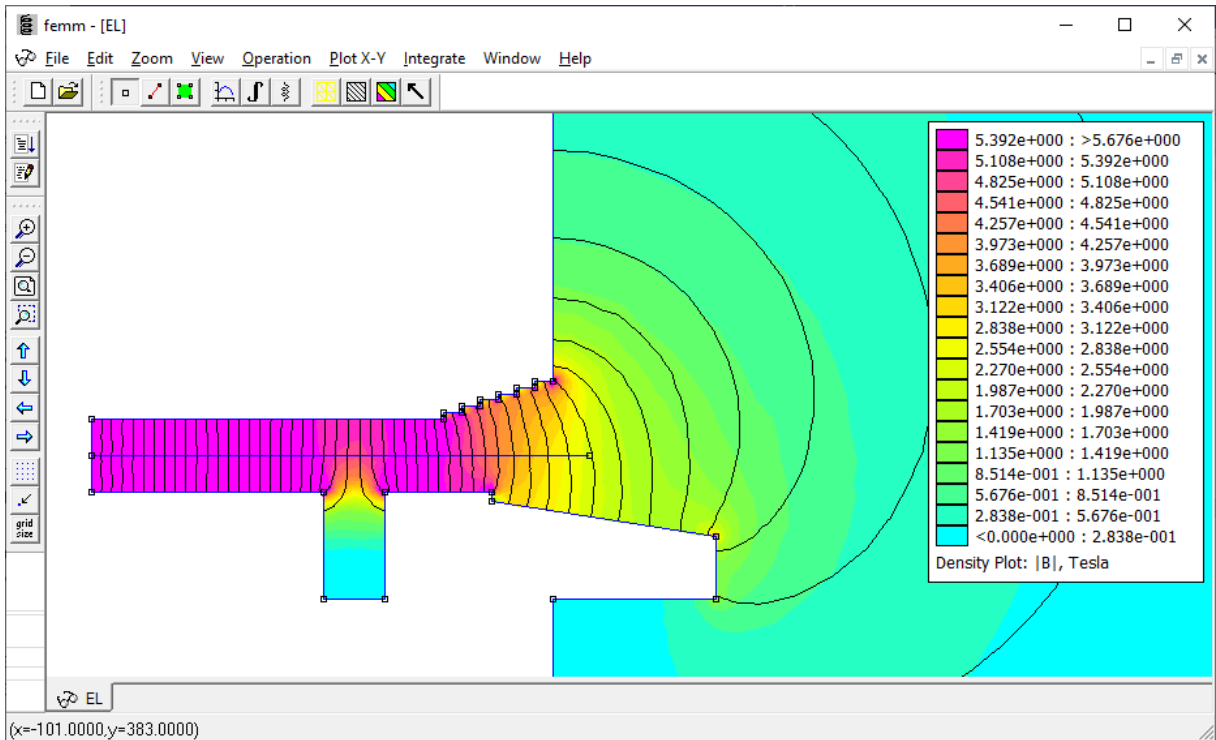


Figure 3.33 - Magnetic flux lines and color density plot (Detail).

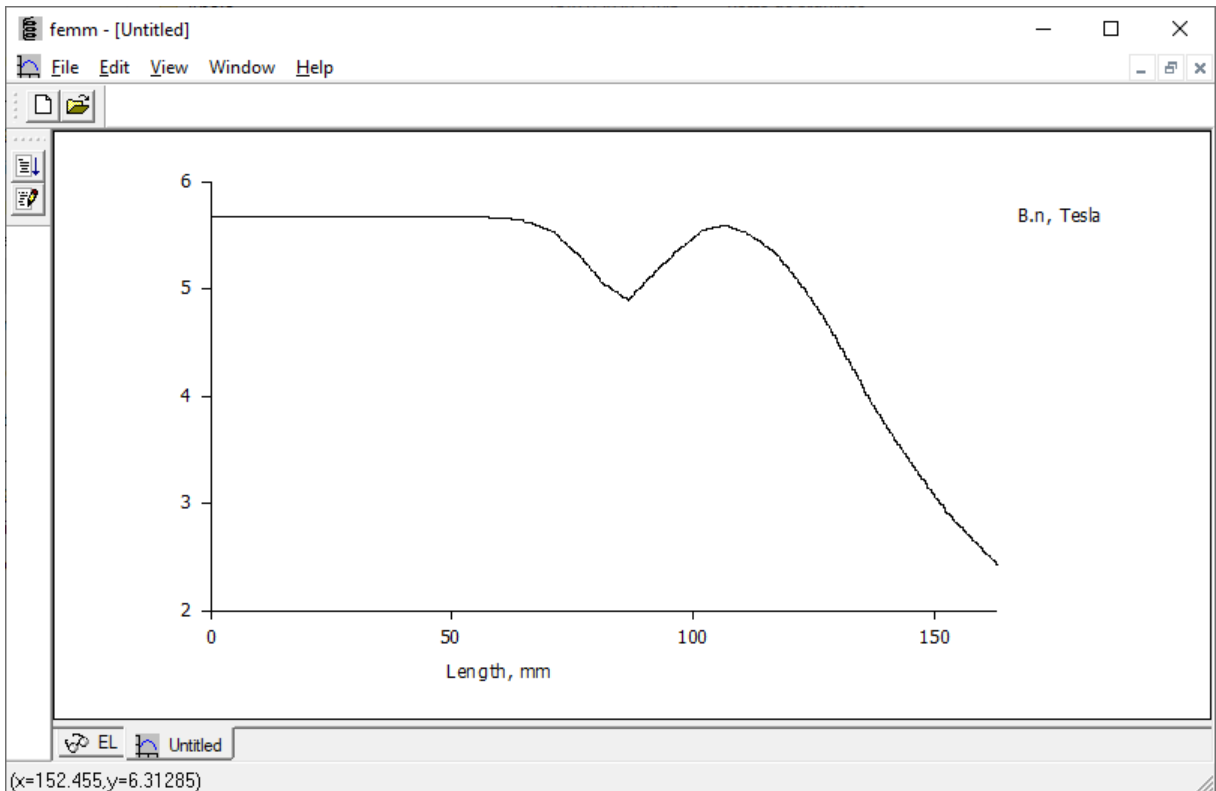


Figure 3.34 - Magnetic flux density over the region of interest.

Figure 3.35 shows the same graphic in Figure 3.34, normalized, and side to side to the geometry simulated, with a dashed line marking the stator end. Red line represents the plotting region.

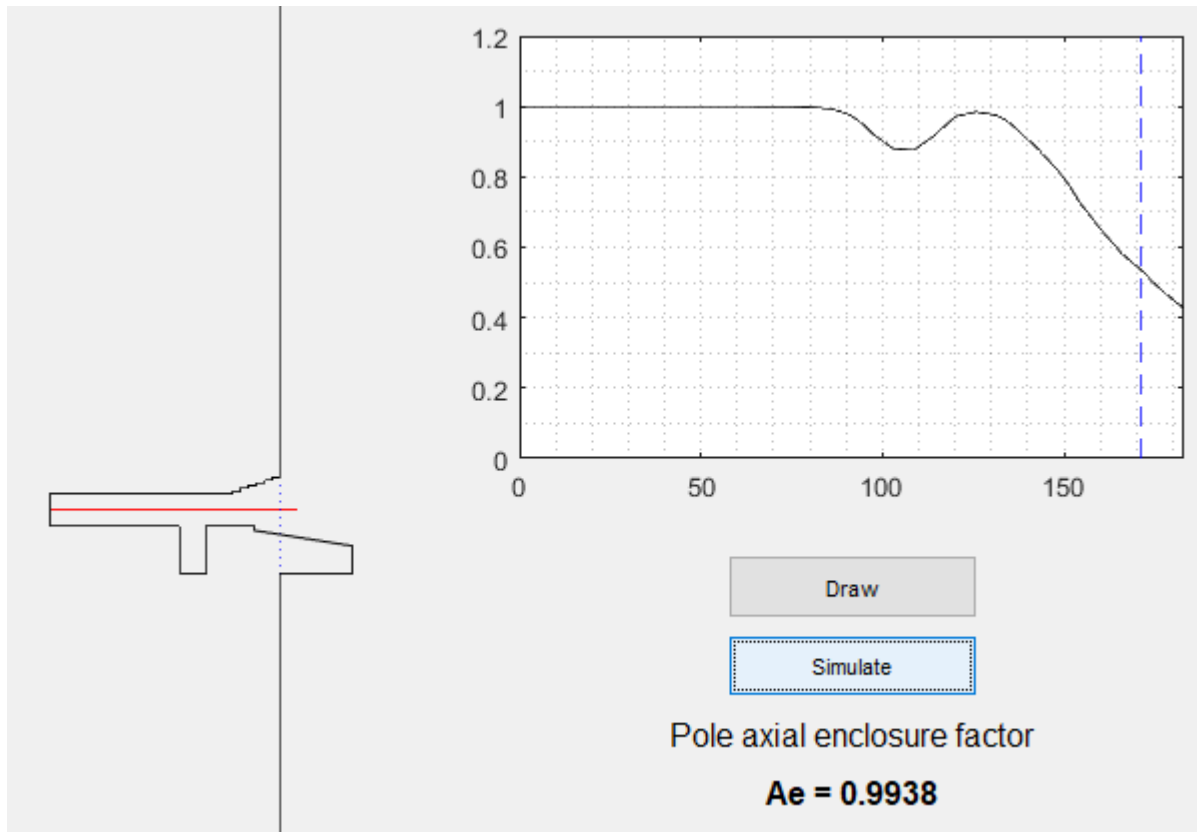


Figure 3.35 - Simulated geometry and normalized magnetic flux density plot.

With density plots in hand, it is possible to calculate α_e using Equation 3.8. The next chapter shows results from three different applications.

4. INTERACTION WITH MATLAB AND APPLICATIONS

MATLAB is a software that has a set of tools to solve engineering problems, mainly when dealing with arrays and matrices. It was chosen for this work due to the availability of a set of commands present in FEMM made to work together with Octave (Same language as MATLAB).

A set of routines were created using MATLAB guide, summarizing the tools described in this work in one application.

Three benchmarks from General Electric are used for this work validation, two of them from real salient pole SG. The third one is created by replicating one of the two and changing its pole shoe shape. Table 4.1 presents all significant data.

Table 4.1 - SGs parameters for validation.

Parameter	SG1	SG2	SG3
Number of stator slots	144	408	144
Number of pair of poles	4	20	4
Stator outer diameter [mm]	3212.0	8900.2	3212.0
Stator inner diameter [mm]	2350.0	8200	2350.0
Stator slot height [mm]	131	150.08	131
Stator slot width [mm]	16.42	22.72	16.42
Type of Pole Shoe	3 arcs	3 arcs	1 arc
Minimum air-gap [mm]	18	24	18
Pole shoe height [mm]	75	35	75
Pole shoe minor width [mm]	-	-	635
Pole shoe greater width [mm]	635	480	635
Corner radius [mm]	-	-	15
Pole shoe greater radius [mm]	1157	4076	1014.4
Pole shoe greater radius width [mm]	403.6	282.1	-
Pole shoe minor radius [mm]	321.44	206.37	-
Pole core height [mm]	201	226	201
Pole core width [mm]	460	350	460

Stator end ladder total height [mm]	12	12	12
Stator end ladder total width [mm]	20	20	20
Number of stator end ladder steps	4	4	4
Pole shoe axial length [mm]	1580	2010	1580
Pole core axial length [mm]	1580	2050	1580
Stator axial length [mm]	1600	2050	1600
Difference height between Pole core and end [mm]	0	0	0
Pole end heel height [mm]	0	0	0
Damper ring slot ramp length [mm]	20	20	20
Pole end minor length [mm]	200	65	200
Pole end greater length [mm]	87.5	85	87.5
Pole end ramp angle [°]	23.2	11.6	23.2
Damper ring slot length [mm]	18	23	18
Damper ring slot height [mm]	35	30	35

4.1. Results for SG1

Results in Figures 4.1 to 4.10.

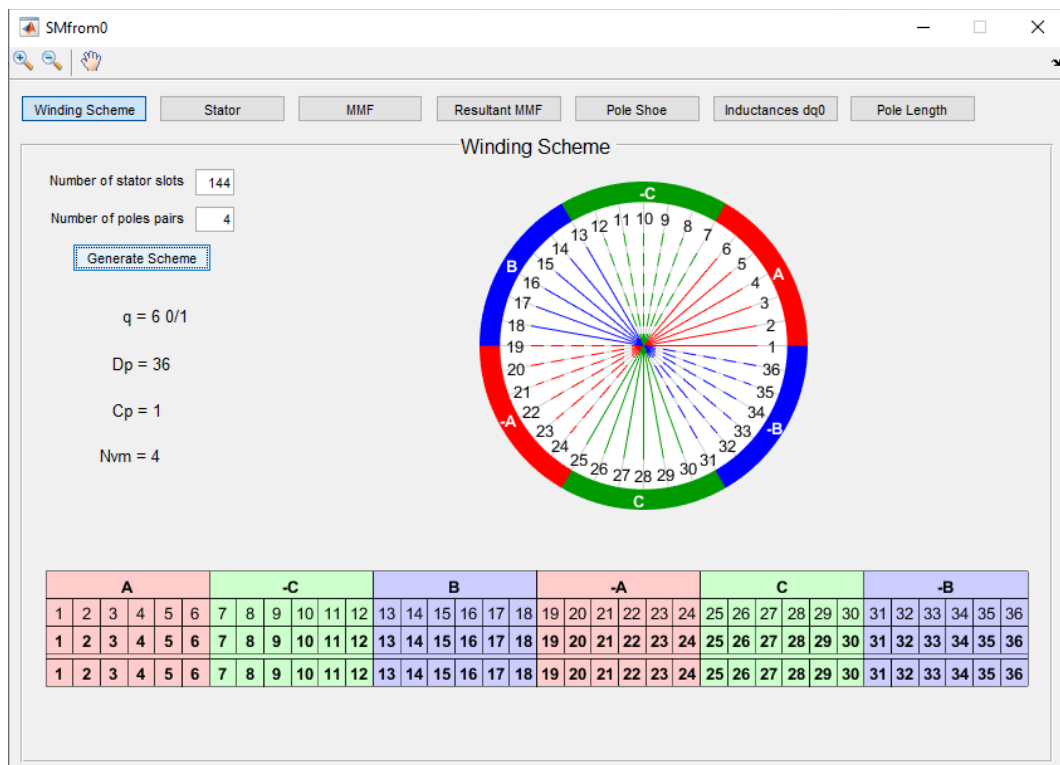


Figure 4.1 - Phasorial rosette and winding scheme for SG1.

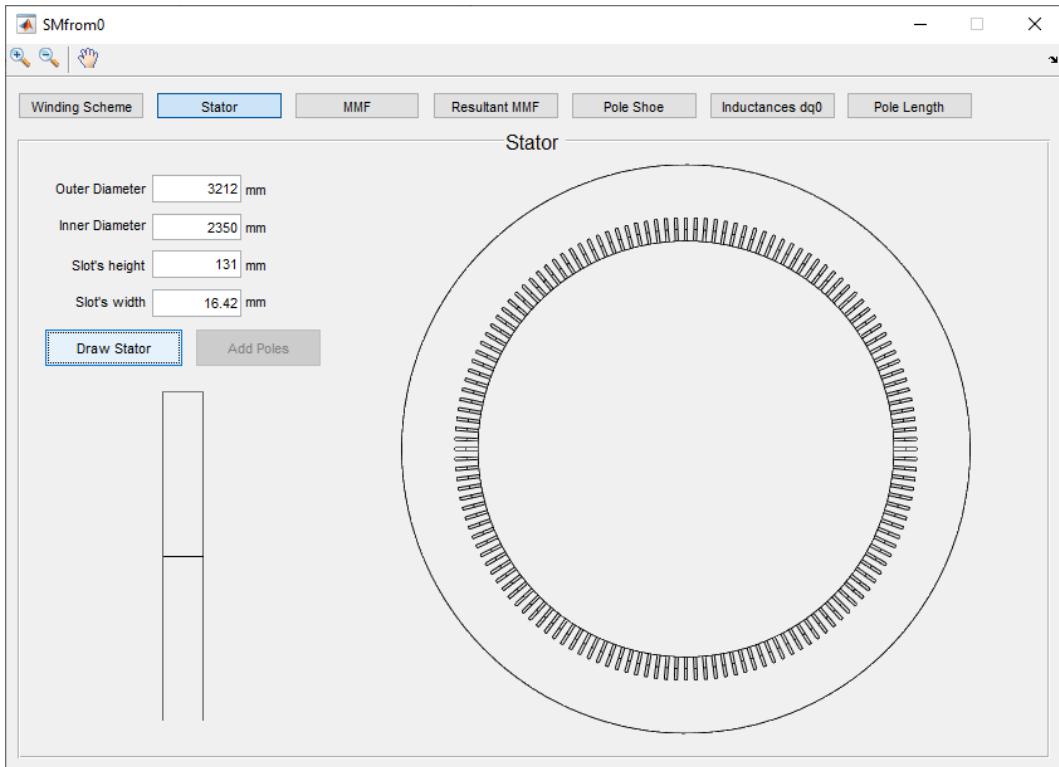


Figure 4.2 - Stator data for SG1.

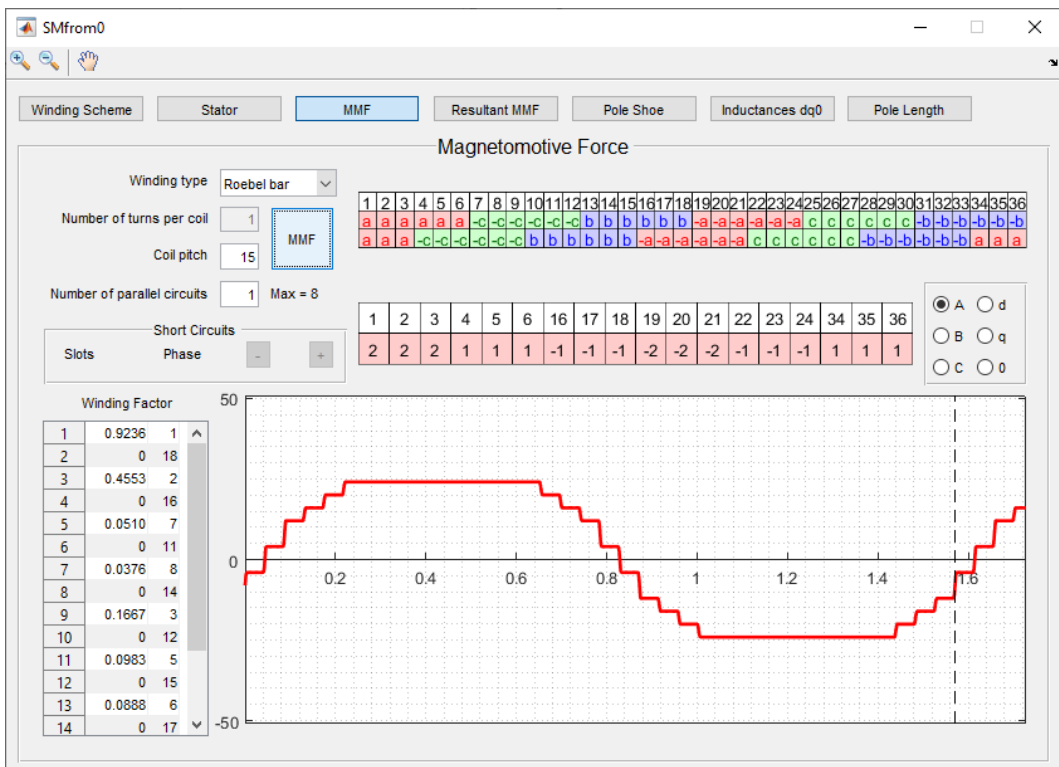


Figure 4.3 - Winding Matrix for SG1.

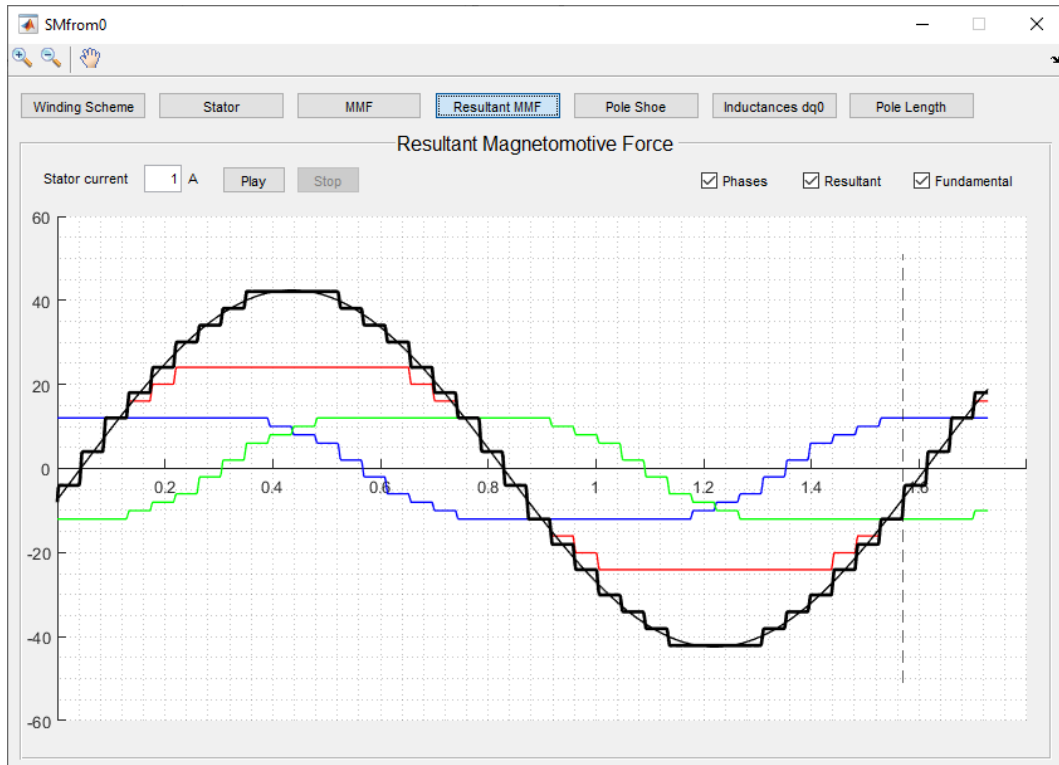


Figure 4.4 - Resulting MMF for SG1.

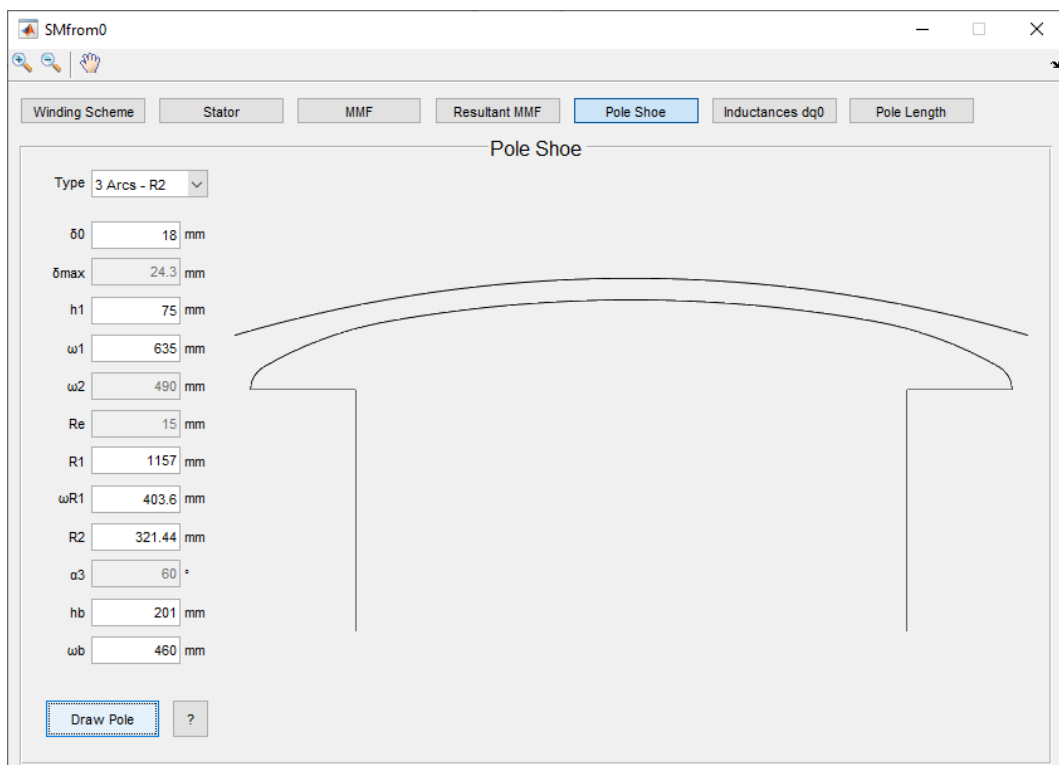


Figure 4.5 - Pole Shoe for SG1.

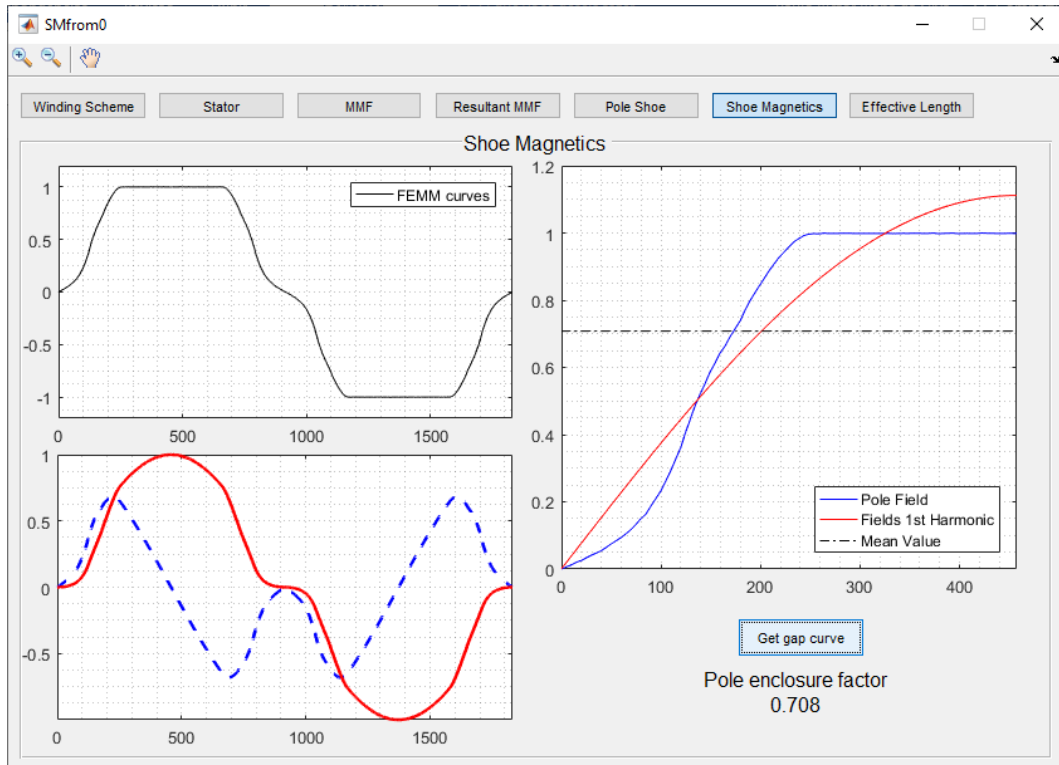


Figure 4.6 - Pole Shoe Magnetic Analysis for SG1.

Pole Field Curve

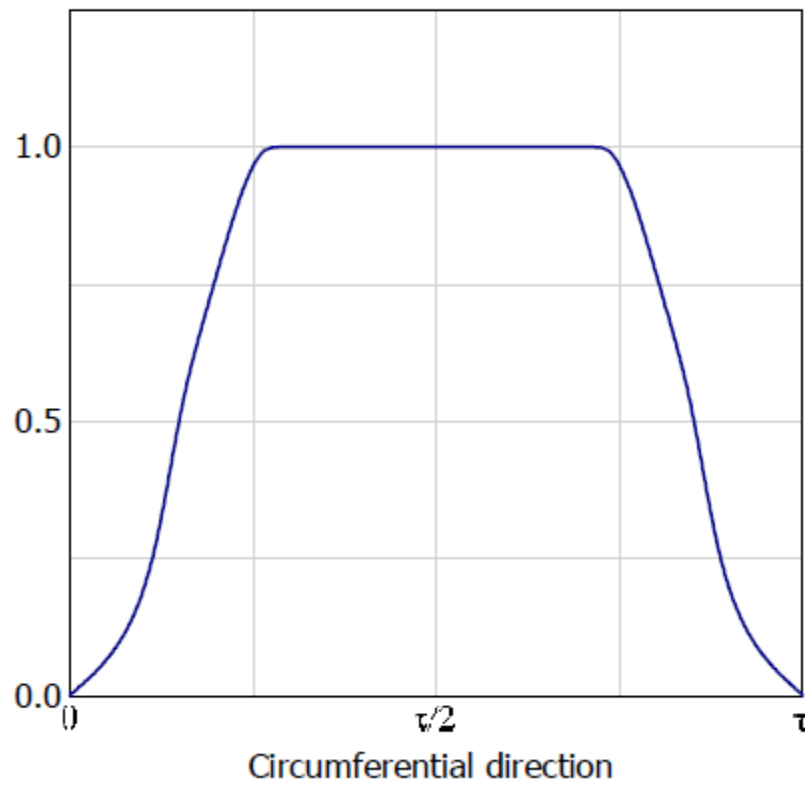


Figure 4.7 - Benchmark pole field curve for SG1.

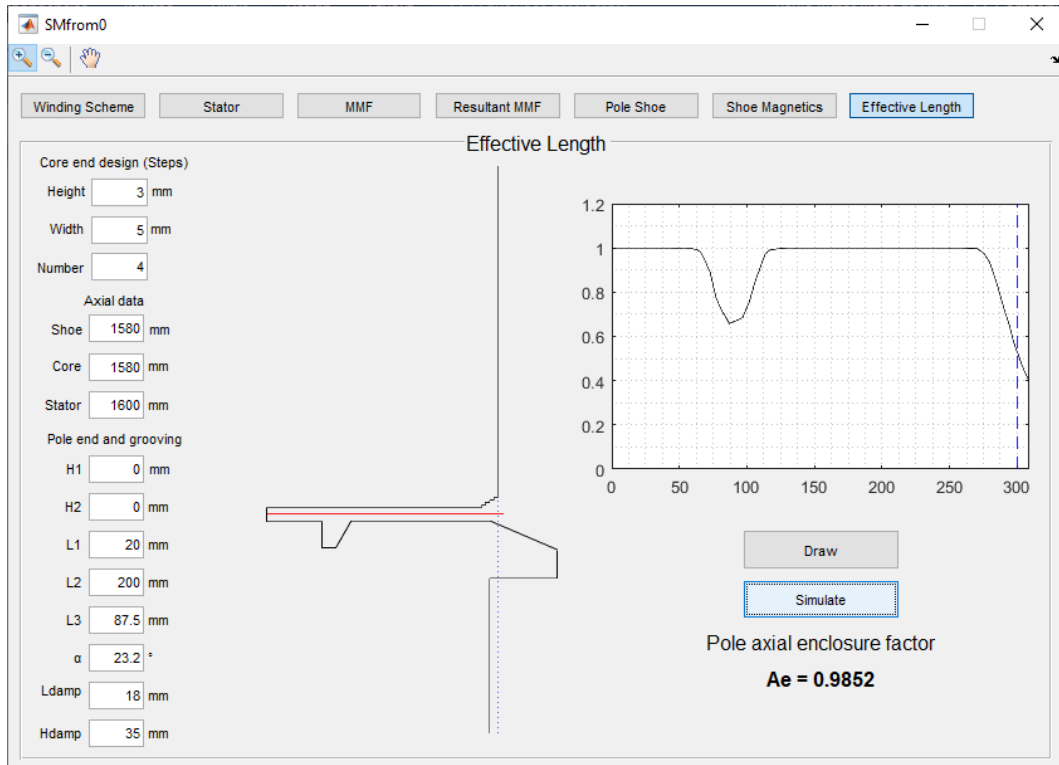


Figure 4.8 - Effective Magnetic Length analysis for SG1.

Airgap Field in Axial Direction

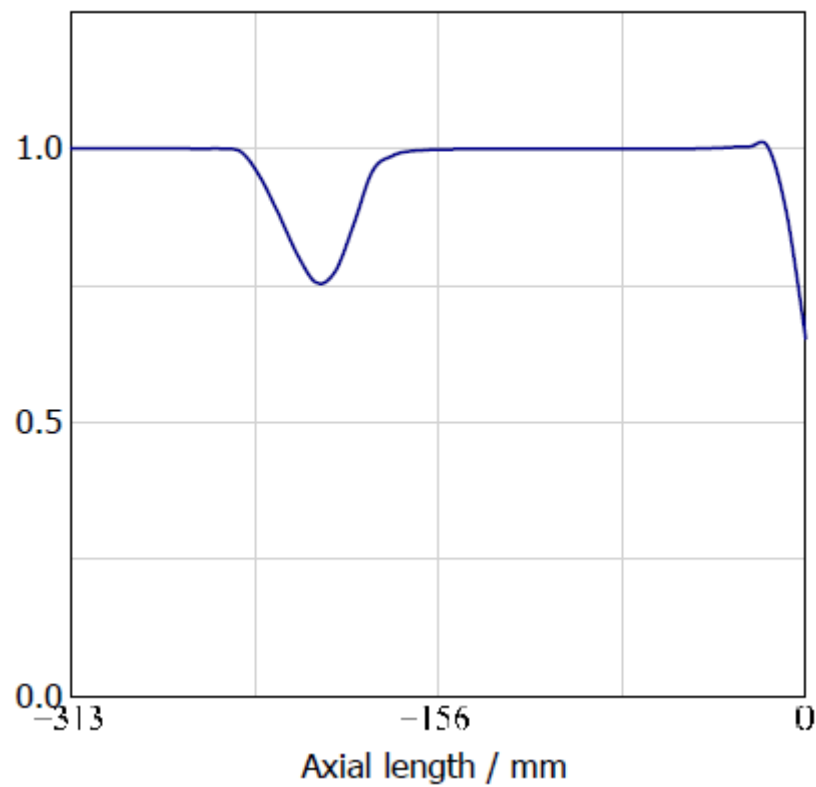


Figure 4.9 - Benchmark airgap field in axial direction for SG1.

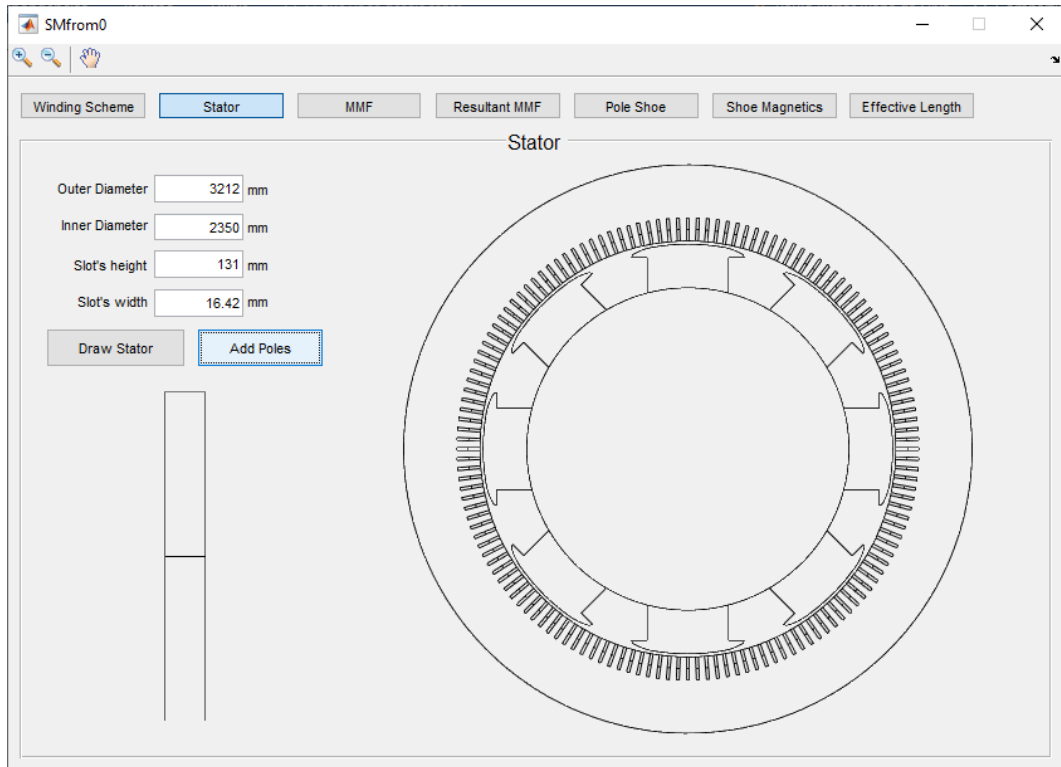


Figure 4.10 - Stator with poles for SG1.

4.2. Results for SG2

Results in Figures 4.11 to 4.20.



Figure 4.11 - Phasorial rosette and winding scheme for SG2.

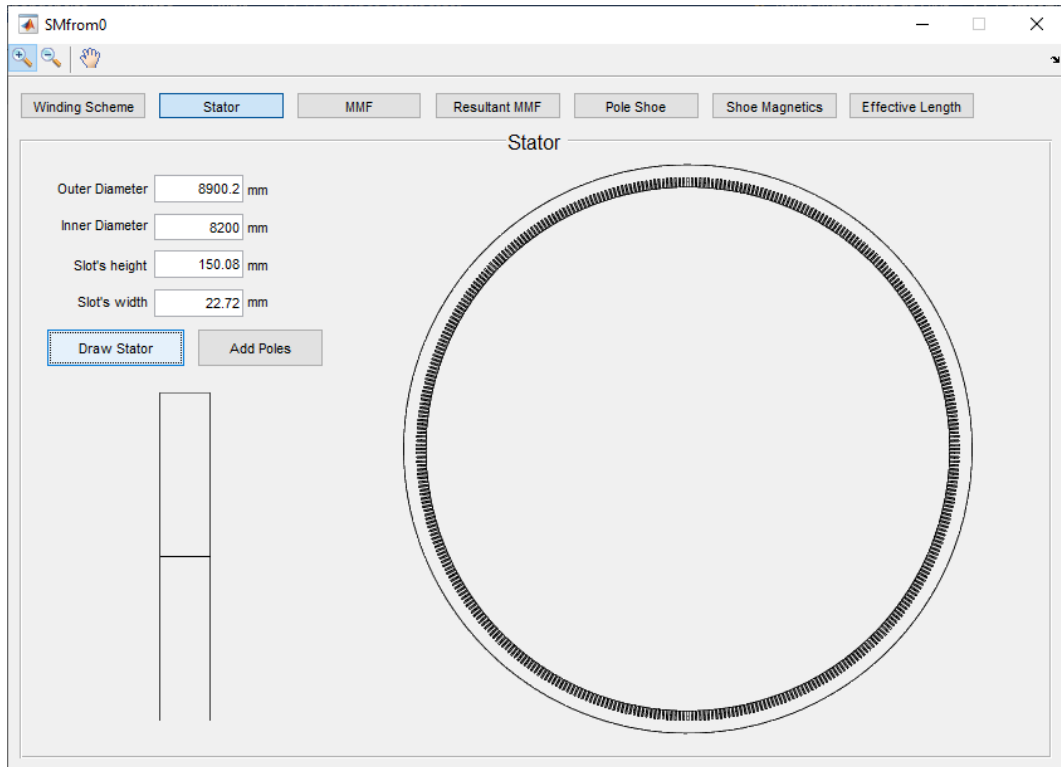


Figure 4.12 - Stator data for SG2

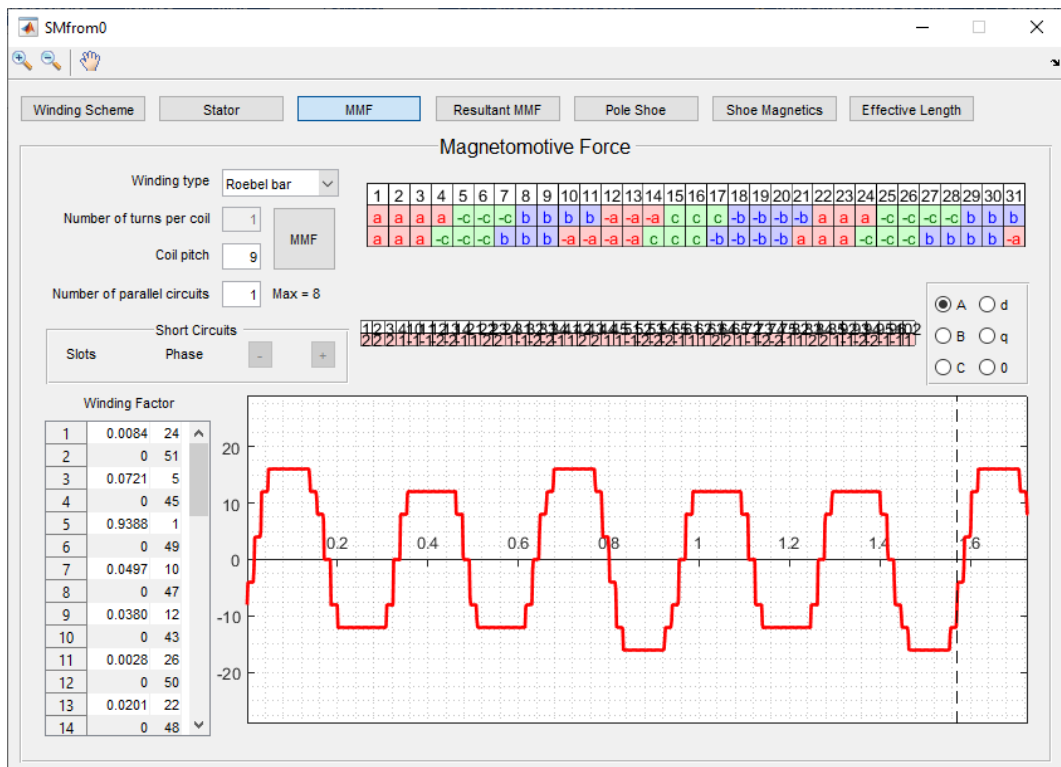


Figure 4.13 - Winding Matrix for SG2.

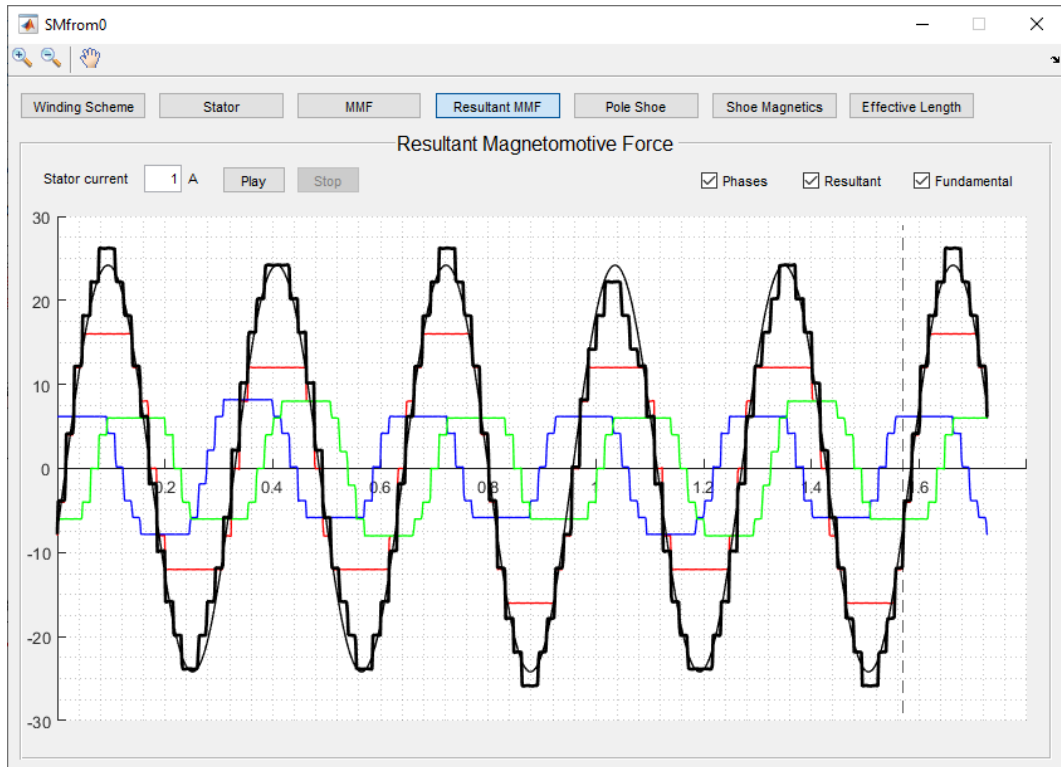


Figure 4.14 - Resulting MMF for SG2.

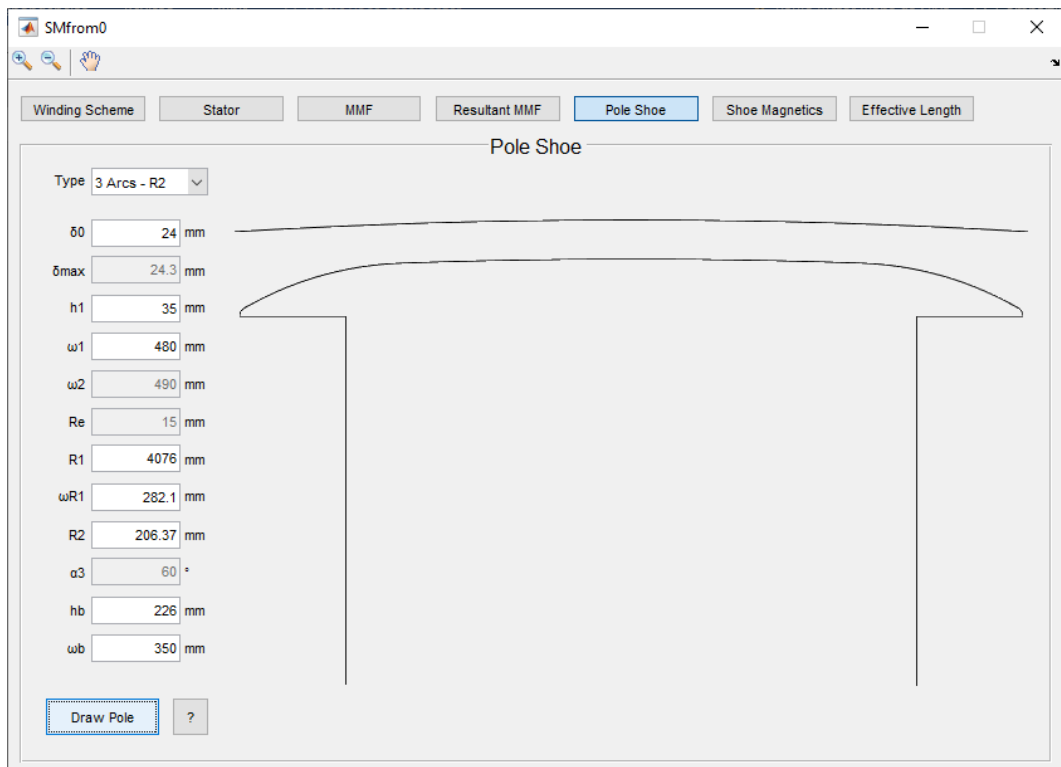


Figure 4.15 - Pole Shoe for SG2.

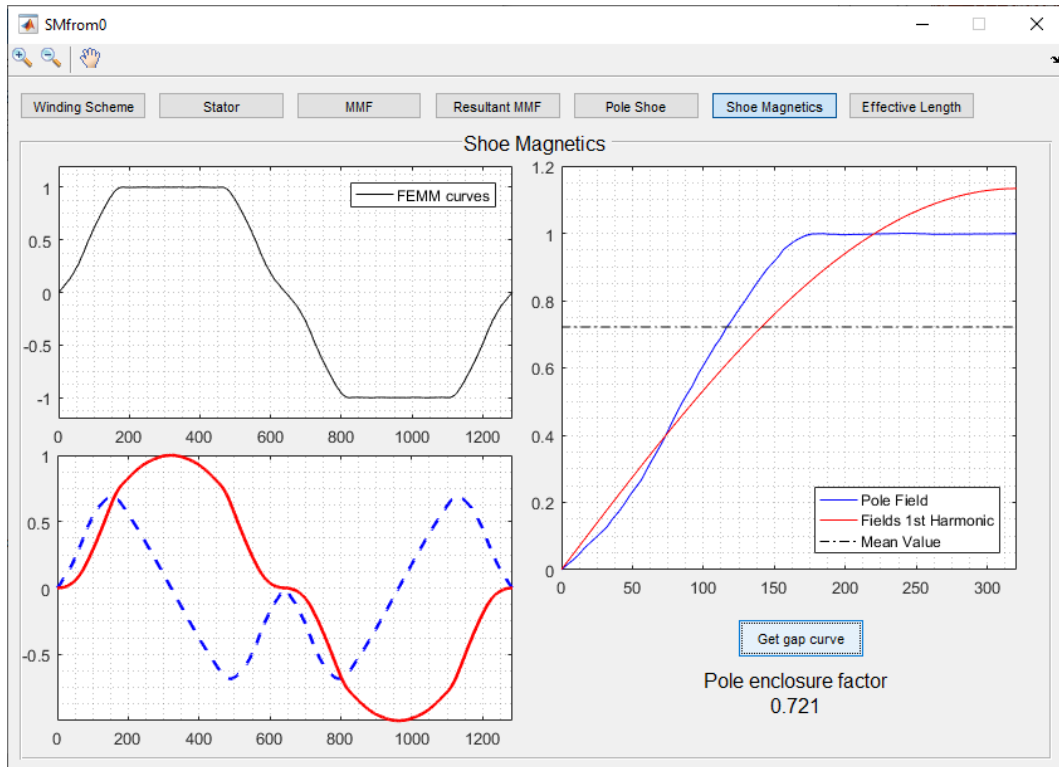


Figure 4.16 - Pole Shoe Magnetic Analysis for SG2.

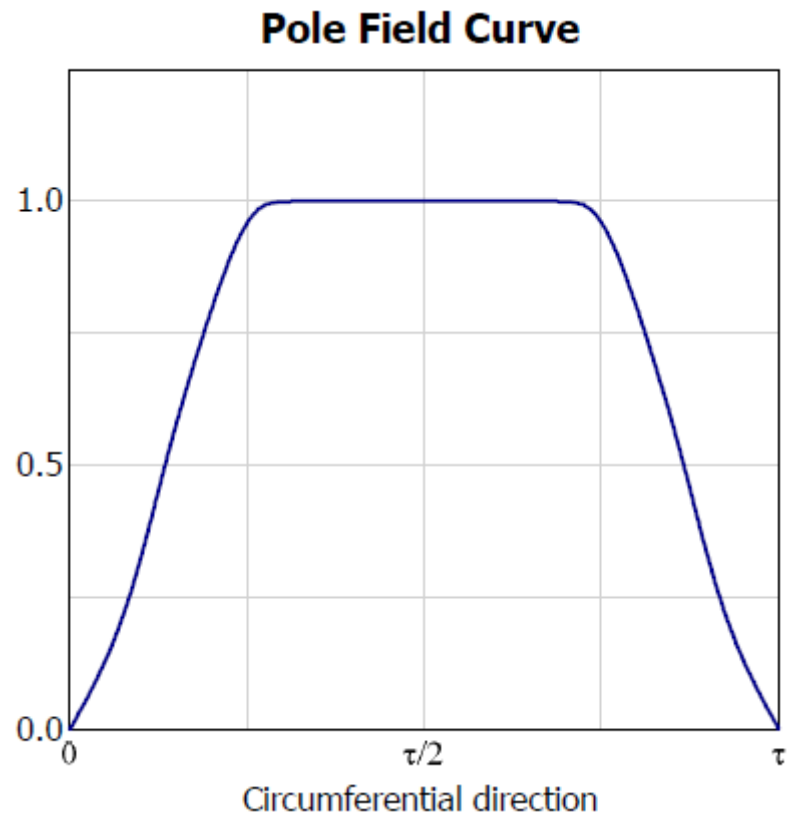


Figure 4.17 - Benchmark pole field curve for SG2.

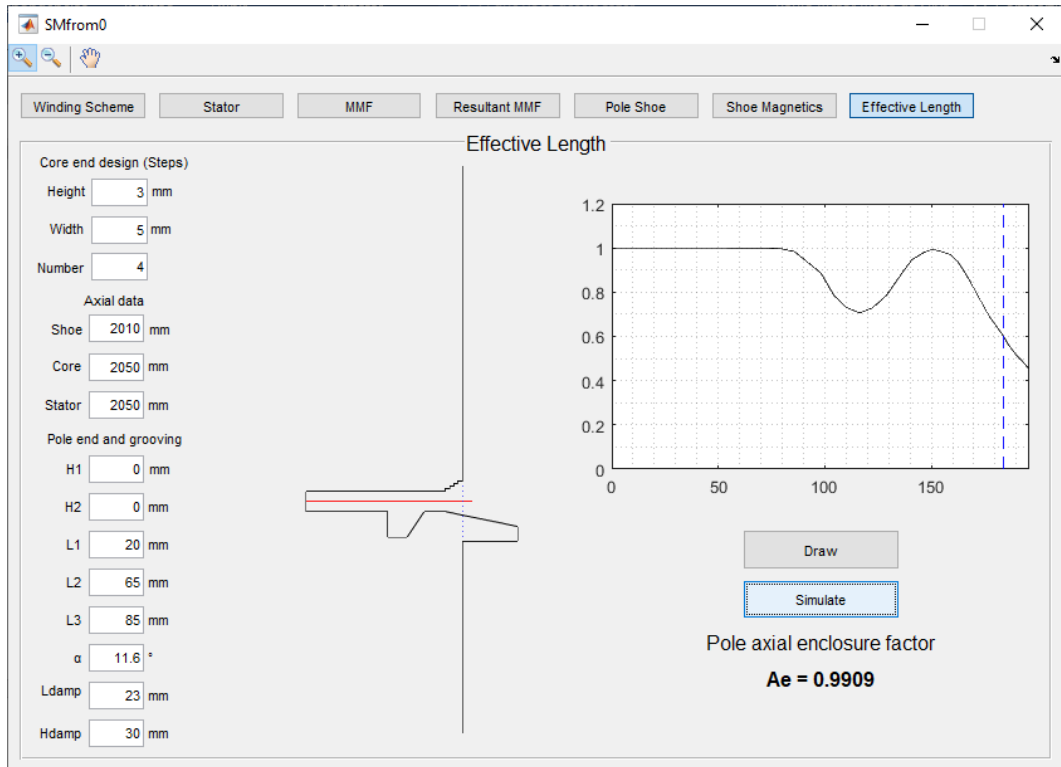


Figure 4.18 - Effective Magnetic Length analysis for SG2.

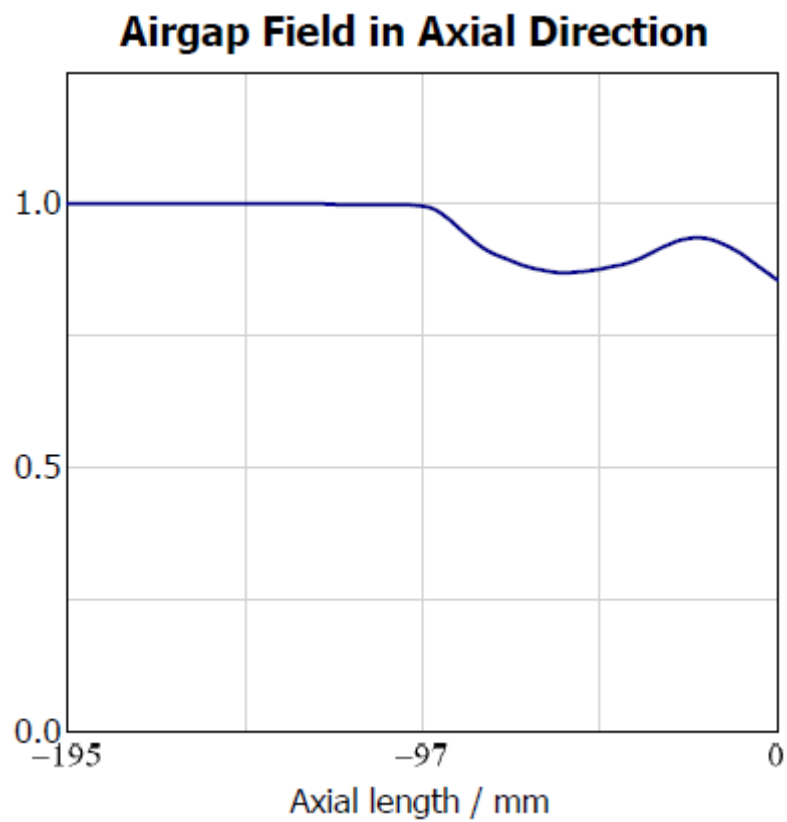


Figure 4.19 - Benchmark airgap field in axial direction for SG2.

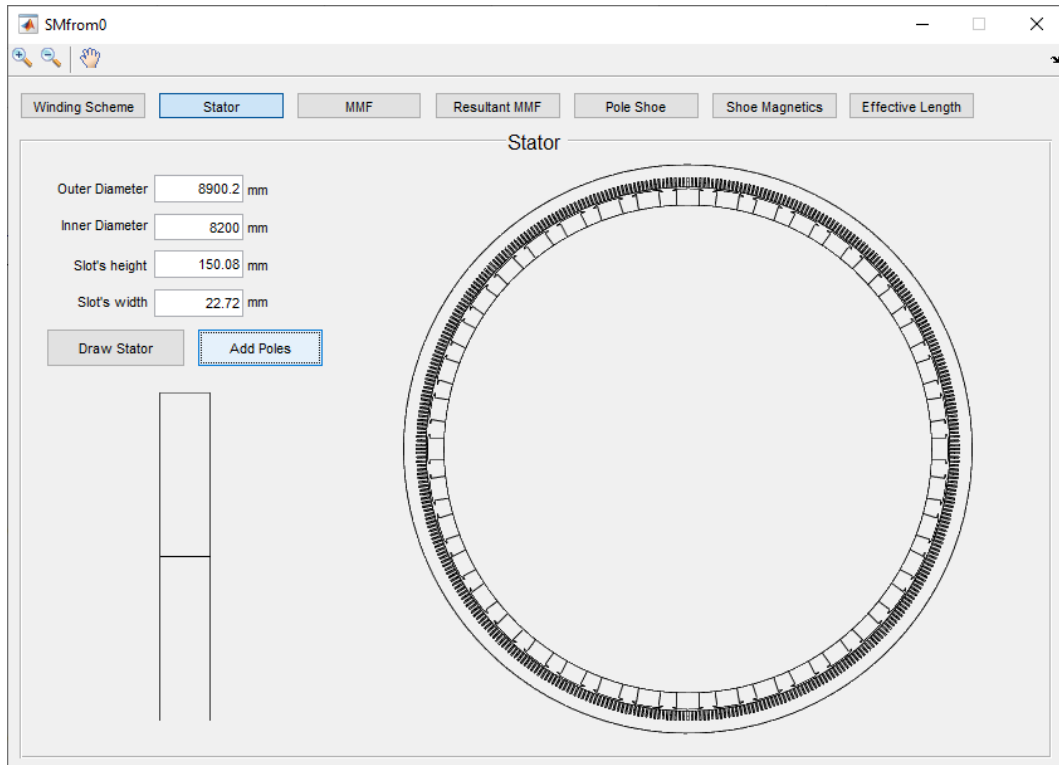


Figure 4.20 - Stator with poles for SG2.

4.3. Results for SG3

Significant results in Figures 4.21 to 4.24.

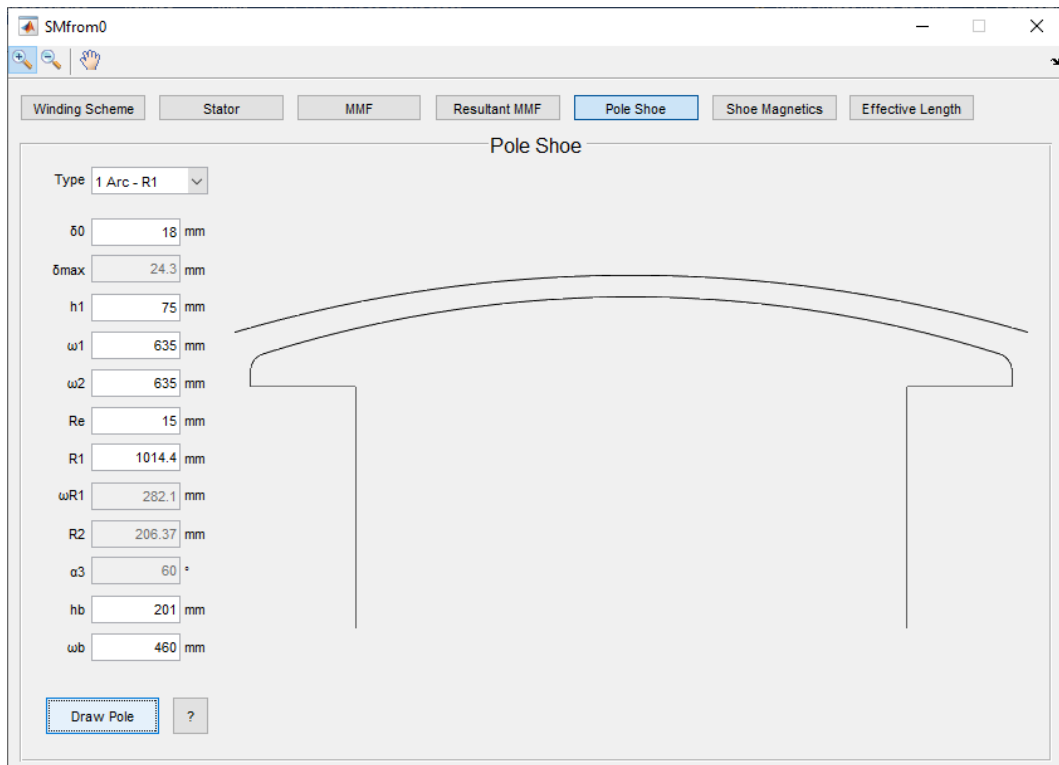


Figure 4.21 - Pole Shoe for SG3.

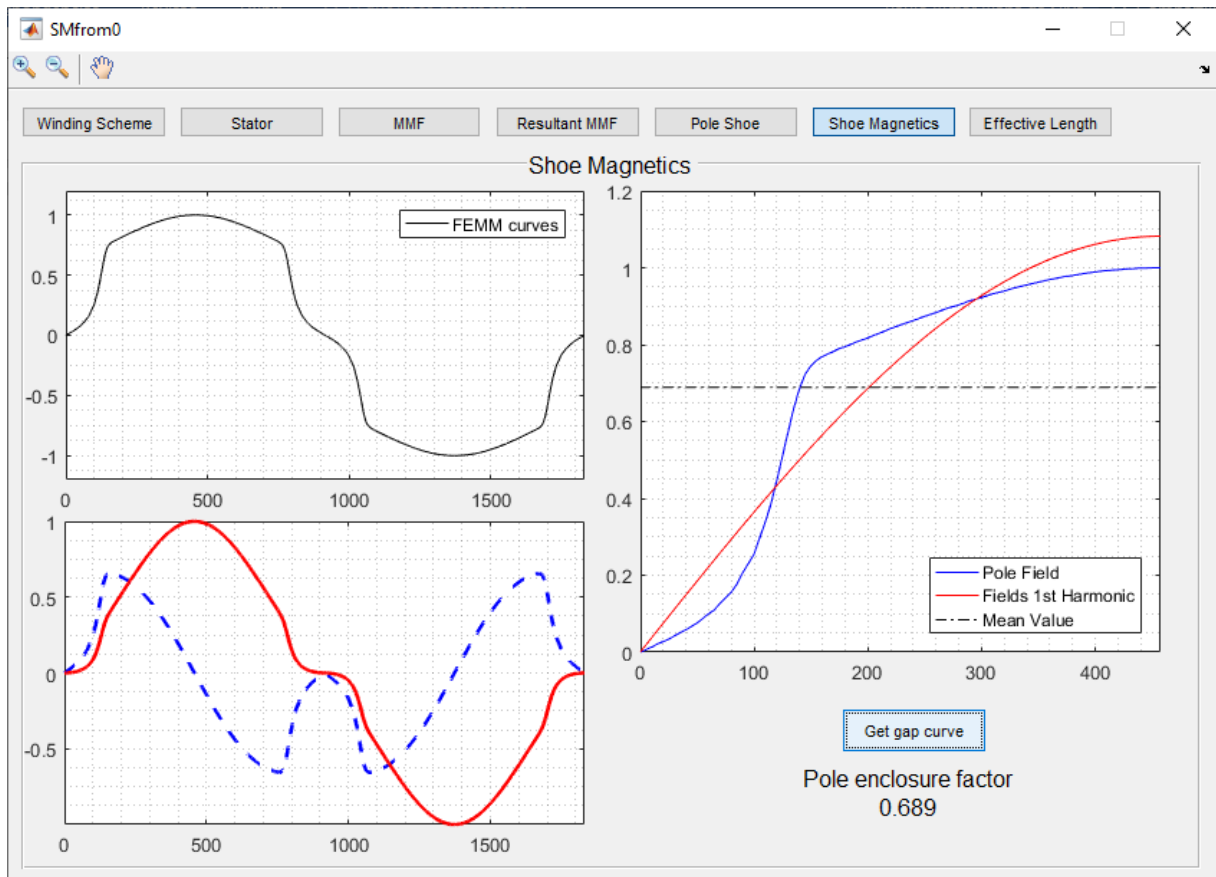


Figure 4.22 - Pole Shoe Magnetic Analysis for SG3.

Pole Field Curve

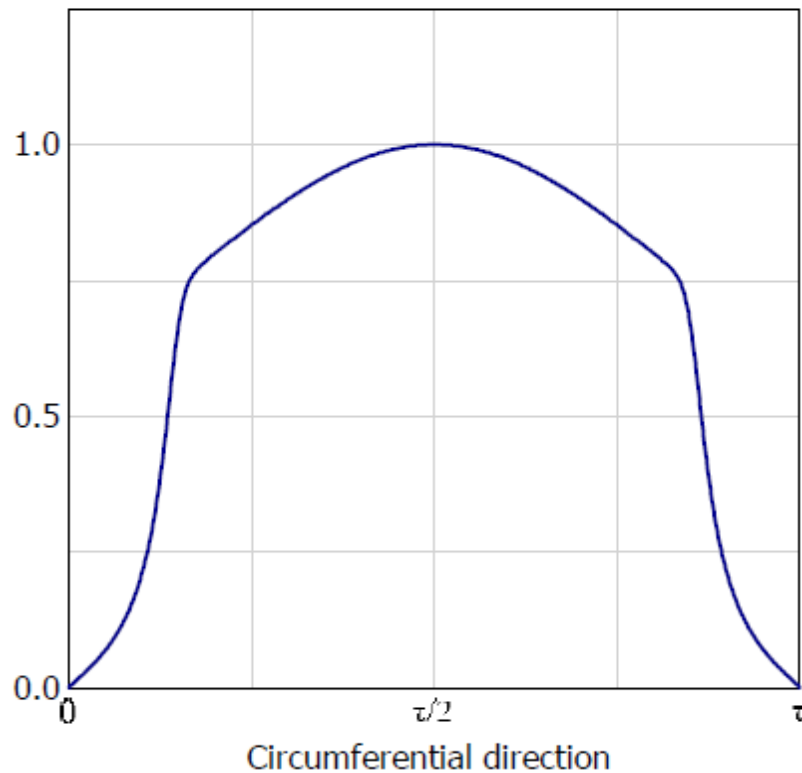


Figure 4.23 - Benchmark pole field curve for SG3.

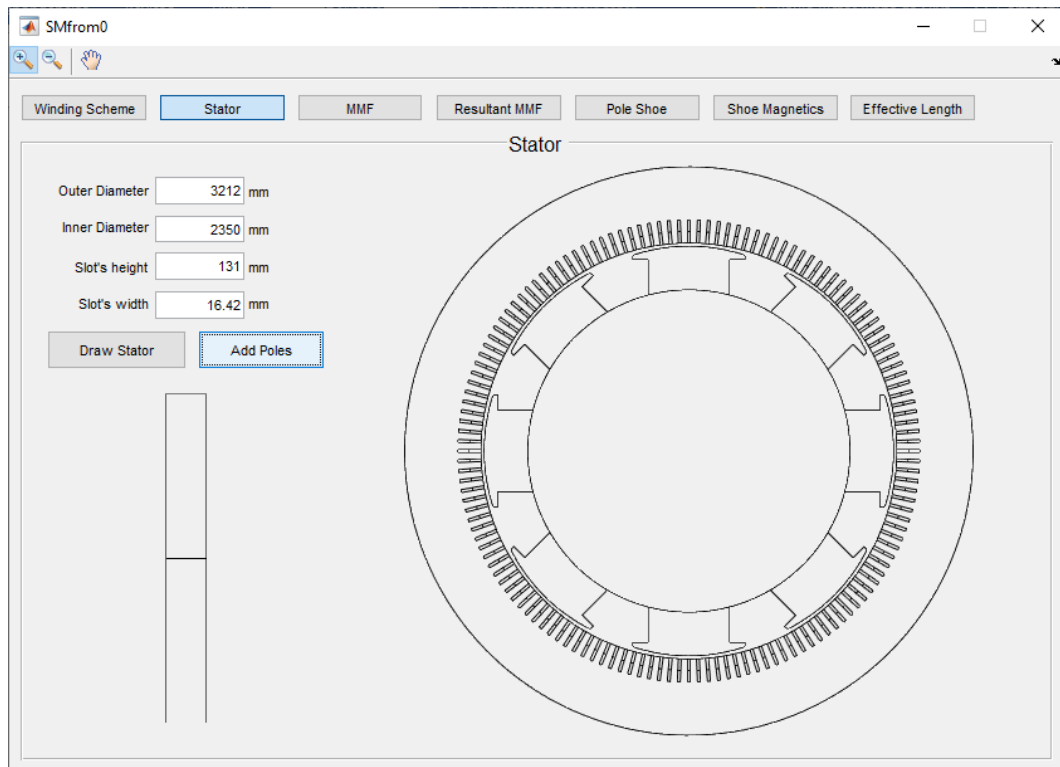


Figure 4.24 - Stator with poles for SG3

4.4. Results

4.4.1. Pole enclosure factor

From Figures 4.6, 4.16 and 4.22 the pole density flux plot is obtained, from that the pole enclosure factor is extracted and both, plot shape and factor value, can be compared with GE benchmark. By visual inspection, the curve shapes obtained coincides with the benchmark ones, even with the lack of information on the benchmark simulation parameters. Table 4.2 presents a comparison between factors obtained using this work tool and from GE benchmark.

Table 4.2 - Pole enclosure results compared to benchmark

SG	GE Benchmark	FEMM + MATLAB	Error
1	0.699	0.708	0.009
2	0.729	0.721	0.008
3	0.688	0.689	0.001

4.4.2. Axial enclosure factor

From Figures 4.8 and 4.18 axial enclosure factors are obtained. Visually, it is notable the difference in pole extremity plots from this work tools and GE benchmark, that is due to the different parameters considered during simulations, for boundaries and materials. The access limitation to benchmark information (only SG dimensions, airgap field in axial direction plot as image and axial enclosure factor) caused this discrepancy. Although, factor values comparison in Table 4.3 shows how accurate results are.

Table 4.3 - Axial enclosure results compared to benchmark.

SG	GE Benchmark	FEMM + MATLAB	Error
1	0.9851	0.9852	0.0001
2	0.9910	0.9909	0.0001

5. CONCLUSIONS

This dissertation presented a collection of procedures together with FEM to provide a general, simple and organized way to evaluate most common salient pole SG magnetics effects with air-gap line as reference, in a form of a set of tools using MATLAB interface. The tools calculate two important machine quantities: Magnetomotive force and factors that are key to estimate magnetic flux. The tools comprehend the study of: winding distribution using Tingley Box; Magnetomotive Force calculation from a given winding matrix; Pole shoe enclosure factor calculation for any salient pole machine; Axial enclosure factor calculation for any usual rotor construction.

In winding distribution, Tingley box proved to be a suitable and simple algorithm to set any combination in number of stator slots and pair of poles into a well-balanced winding scheme. For generators with a large number of slots it is difficult to apply the method by hand, so the implementation of it as an algorithm embraces these cases. Tingley is a clean way to show distribution of windings in slots and provides the winding matrix as output.

Applied examples of Winding Matrix maintains its status as a strong tool to manipulate windings in a more basic level, it allows changing the number of turns in each slot and the pitch of layers with ease, justifying its use, together with the MMF of a single turn formula, to determine the resultant MMF of any usual machine.

The use of Winding Matrix to calculate MMF is the start of more complete analyzes for machines, allowing the inclusion of unbalances as short-circuits in turns in specific slots, which is a common fault in SGs. This aspect allied with a real-time simulation is a strong utility toward predictive maintenance of power systems.

The two other tools presented in this dissertation makes a magnetic study using Finite Element Analysis in order to obtain enclosure factors, which are central to determine magnetic quantities that represent the machine. The use of MATLAB and FEMM provides a user-friendly interface that simulates salient pole shoes and their axial extremities with accuracy, which is confirmed when using GE benchmark data and comparing results.

Individually, the tools have proven their value by presenting valuable outputs as winding matrix, MMF, pole shoe enclosure factor and axial enclosure factor. And yet, when mutually applied, they allow the estimation of important magnetic quantities that are for use of machine manufacturers and for dynamic studies and simulation, using input parameters known from design and rated information, for any usual salient pole SM.

6. FUTURE WORKS

It is left to quantify the magnitudes of MMF and magnetic flux curves obtained in this work, and use this information to determine the machine reactance matrix.

To include the fault analysis in the MMF determination tool, allowing one to add faulty turns in one or more specific slots. Consecutively, combine this tool to a real-time simulator that analyzes fault in power systems.

To consider field and damper windings in the salient pole magnetic study, adapting the existing tools for their cases, completing the salient pole SM representation.

7. BIBLIOGRAPHY

- [1] International Energy Agency, "Data and Statistics," 2017. [Online]. Available: <https://www.iea.org/data-and-statistics>.
- [2] International Hydropower Association, "World Hydropower Statistics," [Online]. Available: <https://www.hydropower.org/maps/worldhydropowerstatistics>.
- [3] R. H. Park, "Two Reaction Theory of Synchronous Machines," *AIEE Transactions*, pp. 48:716-730, 1929.
- [4] M. N. Al-Din and I. Al-Adwan, "Finite Element Analysis of an Outer Rotor Permanent Magnet Brushless DC," *International Journal of Electrical Engineering*, pp. 99-116, 2013.
- [5] O. Chiver, C. Barz, L. Neamt and Z. Erdei, "Induction Motor Analysis by Finite Elements Method," *Journal of Electrical and Electronics Engineering*, 2010.
- [6] D. W. Ferreira, S. I. Nabeta and L. Lebensztajn, "Finite Element Analysis and Synchronous Machine Parameter Determination," *Journal of Microwaves and Optoelectronics*, vol. 6, no. 1, pp. 178-188, 2007.
- [7] E. Schmidt, M. Sušć and A. Eilenberger, "Finite element analysis of a permanent magnet synchronous machine with an external rotor for a position sensorless control," *2009 Australasian Universities Power Engineering Conference*, pp. 1-6, 2009.
- [8] I. Boldea, *Synchronous Generators*, CRC Press, Taylor & Francis Group, 2015.
- [9] C. Concordia, *Synchronous Machines, Theory and Performance*, New York: John Wiley & Sons, 1951.
- [10] B. Ban, S. Stipetic and M. Klanac, "Synchronous Reluctance Machines: Theory, Design and the Potential Use in Traction Applications," *2019 International Conference on Electrical Drives & Power Electronics (EDPE)*, August 2019.
- [11] Henry, "Introduction to Synchronous Generator," 03 December 2019. [Online]. Available: <https://www.theengineeringknowledge.com/introduction-to-synchronous-generator/>.
- [12] M. P. Kostenko and L. M. Piotrovski, *Electrical Machines II*, Moskow: MIR Publishers, 1969.

- [13] K. B. Lee, H. U. Shin and Y. Bak, "Basic Control of AC Motor Drives," *Control of Power Electronic Converters and Systems*, pp. 301-329, 2018.
- [14] "Memória Rondonense," [Online]. Available: <http://www.memoriarondonense.com.br/galeria-single/itaipu-binacional-em-fotos/24/>.
- [15] "Tutors Globe," [Online]. Available: <http://www.tutorsglobe.com/>.
- [16] B. Adkins and R. G. Harley, *The general theory of alternating current machines : application to practical problems*, London: Chapman and Hall Distributed by Halsted Press, 1978.
- [17] W. A. Lewis, *The Principles of Synchronous Machines*, Illinois Institute of Technology, 1959.
- [18] P. Krause, O. Wasynczuk, S. D. Sudhoff and S. Pekarek, *Analysis of Electric Machinery and Drive Systems*, Piscatawy, NJ: Wiley-IEEE Press, 2013.
- [19] A. Hrennikoff, "Solution of problems of elasticity by the framework method," *Journal of Applied Mechanics*, p. 169–175, 1941.
- [20] R. Courant, "Variational methods for the solution of problems of equilibrium and vibrations," *Bulletin of the American Mathematical Society*, p. 49: 1–23, 1943.
- [21] "FEATool Multiphysics," [Online]. Available: <https://www.featool.com/tutorial/>.
- [22] J. N. Reddy, *An Introduction to the Finite Element Method*, Third Edition, McGraw-Hill, 2006.
- [23] Finite Element Method Magnetics, "Finite Element Method Magnetics," [Online]. Available: <http://www.femm.info/wiki/Documentation/>.
- [24] E. M. Tingley, "Two-Phase and Three-Phase Lap Windings in Unequal Groups," *Electrical Review and Western Electrician*, pp. 166-168, 23 January 1915.
- [25] N. Bianchi, S. Bolognani, M. D. Pre and G. Grezzani, "Design considerations for fractional-slot winding configurations of synchronous machines," *IEEE TRANSACTIONS ON INDUSTRY APPLICATIONS*, vol. 42, no. 4, pp. 997-1006, 2006.
- [26] H. Grop and J. Soulard, "Theoretical investigation of fractional conductor windings for AC-machines," in *Proceedings of the 2008 International Conference on Electrical Machines*, 2008.

- [27] M. Caruso, A. O. Di Tommaso, F. Marignetti, R. Miceli and G. R. Galluzzo, "A General Mathematical Formulation for Winding Layout Arrangement of Electrical Machines," *Energies*, pp. 11(2), 446, 2018.
- [28] E. J. J. Rocha, P. V. V. Silva and E. C. Bortoni, "The conductor as the cornerstone of winding magnetomotive force," *2017 IEEE Power & Energy Society General Meeting*, pp. 1-5, 2017.
- [29] A. Ivanov-Smolensky, *Electrical Machines*, vol. 3, Moskow: MIR Publishers, 1983.

ANNEX A

$$\begin{bmatrix} \lambda_a \\ \lambda_b \\ \lambda_c \\ - \\ \lambda_F \\ \lambda_D \\ \lambda_Q \end{bmatrix} = \begin{bmatrix} \frac{1}{\sqrt{3}} & \frac{1}{\sqrt{3}} & \frac{1}{\sqrt{3}} & | & 0 & 0 & 0 \\ \sqrt{\frac{2}{3}} \cos \theta & \sqrt{\frac{2}{3}} \cos \left(\theta - \frac{2\pi}{3} \right) & \sqrt{\frac{2}{3}} \cos \left(\theta + \frac{2\pi}{3} \right) & | & 0 & 0 & 0 \\ \sqrt{\frac{2}{3}} \sin \theta & \sqrt{\frac{2}{3}} \sin \left(\theta - \frac{2\pi}{3} \right) & \sqrt{\frac{2}{3}} \sin \left(\theta - \frac{2\pi}{3} \right) & | & 0 & 0 & 0 \\ \hline 0 & 0 & 0 & | & 1 & 0 & 0 \\ 0 & 0 & 0 & | & 0 & 1 & 0 \\ 0 & 0 & 0 & | & 0 & 0 & 1 \end{bmatrix} \dots$$

$$\begin{bmatrix} \mathbb{P} & 0 \\ 0 & u_3 \end{bmatrix}$$

$$\begin{bmatrix} L_s + L_m \cos(2\theta) & -M_s - L_m \cos \left[2 \left(\theta + \frac{\pi}{6} \right) \right] & -M_s - L_m \cos \left[2 \left(\theta + \frac{5\pi}{6} \right) \right] & | & M_F \cos \theta & M_D \cos \theta & M_Q \sin \theta \\ -M_s - L_m \cos \left[2 \left(\theta + \frac{\pi}{6} \right) \right] & L_s + L_m \cos \left[2 \left(\theta - \frac{2\pi}{3} \right) \right] & -M_s - L_m \cos \left[2 \left(\theta - \frac{\pi}{2} \right) \right] & | & M_F \cos \left(\theta - \frac{2\pi}{3} \right) & M_D \cos \left(\theta - \frac{2\pi}{3} \right) & M_Q \sin \left(\theta - \frac{2\pi}{3} \right) \\ -M_s - L_m \cos \left[2 \left(\theta + \frac{5\pi}{6} \right) \right] & -M_s - L_m \cos \left[2 \left(\theta - \frac{\pi}{2} \right) \right] & L_s + L_m \cos \left[2 \left(\theta + \frac{2\pi}{3} \right) \right] & | & M_F \cos \left(\theta + \frac{2\pi}{3} \right) & M_D \cos \left(\theta + \frac{2\pi}{3} \right) & M_Q \sin \left(\theta + \frac{2\pi}{3} \right) \\ \hline M_F \cos \theta & M_F \cos \left(\theta - \frac{2\pi}{3} \right) & M_F \cos \left(\theta + \frac{2\pi}{3} \right) & | & L_F & M_R & 0 \\ M_D \cos \theta & M_D \cos \left(\theta - \frac{2\pi}{3} \right) & M_D \cos \left(\theta + \frac{2\pi}{3} \right) & | & M_R & L_D & 0 \\ M_Q \sin \theta & M_Q \sin \left(\theta - \frac{2\pi}{3} \right) & M_Q \sin \left(\theta + \frac{2\pi}{3} \right) & | & 0 & 0 & L_Q \end{bmatrix} \dots$$

$$[L]$$

$$\begin{array}{c}
 \dots \\
 \left[\begin{array}{ccc|ccc}
 \frac{1}{\sqrt{3}} & \frac{1}{\sqrt{3}} & \frac{1}{\sqrt{3}} & 0 & 0 & 0 \\
 \sqrt{\frac{2}{3}} \cos \theta & \sqrt{\frac{2}{3}} \cos \left(\theta - \frac{2\pi}{3} \right) & \sqrt{\frac{2}{3}} \cos \left(\theta + \frac{2\pi}{3} \right) & 0 & 0 & 0 \\
 \sqrt{\frac{2}{3}} \sin \theta & \sqrt{\frac{2}{3}} \sin \left(\theta - \frac{2\pi}{3} \right) & \sqrt{\frac{2}{3}} \sin \left(\theta + \frac{2\pi}{3} \right) & 0 & 0 & 0 \\
 \hline
 0 & 0 & 0 & 1 & 0 & 0 \\
 0 & 0 & 0 & 0 & 1 & 0 \\
 0 & 0 & 0 & 0 & 0 & 1
 \end{array} \right] \begin{bmatrix} i_a \\ i_b \\ i_c \\ i_F \\ i_D \\ i_Q \end{bmatrix} = \begin{array}{c}
 \left[\begin{array}{ccc|ccc}
 L_s - 2M_s & 0 & 0 & 0 & 0 & 0 \\
 0 & L_s + M_s + 3/2 L_m & 0 & \sqrt{3/2} M_F & \sqrt{3/2} M_D & 0 \\
 0 & 0 & L_s + M_s - 3/2 L_m & 0 & 0 & \sqrt{3/2} M_Q \\
 \hline
 0 & \sqrt{3/2} M_F & 0 & L_F & M_R & 0 \\
 0 & \sqrt{3/2} M_D & 0 & M_R & L_D & 0 \\
 0 & 0 & \sqrt{3/2} M_Q & 0 & 0 & L_Q
 \end{array} \right] \begin{bmatrix} i_a \\ i_b \\ i_c \\ i_F \\ i_D \\ i_Q \end{bmatrix} \\
 \text{[LT]}
 \end{array}
 \end{array}$$

$$\begin{bmatrix} \mathbb{P} & 0 \\ 0 & u_3 \end{bmatrix}$$